

MOLECULAR STRUCTURES AND PROPERTIES OF POLYMERS FOR
GEL ELECTROLYTES AND POLYMERIZED IONIC LIQUIDS



A Thesis Submitted in Partial Fulfillment of the Requirements for the
Degree of Master of Science in Chemistry
Suranaree University of Technology
Academic Year 2024

โครงสร้างโมเลกุลและสมบัติของพอลิเมอร์สำหรับอิเล็กทรอนิกส์เจลและระบบ
ของเหลวของไอออนิกที่ถูกทำให้เป็นพอลิเมอร์

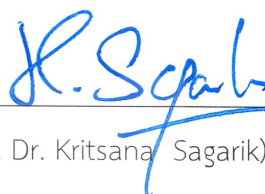


วิทยานิพนธ์นี้เป็นส่วนหนึ่งของการศึกษาตามหลักสูตรปริญญาวิทยาศาสตรมหาบัณฑิต
สาขาวิชาเคมี
มหาวิทยาลัยเทคโนโลยีสุรนารี
ปีการศึกษา 2567

MOLECULAR STRUCTURES AND PROPERTIES OF POLYMERS FOR GEL
ELECTROLYTES AND POLYMERIZED IONIC LIQUIDS

Suranaree University of Technology has approved this thesis submitted in
partial fulfillment of the requirements for a Master's Degree.

Thesis Examining Committee



(Prof. Dr. Kritsana Sagarik)

Chairperson



(Assoc. Prof. Dr. Visit Vao-soongnern)

Member (Thesis Advisor)



(Assoc. Prof. Dr. Chaiwat Ruksakulpiwat)

Member



(Asst. Prof. Dr. Khongvit Prasitnok)

Member



(Assoc. Prof. Dr. Yupaporn Ruksakulpiwat)

Vice Rector for Academic Affairs
and Quality Assurance



(Prof. Dr. Santi Maensiri)

Dean of Institute of Science

จิตาภา กุสินรัมย์ : โครงสร้างโมเลกุลและสมบัติของพอลิเมอร์สำหรับอิเล็กโทรไลต์เจลและระบบของเหลวของไอออนิกที่ถูกทำให้เป็นพอลิเมอร์ (MOLECULAR STRUCTURES AND PROPERTIES OF POLYMERS FOR GEL ELECTROLYTES AND POLYMERIZED IONIC LIQUIDS) อาจารย์ที่ปรึกษา : รองศาสตราจารย์ ดร.วิสิทธิ์ แวสูงเนิน, 152 หน้า.

คำสำคัญ: การจำลองหลากหลายระดับ, พอลิเมอร์โครงสร้างอสัณฐาน, พอลิไวนิลฟลูออไรด์, พอลิไวนิลคลอไรด์, ความแข็งของสายโซ่, พื้นผิวสัมผัสของพอลิเมอร์, การจำลองแบบมอนติคาร์โล, การตกผลึกของพอลิเมอร์, แบบจำลองเสมือนของโครงสร้างพอลิเอทิลีน, การขนส่งไอออน, การจำลองแบบทางพลวัตเชิงโมเลกุล, ของเหลวไอออนิกที่ถูกทำให้เป็นพอลิเมอร์

วิทยานิพนธ์นี้มีการใช้การจำลองคอมพิวเตอร์แบบหลายระดับเพื่อตรวจสอบปัจจัยระดับโมเลกุลที่สามารถควบคุมคุณสมบัติเชิงโครงสร้างของพอลิเมอร์โฮสต์ในการประยุกต์ใช้อิเล็กโทรไลต์เพื่อพัฒนาการเพิ่มสภาพการนำไฟฟ้าไอออนิกของอิเล็กโทรไลต์พอลิเมอร์ จึงมีการเสนอวิธีที่สามารถเป็นไปได้บางวิธีเพื่อปรับเปลี่ยนหน่วยของพอลิเมอร์ที่ทำซ้ำเพื่อปรับความแข็งแรงภายในสายโซ่และปฏิสัมพันธ์ระหว่างโมเลกุล ซึ่งสามารถส่งผลกระทบต่อลักษณะทางโครงสร้าง มิติของโมเลกุล การก่อตัวของสายโซ่บริเวณใกล้พื้นผิว การตกผลึกเมื่ออุณหภูมิเย็นลงจากของเหลวที่สถานะหลอมละลาย โครงสร้างแบบอสัณฐานเชิงอะตอมเสมือนจริง และระดับการแตกตัวของไอออนิกในของเหลวไอออนิกที่ถูกทำให้เป็นพอลิเมอร์ โดยวิทยานิพนธ์เล่มนี้แบ่งออกเป็น 4 ส่วนหลักดังนี้

ในส่วนแรก ได้มีการศึกษาการจำลองโมเลกุลหลายระดับสำหรับคุณสมบัติเชิงโครงสร้างและวัสดุของโฮสต์พอลิเมอร์สองตัวสำหรับอิเล็กโทรไลต์เจล โดยแบบจำลองสถานะไอโซเมอร์กึ่งหมุน (RIS) ที่ได้จากการคำนวณโครงสร้างอิเล็กทรอนิกส์เบื้องต้นถูกนำมาใช้เพื่อทำนายสถิติทางโครงสร้างของพอลิไวนิลฟลูออไรด์ (พีวีเอฟ) เมื่อเปรียบเทียบกับพอลิไวนิลคลอไรด์ (พีวีซี) ซึ่งความแข็งแรงของสายโซ่หรือค่า C_n ถูกนำเสนอในส่วนของอัตราส่วนลักษณะเฉพาะทางความแข็งแรง (C_n) นั้น มีค่ามากกว่าอย่างมีนัยสำคัญสำหรับสายโซ่พีวีซี ซึ่งสายโซ่ของพีวีซีและพีวีเอฟจะถูกทำให้เป็นแบบจำลองเม็ดหยาบและแมปกับโครงสร้างแบบตาข่ายเพชรในบริเวณที่ใกล้ที่สุดเป็นอันดับสองหรือที่เรียกว่า 2^{nd} lattice โดยสมบัติบนโครงตาข่าย เช่น ขนาดของโมเลกุลและสถิติเชิงโครงสร้างที่สอดคล้องกับการทำนายเชิงทฤษฎีเป็นอย่างดี โดยแบบจำลองของสองระบบแบบอสัณฐานเชิงอะตอมเสมือนจริงซึ่งสามารถทำได้โดยการทำแมปย้อนกลับเพื่อคืนค่าอะตอมที่หายไป และหลังจากลดพลังงานให้เหลือน้อยที่สุด ผลลัพธ์ทั้งหมดนี้จะถูกรายงานและเปรียบเทียบระหว่างระบบพีวีเอฟและพีวีซี

ในส่วนที่สอง ศึกษาบทบาทของความแข็งแรงของสายโซ่ต่อคุณสมบัติเชิงโครงสร้างและโมเลกุลสำหรับพื้นผิวอิสระของพอลิเมอร์หลอมเหลวโดยใช้วิธีการตรวจสอบจากการจำลอง MC ของสายโซ่

พอลิเอทิลีน (PE) ที่มีโครงสร้างคล้าย PE ที่เป็นการจำลองแบบเนื้อหยาบ (CG) บนโครงตาข่ายที่ 2 หรือ 2nm lattice ซึ่งมีการเสนอแบบจำลองคล้ายโครงสร้าง PE โดยการคูณค่าน้ำหนักทางสถิติของ RIS กับพารามิเตอร์ความแข็งของสายโซ่ (k) เพื่อแสดงถึงสายโซ่ที่มีความยืดหยุ่นของโครงสร้างมากกว่า ($k = 0.0$ และ 0.5) และโครงสร้างที่แข็งกว่า ($k = 1.5$ และ $k = 2.0$) เมื่อเทียบกับ PE ที่มีโครงสร้างปกติ ($k = 1.0$) สำหรับพื้นผิวหลอมเหลว-สุญญากาศของสายโซ่ที่มีความแข็งกว่า ซึ่งความหนาแน่นของมวลรวมจะลดลงตามโปรไฟล์พื้นผิวที่กว้างขึ้น โดยอิงตามพลังงานภายในและระหว่างโมเลกุล พบว่าสายโซ่ที่มีความยืดหยุ่นมากขึ้นจะมีโครงสร้างแบบโกชมากขึ้นโดยมีโครงสร้างที่บริเวณเป็นกลุ่มที่หนาแน่นกว่า แต่จะมีโครงสร้างทรานส์มากขึ้นเมื่อเข้าใกล้พื้นผิว

ในส่วนที่สาม บทบาทของปฏิสัมพันธ์ระหว่างโมเลกุลที่เกี่ยวข้องกับการจับกันของสายโซ่ในเฟสควบแน่น ซึ่งอาจเกี่ยวข้องอย่างใกล้ชิดกับการตกผลึกของพอลิเมอร์ ซึ่งได้รับการตรวจสอบผ่านการจำลอง MC ด้วยวิธีการจำลองระบบแบบหยาบ(CG) เพื่อศึกษาผลกระทบของปฏิสัมพันธ์ระหว่างโมเลกุลต่อการตกผลึกของพอลิเมอร์จากสถานะหลอมเหลว สำหรับแบบจำลองคล้ายโครงสร้างของระบบ PE ที่มีพารามิเตอร์พลังงานศักย์ Lennard-Jones (LJ) ต่างกัน นั่นคือ ขนาดลูกบดเท่ากัน ($\sigma = 0.44$ นาโนเมตร) แต่มีความลึกของหลุมศักย์ต่างกัน (ϵ), ในช่วงของ $185 \text{ K} < \epsilon/kT < 205 \text{ K}$ คือระบบที่มีแรงดึงดูดมากกว่า ส่วนในช่วง $125 \text{ K} < \epsilon/kT < 185 \text{ K}$ คือระบบที่มีแรงผลึกมากกว่า โดยเปรียบเทียบกับระบบสายโซ่ของ PE แบบปกติ ($\sigma = 0.44\text{nm}$, $\epsilon/kT = 185 \text{ K}$) ผลลัพธ์โดยรวมชี้ให้เห็นว่ามีเพียงสายโซ่คล้าย PE เท่านั้นที่มีปฏิสัมพันธ์ระหว่างโมเลกุลที่เหมาะสมจึงสามารถสร้างโครงสร้างแบบมีระเบียบได้อย่างมีประสิทธิภาพที่อุณหภูมิการตกผลึก

ในส่วนสุดท้าย คุณสมบัติเชิงโครงสร้างพลวัตและการขนส่งไอออนของไอออนิกของเหลว (ILs) ที่เป็นพอลิเมอร์ที่มีฐานเป็นอิมิดาโซเลียม (imidazolium) ผสมกับอิลิกโทรไลต์ของ 1-บิลทิล-3-เมทิลลิมาโซเลียม บิสไตรฟลูออโรเมเทนซัลโฟนิลอิมิด: (Bmim-TFSI) ซึ่งถูกศึกษาด้วยวิธีการจำลองแบบทางพลวัตเชิงโมเลกุล ผลลัพธ์แสดงให้เห็นว่าการเติมอิลิกโทรไลต์ ILs ช่วยให้การเคลื่อนที่แบบแบ่งส่วนของสายโซ่พอลิเมอร์เร็วขึ้น และยังช่วยเพิ่มการนำไฟฟ้าของไอออน ซึ่งสอดคล้องกับที่สังเกตได้ในการทดลอง สำหรับการศึกษาสถิติความสัมพันธ์ของแอนไอออนแสดงให้เห็นว่ากลไกการขนส่งภายในสายโซ่เป็นโหมดที่โดดเด่นเมื่อเทียบกับกลไกการขนส่งอื่น ๆ สิ่งนี้สอดคล้องกับการค้นพบในการทดลองครั้งก่อนที่ทำโดย Inoue et al. (Inoue, 2013) ซึ่งระบุว่าโหมดย่อย Rouse มักปรากฏในสารละลายที่เป็นโหมดหลักของการเคลื่อนไหวในโพลีเมอร์โดยได้รับผลกระทบจากปฏิสัมพันธ์ภายในสายโซ่

สาขาวิชาเคมี

ปีการศึกษา 2567

ลายมือชื่อนักศึกษา

จิตาภา นิลนัมย์

ลายมือชื่ออาจารย์ที่ปรึกษา

วิชัย นิลนัมย์

CHIDAPHA KUSINRAM : MOLECULAR STRUCTURES AND PROPERTIES OF
POLYMERS FOR GEL ELECTROLYTES AND POLYMERIZED IONIC LIQUIDS
ELECTROLYTE THESIS ADVISOR : ASSOC. PROF. VISIT VAO-SOONGNERN, Ph.D.
152 PP.

Keyword: Multiscale simulation, Amorphous polymer, Poly vinylfluoride (PVF), Poly vinylchloride (PVC), Chain stiffness, Polymer surface, Monte Carlo simulation, Polymer crystallization, Ion Transportation, MD simulation, Polymerized Ionic Liquid

Multiscale computer simulations were employed to investigate molecular factors that can control structural properties of the host polymers in electrolyte application. To Increase the ionic conductivity of polymer electrolytes, some possible routes are proposed to modify the repeating units to adjust the intrachain stiffness and intermolecular interaction that can affect conformational characteristics, molecular dimension, chain perturbation near the surface, crystallization, upon cooling from the melts, atomistic amorphous structures and the degree of ionic dissociation in polymerized ionic liquids. There are 4 main parts in this thesis.

In the first part, multiscale molecular simulations for structural and material properties of two polymer hosts for gel electrolytes were studied. The rotational isomeric state (RIS) models derived from *ab initio* electronic structure calculation were employed to predict the conformational statistics of poly(vinyl fluoride), PVF, in comparison with poly(vinyl chloride), PVC. The chain stiffness, as represented by the characteristic ratio, is significantly larger for PVC chains. PVC and PVF chains were coarse-grained and mapped onto the second nearest neighbor diamond ($2nd$) lattice. The on-lattice properties such as molecular size and conformational statistics agree well with theoretical prediction. Fully atomistic amorphous PVF and PVC models can be obtained by reverse-mapping to restore the missing atoms. After energy minimization, all results are reported and compared between PVF and PVC.

In the second part, the role of chain stiffness on structural and molecular properties for the free surface of polymer melts was examined by MC simulations of the coarse-grained (CG) polyethylene *PE-like* chains on the $2nd$ lattice. *PE-like* models

were proposed by multiplying the RIS statistical weights with the chain stiffness parameter (k) to represent more flexible ($k = 0.0$ and 0.5) and stiffer ($k = 1.5$ and $k = 2.0$) chains than normal PE ($k = 1.0$). For the melt-vacuum surfaces of stiffer chains, bulk densities become lower with broader surface profiles. Based on intra- and intermolecular energetics, more flexible chains have a larger amount of gauche conformation with denser bulk structures, but they adopt more trans conformation near the surface.

In the third part, the role of the intermolecular interaction related to the chain packing in the condensed phase, which can be intimately associated with polymer crystallization was investigated via MC simulations of CG *PE-like* models to study the effect of intermolecular interaction on polymer crystallization from the molten state. *PE-like* models with different Lennard-Jones (LJ) potential energy parameters i.e. the same bead size ($\sigma = 0.44$ nm) but different potential well depth (ϵ), in the range of $185 \text{ K} < \epsilon/kT < 205 \text{ K}$ and $125 \text{ K} < \epsilon/kT < 185 \text{ K}$, respectively, for more attractive and more repulsive interaction than those for normal PE chains ($\sigma = 0.44 \text{ nm}$, $\epsilon/kT = 185 \text{ K}$). Overall results suggest that only *PE-like* chains with the appropriated intermolecular interaction can be effectively formed the ordered structure at the crystallization temperature.

In the final part, the structural, dynamics, and ion transportation properties of imidazolium-based polymerized ionic liquids (ILs) blended with 1-butyl-3-methylimidazolium bis(trifluoromethanesulfonyl)imide: (Bmim-TFSI) electrolytes were investigated using molecular dynamics (MD) simulations. Results showed that the addition of ILs electrolytes facilitates faster segmental dynamics of the polymer chains and enhances the ionic conductivity, in agreement with what was observed in the experiments. The study of anion association statistics suggests that the intrachain transportation mechanism is the dominant mode compared to other transport mechanisms.

School of Chemistry

Academic Year 2024

Student's Signature จิตภาณุ นุติธรรมชัย
 Advisor's Signature วิมลวรรณ

ACKNOWLEDGEMENTS

My sincere gratitude goes out to Associate Professor Dr. Visit Vao-soongnern, my supervisor, for all of his support and inspiration. I genuinely appreciate all of the learning opportunities he has provided for me. This project could not be completed without the support of my classmates. I cannot express enough thanks to them. I would like to thank DPST scholarship for supporting my study at Suranaree University of Technology (SUT). I thank SUT for providing the working space and computer resources for this research project.

I would like to thank my supervisor for internship, Prof. Tadashi Inoue, for giving me the opportunity of internship and join his laboratory at Osaka University. I was grateful by his research sources, this has given me a lot of new experience for instrument and additional experimental knowledge. I would also like to thank Assoc. Prof. Osamu Urakawa, who suggested and offered ideas for this research and helpful discussions in experiments and simulations about polymerized ionic liquids. I would like to thank my friends in Inoue's laboratory member, especially Mr. Izutsu Haruki, he teaches me how to use the instruments, experiment and help discuss experiment results. And I would also like to thank Assist. Prof. Khongvit Prasitnok, who guidance carried me through all the processes and helpful discussion about MD simulation.

Finally, I would like to thank my wonderful family for encouragement, financial support and belief.

Chidapha Kusinram

CONTENTS

	Page
ABSTRACT IN THAI	I
ABSTRACT IN ENGLISH.....	III
ACKNOWLEDGEMENTS.....	V
CONTENTS.....	VI
LIST OF TABLES.....	X
LIST OF FIGURES.....	XI
LIST OF ABBREVIATIONS.....	XVIII
CHAPTER	
I INTRODUCTION	1
1.1 Research objectives.....	5
1.2 Scope and limitations.....	5
1.2.1 Molecular Simulation.....	5
1.2.2 Experiments.....	6
II LITERATURE REVIEWS.....	7
2.1 Multiscale molecular simulations of two polymer hosts for gel electrolytes: poly(vinyl chloride) and poly(vinyl fluoride).....	7
2.1.1 Rotational isomeric state (RIS) model of PVC.....	8
2.1.2 Rotational isomeric state (RIS) model of PVF.....	11
2.2 Monte Carlo simulation : Effect of chain stiffness on the free surface of polymers.....	13
2.3 The effect of intermolecular interaction on polymer crystallization...	14
2.4 Molecular dynamics (MD) simulation of detailed structures and ion transportation of polymerized ionic liquid/ionic liquid blends.....	17
2.4.1 Ionic conductivity in Experiment.....	17

CONTENTS (Continued)

	Page
2.4.2 The charge screening on the viscoelastic properties and the conformation of polymerized ionic liquids (PILs) in ionic liquid (IL) solutions.....	19
2.4.3 Molecular Dynamics (MD) Simulation of polymerized ionic liquids.....	20
2.4.4 Molecular Dynamics (MD) Simulation of Ionic conductivity.	22
2.4.5 Ion Transport Mechanisms.....	23
III RESEARCH METHODOLOGY	26
3.1 A multiscale molecular simulations for structural and material properties of two polymer hosts for gel electrolytes of poly(vinyl chloride) : PVC and poly(vinyl fluoride): PVF.....	26
3.1.1 Rotational Isomeric State (RIS) Model.....	26
3.1.2 RIS model of vinyl polymers.....	29
3.1.3 RIS parameters by quantum chemistry calculation.....	30
3.1.4 Monte Carlo Simulation of polymer.....	33
3.1.5 Moves in the Simulation.....	37
3.1.6 System Description.....	37
3.1.7 Fully atomistic models.....	38
3.2 Monte Carlo simulation : Effect of chain stiffness on the free surface of polymers.....	38
3.2.1 Rotational Isomeric State (RIS) Model.....	38
3.2.2 Monte Carlo simulation.....	41
3.2.3 Free surface formation.....	42
3.3 The effect of intermolecular interaction on polymer crystallization..	43

CONTENTS (Continued)

	Page
3.4 Molecular dynamics (MD) simulation of detailed structures and ion transportation of polymerized ionic liquid/ionic liquid blends.....	45
3.4.1 Experimental Methods	45
3.4.2 Molecular dynamics simulation.....	48
IV RESULTS AND DISCUSSION	54
4.1 Multiscale molecular simulations of two polymer hosts for electrolytes: poly(vinyl chloride) and poly(vinyl fluoride).....	54
4.1.1 Conformational Energy.....	54
4.1.2 Structural relaxation.....	61
4.1.3 Molecular dimension.....	63
4.1.4 Conformational statistics.....	63
4.1.5 Cohesive energy and solubility parameter.....	65
4.1.6 Coarse-grained structures.....	66
4.1.7 Radial distribution function.....	67
4.2 Monte Carlo simulation : Effect of chain stiffness on the free surface of polymers.....	70
4.2.1 Equilibration.....	70
4.2.2 Density profiles.....	72
4.2.3 Bond orientation.....	79
4.2.4 Molecular properties.....	80
4.2.5 Molecular orientation.....	83
4.2.6 Energetics.....	84
4.3 The effect of intermolecular interaction on Polymer crystallization..	86
4.3.1 Equilibration.....	86
4.3.2 Conformation.....	92

CONTENTS (Continued)

	Page
4.3.3 Chain dimension.....	94
4.3.4 Chain orientation.....	95
4.3.5 Structural packing.....	100
4.4 Molecular dynamics (MD) simulation of detailed structures and ion transportation of polymerized ionic liquid/ionic liquid blends.....	102
4.4.1 Validated method for equilibration: PolyIL–IL Blends at 600K.....	102
4.4.2 Polymer dynamics: PolyIL–IL Blends.....	104
4.4.3 Radial Distribution Functions (RDF) and Coordination numbers (CN).....	112
4.4.4 Ion Transport Mechanisms	115
4.4.5 Glass Transition Temperatures (T _g) for PolyIL–IL Blends.....	117
4.4.6 Transference Numbers for PolyIL–IL Blends.....	120
4.4.7 The ideal ionic conductivity in PolyIL-IL Blends.....	123
4.4.8 Ion Transport Events in PolyIL-IL Blends at 600 K.....	127
V CONCLUSION.....	131
REFERENCES.....	134
APPENDICES.....	153
APPENDIX A THESIS OUTPUT (PUBLICATIONS).....	154
APPENDIX B INTERNATIONAL CONFERENCE I.....	155
APPENDIX C INTERNATIONAL CONFERENCE II.....	156
CURRICULUM VITAE.....	157

LIST OF TABLES

Table	Page
3.1 The characteristics ratio and probability of the conformational states with different chain stiffness parameters at 473 K.....	41
3.2 Composition details of PolyIL-IL blend electrolytes with varying ILs loadings.....	49
3.3 Box size, density (ρ), radius of gyration (R_g), and average end to end distance (R_{ee}) of PolyIL-IL Blend Electrolytes with Varying ILs Loadings.....	50
4.1.1 Conformational energies of 2,4-dichloroethane (DCE) and 2,4-difluoroethane (DFE).....	56
4.1.2 Statistical weights parameter of various RIS models for PVC.....	57
4.1.3 Statistical weights parameter of various RIS models for PVF.....	57
4.1.4 Comparison of the characteristic ratio of PVC and PVF determined by experiment and RIS calculation.....	60
4.1.5 Molecular dimension and chain mobility.....	63
4.1.6 Torsional angle distribution of PVC and PVF models.....	65
4.2.1 Parameters of polymer surfaces.....	74
4.2.2 Chain dimension and shape parameters.....	81
4.4.1 The absolute displacement (in 500 ps increments) of ILs, PolyILs and PolyIL-IL blends.....	112
4.4.2 Comparison between the total ionic conductivity from the experiment and the ideal ionic conductivity from MD simulation of PolyIL-ILs blend systems at different temperatures.....	125

LIST OF FIGURES

Figure	Page
2.1	10
<p>The characteristic ratios, ($C_n = \langle r^2 \rangle_0 / n l^2$), and dipole moment ratio, ($C_m = \langle m^2 \rangle_0 / n m^2$), for PVC chains with Bernoullian tacticity and a probability for a repeating diad P_r (equivalent to the probability of <i>meso</i> diad).....</p>	
2.2	12
<p>Characteristic interactions of PVF.....</p>	
2.3	18
<p>Schematic presentation of two possible mechanisms of ion transport in polymers: the liquid-like (lower left) requires the motion of the polymer segment and depends on the rate of segmental relaxation, whereas the solid-like (lower right) is based on ion jumps over an energy barrier in the frozen (on the time scale of ion jumps) polymer matrix.....</p>	
2.4	20
<p>Specific viscosity as a function of the concentration of Bmim-TFSI for PC₄-TFSI solutions at $c_p = 4.0 \times 10^{-2}$ M. The values of η_{sp} via a bulk shear rheometer (ARES-G2; open circles), a microfluidic-based rheometer (m-VROC; open diamonds), and a gravity-driven capillary viscometer (Ubbelohde; filled circles) are compared. Blue solid and red dashed curves represent the scaling prediction of η_{sp} for semidilute unentangled (SUF) and DF* solutions, respectively.....</p>	
3.1	34
<p>Schematic representation of three numbered steps in a MC simulation on a high coordination lattice that replaces a simulation of the fully atomistic system in a continuous space.....</p>	
3.2	35
<p>Graphical demonstration of how a tetrahedral lattice can be converted into a <i>2nd</i> lattice.....</p>	

LIST OF FIGURES (Continued)

Figure	Page
3.3 NMR spectra of Bvim-TFSI	47
3.4 The definition of the mean squared displacement (MSD) and Diffusion coefficient (D).....	51
4.1.1 Newman projections of the t , g^+ and g^- conformations of the C-CH ₂ CH(Cl)-C and C-CH ₂ CH(F)-C three-bond sequences.....	54
4.1.2 The representative conformation and statistical weight matrices of the second order interaction for PVC and PVC chains with the LL configuration of 2,4-dichloropentane (DCP) and 2,4-difluoropentane (DFP).....	55
4.1.3 (a) Characteristics ratio and (b) dipole moment ratio for PVC and PVF chains based on statistical weight matrices determined in this work.....	59
4.1.4 (a) Orientation autocorrelation function (OACF) of the end-to-end vectors (b) the mean-square displacement (MSD) for the chain center of mass and (c) the MSDs of the individual monomer from MC simulation of bulk PVC and PVF at 600 K.....	62
4.1.5 Example of the snapshot of coarse-grained and fully atomistic models of atactic PVC (above) and PVF (below) at their bulk densities.....	62
4.1.6 Distribution of the backbone torsional angles for amorphous (a) <i>a</i> PVC and (b) <i>a</i> PVF bulks from the reverse-mapping structures before and after energy minimization.....	64
4.1.7 The intermolecular pair correlation function from MC simulation of the coarse-grained PVC and PVF bulk structures at 600 K.....	67

LIST OF FIGURES (Continued)

Figure	Page
4.1.8 (a) intermolecular RDF of all carbon backbone atoms (b) intermolecular RDF of methine (CH) and methylene (CH ₂) carbons and (c) Intermolecular RDFs of Cl...Cl, and F...F atom pairs from the fully atomistic models of amorphous structures.....	69
4.2.1 (a) the OACFs of the chain end-to-end vectors, (b) the MSDs of the chain center of mass, and (c) the MSDs of the individual monomer of polyethylene-like models.....	71
4.2.2 Representative structures of the free surfaces of polymer melt with different degrees of chain stiffness, $k = 0.0$ (top), 1.0 (middle), and 2.0 (bottom).....	73
4.2.3 Density profiles of melt-vacuum surfaces of polymer with different chain stiffness as a function of the displacement from the center of structures.....	74
4.2.4 (a) Distribution of chain center of mass and (b) the corresponding cumulative profiles of polymer surfaces.....	77
4.2.5 (a) Relative end-monomer and (b) middle-monomer densities of the free surface of polymer melts at different positions in the structures.....	78
4.2.6 The order parameter of (a) middle-bonds and (b) end-bonds of the free surface of polymer melts.....	80
4.2.7 The components of the mean-squared radius of gyration in (a) the parallel (XY) and (b) the perpendicular (Z) direction to the surface and (c) the first and the third principal axes of polymer molecules.....	82
4.2.8 The chain order parameter of (a) the first and (b) the third principal axes of polymer chains.....	84

LIST OF FIGURES (Continued)

Figure	Page
4.2.9 The profiles of (a) intramolecular and (b) intermolecular energies at different positions in polymer surfaces.....	85
4.3.1 (a) Intramolecular energies (E_{intra}) and (b) intermolecular energies (E_{inter}), of <i>PE-like</i> chains with different intermolecular interactions.....	87
4.3.2 (a) The OACFs of the chain end-to-end vectors (b) the MSDs of the chain center of mass and (c) the MSDs of individual CG beads of PE-like models with different intermolecular interactions at 298 K.....	90
4.3.3 The final structures after 100 million MCS trajectories at 298 K of PE-like models with different intermolecular interactions (a) E125, (b) E 145 (c) E165 (d) E185 and (d) E205 systems.....	92
4.3.4 The fraction of trans conformation of PE-like models with different intermolecular interactions.....	94
4.3.5 The mean square radius of gyration of PE-like models with different intermolecular interactions.....	96
4.3.6 The global order parameter for PE-like models with different intermolecular interactions.....	96
4.3.7 The intramolecular bond orientation correlation functions for PE-like models with different intermolecular interactions.....	99
4.3.8 The correlation function of intermolecular bond orientation for <i>PE-like</i> models with different intermolecular interactions.....	99
4.3.9 The intermolecular pair correlation function for the <i>PE-like</i> models with different intermolecular interactions.....	101
4.4.1 Time evolution of potential energy (left) and density (right).....	102

LIST OF FIGURES (Continued)

Figure	Page
4.4.2 Time evolution of the radius of gyration (R_g) for IL, PolyIL and PolyIL-IL blends from the 110 ns equilibration runs. The dashed lines indicate the equilibration time of the R_g	103
4.4.3 The initial [non-equilibrium] : (a), (b) and (c) and final structures [equilibrium] : (d), (e) and (f) at 600 K.....	104
4.4.4 The mean-square displacement for the center of mass of (a) PolyIL-IL blends, (b) Bmim ⁺ cation, (c) TFSI ⁻ anion and (d) Pbvim ⁺ (polycation).....	105
4.4.5 The Diffusion coefficient of (a) PolyIL-IL blends, (b) Bmim ⁺ cation, (c) TFSI ⁻ anion and (d) Comparisons between PolyIL, PolyIL-IL blends and IL, respectively.....	106
4.4.6 The Diffusion coefficient of (a) TFSI ⁻ , (b) Bmim ⁺ ions in polyIL-IL blends as a function of IL concentrations at different temperatures. In the figure, D_0 is the respective value obtained for pure ILs. (c) TFSI ⁻ and (d) Bmim ⁺ ions in polyIL-IL blends as a function of T/T_g at different IL concentrations.....	108
4.4.7 (a) The Orientational autocorrelation functions and (b) KWW fitting of PolyIL-IL blends in various IL concentrations. Corresponding KWW relaxation times (τ_{KWW}) for each system.....	109
4.4.8 The Trajectories of Bmim ⁺ , TFSI ⁻ and Pbvim ⁺ recorded every 500 ps...	111
4.4.9 The absolute displacement of ILs system (a) Bmim ⁺ and (b) TFSI ⁻ every 500 ps interval.....	111
4.4.10 The absolute displacement of PolyILs system (a) Pbvim ⁺ and (b) TFSI ⁻ every 500 ps interval.....	111

LIST OF FIGURES (Continued)

Figure	Page
4.4.11 The absolute displacement of PolyIL-IL system (a) Pbvim ⁺ and (b) Bmim ⁺ and (c) TFSI ⁻ every 500 ps interval. Give an example (at ILs conc = 0.4) of a blend system from all systems.....	112
4.4.12 Radial distribution function between (a) the centers of mass for Pbvim ⁺ , TFSI ⁻ and Bmim ⁺ and (b) Coordination numbers (CN) at 600 K.....	113
4.4.13 Radial distribution function between (a) the centers of mass for PolyILs, (b) PolyIL-IL blends and (c) ILs at different temperatures.....	114
4.4.14 Coordination numbers (CN), (a) for PolyILs, ILs at different IL concentrations and (b) for PolyILs, ILs at different temperatures.....	114
4.4.15 Probability that a given TFSI ⁻ is associated with (a) n cations and (b) N polymer chains. The error bars are smaller than the size of the symbol where invisible.....	116
4.4.16 A snapshot of anion (magenta) association to polymerized cations and polymer chains in (a) PolyIL and (b) PolyIL-IL blends. The represent an ion-association determined from a distance cutoff of 6.5 Å. Only the polymer chains within 20 Å spherical radius from the centered anion are shown without any other ions for clarity.....	117
4.4.17 Plots of specific volume versus temperature to determine T _g values for various IL concentrations of blend systems.....	120
4.4.18 (a) T _g from experiment and (b) Comparison (Exp.& Sim.) of Glass Transition Temperatures (T _g).....	120

LIST OF FIGURES (Continued)

Figure	Page
4.4.19 a) the anions and (b) cations transference number as a function of the ILs loading at different temperatures.....	122
4.4.20 The comparison of the anions and cations transference number as a function of the ILs loading at different temperatures.....	122
4.4.21 The ideal ionic conductivity of PolyIL-ILs blend systems obtained as plotted versus 1000/T (a) Total ionic conductivity from experiment, (b) Total of systems, (c) Bmim ⁺ and (d) TFSI ⁻ for ideal ionic conductivity from MD simulation.....	124
4.4.22 The Nernst-Einstein predictions a function of the loading of ILs for (a) system, (b) TFSI ⁻ and (c) Bmim ⁺ as a function of T/T _g	126
4.4.23 Definition of ion hopping mechanisms adopted in this work to distinguish different types of ion hopping events in polyIL-IL blend electrolytes from Mogurampelly et al. The transition events are categorized into three types to represent (a) intrachain, (b) interchain, and (c) the to and from polymer chain hopping events.....	129
4.4.24 Fraction of transition rate of different hopping types as a function of pure ILs loading at 600K (a) Experimental result from (Inoue, 2013) (b) Result from MD simulation and (c) Individual result from MD simulation.....	130

LIST OF ABBREVIATIONS

RIS	Rotational isomeric state
MC	Monte Carlo
PVF	Poly(vinyl fluoride)
PVC	Poly(vinyl chloride)
$2nd$	Second nearest neighbor diamond lattice
PE	Polyethylene
k	Chain stiffness parameter
SPEs	Solid polymer electrolytes
PEO	Poly(ethylene oxide)
S	Siemen
cm	Centimeter
ILs	Ionic liquids
PILs	Polymer ionic liquids
MD	Molecular dynamic
Bmim-TFSI	1-butyl-3-methylimidazolium bis(trifluoromethanesulfonyl)imide
Pbvim-TFSI	Poly(1-butyl-3-vinylimidazolium bis(trifluoromethanesulfonyl)imide
GPEs	Gel polymer electrolytes
P_m	Probability for a meso
m	<i>Diads</i>
r	<i>Racemo</i>
$^{\circ}\text{C}$	Degree Celsius
$\langle r^2 \rangle_0$	Mean-square unperturbed end-to end distance
C_n	Characteristic ratio
U	Statistical weight matrices
g^+	Gauche plus
g^-	Gauche minus

LIST OF ABBREVIATIONS (Continued)

t	<i>trans</i>
C_m	Dipole moment ratio
LJ	Lennard–Jones energy
B_2	Second virial coefficient
ε	Potential well depth
σ	Ionic conductivity
Br^-	Bromide ion
BF_4^-	Boron fluoride
PF_6^-	Hexafluorophosphate
Tf_2N^-	Bis(trifluoromethane)sulfonimide
Å	Angstroms
MCS	Monte Carlo Step
K	Kelvin
PCFF	Polymer consistent force-field
NVT	Canonical ensemble
NPT	Isobaric-isothermal ensemble
NMR	Nuclear magnetic resonance spectroscopy
T_g	Glass transition temperature
OPLS-AA	Optimized potentials for liquid simulations-all atom
R_g	Radius of gyration
R_{ee}	Average end-to-end distance
MSD	Mean squared displacement
D	Diffusion coefficient
ACF	Orientational autocorrelation functions
RDF	Radial Distribution Functions
CN	Coordination Number
PCF	Pair correlation function
S_b	Bond order parameter

LIST OF ABBREVIATIONS (Continued)

$\langle r^2 \rangle^{1/2}$	Mean square end-to-end vector
$\langle s^2 \rangle^{1/2}$	Mean square radius of gyration
S_G	Orientation order parameter of polymer chains
$M_1(j)$	First-order intramolecular bond order parameter
S_L	Intermolecular bond orientation order



CHAPTER I

INTRODUCTION

There has long been interest in the development of lithium-ion batteries for more efficiency and safety with potential usage in various applications. From the beginning, these batteries are composed of organic liquid electrolytes with high ionic conductivity. However, liquid electrolytes usually have low thermal stability, high flammability, toxic, restrictive electrochemical stability window, and no hindrance to dendrite expansion. The major challenge to these problems is to achieve a long battery life (charge-discharge cycle) with high conductivity (Tarascon, 2001; Quartarone, 2011; Manthiram, 2017).

Molecular simulations at fully atomistic scale of polymeric materials have been developed since 1980s to investigate molecular and material properties (Kotelyanskii, 2004). Most early works had been focused on synthetic polymers with structurally simple and nonpolar polyolefins. The earlier methods were often simplified by the models such as "united" atoms to reduce the computational cost. A method to generate amorphous polymeric materials at fully atomistic scale was first reported for atactic polypropylene glasses (Theodorou, 1985). In general, atomistic simulation of polymeric materials requires accurate conformational statistics for generation of initial guess structure and readily equilibration afterward. Thus, the crucial step for polymer simulations is to find a way to generate the realistic molecular model especially for chain conformation and interatomic correlation function.

The rotational isomeric state (RIS) models of PVF and PVC had been derived from ab initio electronic structure calculation. The RIS calculation predicted a higher chain stiffness (larger characteristic ratio) for PVC than PVF chain at all meso diad content. PVF and PVC chains were then coarse-grained by grouping each monomer unit into one bead and mapped onto the second nearest diamond (2nd) lattice. The fully atomistic models of amorphous PVF and PVC structures can be obtained through

the reverse-mapping procedure to restore the missing atoms followed by energy minimization. To validate these atomistic models, some molecular and material properties of amorphous structures were determined and compared with experimental data including conformational statistics, solubility parameters and the static structure factor.

Polymer surface is an essential part of various technological applications (Feast, 1987). Their importance covers many issues in designing high-performance materials including wettability and contact angle, interactions and reactions at surfaces, tribology, adhesion and adsorption, and surface modification (Mittal 1 and 2, 1983). There have been numerous past studies on the structures and properties of polymer surfaces (Garbassi, 1994) and a better understanding should provide the great capacity to alter the chemical structure of polymer chains to improve surface properties to meet specific purposes (Stamm, 1992). Properties of polymers near the surfaces can be remarkably different from the bulk structures including local density, conformation, chain size/shape, and bond/chain orientation which can be varied at different positions from the surface (Forrest, 1992). The role of chain stiffness on structural and molecular properties for the free surface of polymer melts was examined by Monte Carlo (MC) simulations of the coarse-grained (CG) polyethylene-like chains on the second nearest neighbor diamond (2nd) lattice. Polyethylene-like model by multiplying the statistical weights with the chain stiffness parameter (k) to represent more flexible ($k = 0.0$ and 0.5) and stiffer ($k = 1.5$ and $k = 2.0$) chains than normal polyethylene ($k = 1.0$). For the melt-vacuum surfaces of stiffer chains, bulk densities become lower with broader surface profiles. For more flexible chains, monomers at the end/middle position are more segregated/depleted near the surface. The chain stiffness arising from barriers to bond rotation and structural constraints are closely related to the macroscopic properties of polymers. For computer simulation, the degree of local flexibility can be adjusted by manipulating the intramolecular energetics can affect the molecular and structural properties of polymer surfaces. In principle, the simulation of fully atomistic models should provide the most detailed information as one can consider the specific chemistry of polymer chains.

The first SPE was reported in the 1970s using poly (ethylene oxide), PEO (Fenton, 1973; Wright, 1975). For ionic conductivity in alkali metal-PEO complexes, it has been proposed that metal ions work as charge carriers in the non-crystalline phase of the polymer host. Ionic diffusion occurs through the formation and dissociation of the coordination structure between cations and oxygen atoms in PEO (Ratner, 1988). The disadvantage of PEO is a very low metal ion transportation caused by the crystallization and trapping effects due to the strong coordination between the PEO backbone and metal ions (Capiglia, 1999; Zhang, 2014; Itoh, 2017;). In addition, the poor mechanical, thermal stability and semi-crystalline property of PEO reduce its efficiency as SPEs. Although inorganic salt can be dissolved well in PEO, the ionic conductivity of SPEs is 10^{-8} - 10^{-5} Scm^{-1} , still lower than 10^{-3} Scm^{-1} for practical applications.

Therefore, the role of the intermolecular interaction related to the chain packing in the condensed phase, which can be intimately associated with polymer crystallization. The role of the intermolecular interaction related to the chain packing in the condensed phase, which can be intimately associated with polymer crystallization. Monte Carlo (MC) simulations of coarse-grained (CG) polyethylene (PE)-like models with different non-bonded interaction parameters between monomer beads were proposed to study the effect of intermolecular interaction on polymer crystallization from the molten state. It is also very important for technological application because more than 60% of industrial polymers are semi-crystalline materials and their functional properties are closely connected with polymer morphologies. Crystallization of flexible chains, with many intrinsic bond conformations, contains complex dynamics over broad lengths and time scales, spanning from large-amplitude molecular motions to atomic-scale rearrangements to optimize crystal order.

Polymer electrolytes are an attractive option to substitute liquid solutions due to their thermal stability and high flexibility (Hallinan, 2013). Polymer electrolytes can be divided into two groups: solid and gel electrolytes. Solid polymer electrolytes (SPEs) are electrolytes in which alkali salts can be dissolved in the appropriate polymers. The host polymers play a role in the diffusion of alkali ions through the local movement

of chain segments. The first SPE was reported in the 1970s using poly (ethylene oxide), PEO (Fenton, 1973; Wright, 1975).

Ionic liquids (ILs) have been studied as solvents for polymerization reactions. Most recently, ILs have been shown to be good solvents for radical polymerizations due to their superior properties compared to conventional liquid electrolytes, are organic salts in the liquid state at room temperature. ILs contain cations and anions with low melting temperatures and exhibit high ionic conductivity with good electrochemical stability (Holbrey, 1999; Olivier-Bourbigou, 2010; Lei, 2017). Polymer-in-salt gel membranes have been prepared straightly by polymerization of vinyl monomers in ILs and by polymerization of ILs integrating polymerizable functions. It looked like a formation of IL-polymer gels, such as are explained by Watanabe and Mizumura (Watanabe, 1996), resulting from the plasticizing effects of the IL on the polymer matrix. The togetherness of some ILs with polymers can be advantageous in polymer processing to build plasticized materials. ILs are capable of holding imidazolium or pyridinium cations are identical to some conventional plasticizers, containing an aromatic core and pendant alkyl groups (Cadogan, 2000; Ohno, 2001). Other advantages of ILs depend on their non-flammability and non-volatility which are good for battery applications (Correia, 2018).

The so-called polymer ionic liquids (PILs) are a new subtype of polymer electrolytes that have advantageous properties over simple ionic liquids, such as non-flammability, wide electrochemical windows. and chemical stability. Therefore, it can be used as a promising material for the next generation solid-state battery (Ohno, 2001; Mecerreyes, 2011; Sangoro, 2014; Qian, 2017; Forsyth, 2019; Zhang, 2020). PILs contain charged groups with an ionic liquid structure in the main and/or side chains, which is weakly coordinated with opposite charges counterions. One of the major challenges for the application of polymers such as PIL as electrolytes is to create highly conductive while maintaining strong mechanical properties (Shaplov, 2018; Rochow, 2020; Yoshizawa-Fujita, 2021). Consequently, understanding the structures and dynamics of PILs and counter ions with their correlations is necessary in designing PIL-based materials with better performance.

1.1 Research objectives

- 1.1.1 To describe the conformational statistics and determine the conformational-dependent properties of vinyl polymer chains using the refined rotational isomeric state (RIS) model based on quantum chemistry calculation.
- 1.1.2 To generate the atomistic models and to predict material properties of amorphous structures of vinyl polymers and polymerized ionic liquids.
- 1.1.3 To investigate the role of chain stiffness effect and intermolecular interaction on surface properties and crystallization by Monte Carlo (MC) simulation of polyethylene-like model
- 1.1.4 To gain more understanding about the structure and property relationship of polymerized ionic liquids based on both experiments and molecular dynamic (MD) simulation.

1.2 Scope and limitation

1.2.1 Molecular simulation

- 1.2.1.1 **Quantum Chemistry:** for more accurate calculation of the optimized structure and conformational energies of two vinyl polymers (polyvinyl fluoride, PVF and polyvinyl chloride, PVC).
- 1.2.1.2 **Rotation Isomeric State (RIS) model** for the description of conformational statistics of two vinyl polymers (PVF and PVC). The statistical weights will be refined using quantum chemistry calculation and will be used in the Monte Carlo simulation for the multichain system at the bulk state.
- 1.2.1.3 **Monte Carlo (MC) simulation**
 - For the initial generation and equilibration of amorphous bulk structures of two vinyl polymers (PVF and PVC). Fully atomistic models can be recovered by the reverse-mapping procedure to restore all atoms followed by geometry optimization using the forcefield-based method.

- Coarse-grained “Polyethylene (PE) - like” models on the second nearest neighbor diamond (2nd) lattice with the chain stiffness parameter (k) to represent more flexible ($k = 0.0$ and 0.5) and stiffer ($k = 1.5$ and $k = 2.0$) chains than normal PE ($k = 1.0$). And the role of the intermolecular interaction related to the chain packing in the condensed phase, which can study the effect of intermolecular interaction on polymer crystallization from the molten state.

1.2.1.4 Molecular Dynamic (MD) simulation to determine the structures and dynamics of polymerized ionic liquids at the atomic scale. This MD technique may be able to give insight about the underlying mechanism of ion mobility and the estimation of theoretical diffusion coefficients of ionic species.

1.2.2 Experiments

In this research is studied to work on both molecular dynamics simulations and experimental studies of polymerized ionic liquids (Pbvim-TFSI) and polymerized ionic liquids-ionic liquids blends (PbvimTFSI-BmimTFSI). Identification transport effects of such blends and consequently specify the feature by which conductivity can be tuned by the addition of pure ILs to polyOLs. Particularly interesting feature is whether the phenomena of “decoupling” from mechanical properties of transport properties monitored in polyIL systems also broaden to their blends with ILs. And to diagnose the mechanisms underlying ion transport of polyIL–pure IL blends. A final purpose underlying our study was to deliberate the conductivity and transference number characteristics of polyIL–pure IL blends and attempt to comprehend the dependence of each property on the blending proportions.

CHAPTER II

LITERATURE REVIEWS

2.1 Multiscale molecular simulations of two polymer hosts for gel electrolytes: poly(vinyl chloride) and poly(vinyl fluoride)

Polymer electrolytes are an attractive option to substitute liquid solutions due to their thermal stability and high flexibility (Daniel, 2013). Polymer electrolytes can be divided into two groups: solid and gel electrolytes. Solid polymer electrolytes (SPEs) are electrolytes in which alkali salts can be dissolved in the appropriate polymers. The host polymers play a role in the diffusion of alkali ions through the local movement of chain segments. The first SPE was reported in the 1970s using poly (ethylene oxide), PEO (Fenton, 1973; Wright, 1975). For ionic conductivity in alkali metal-PEO complexes, it has been proposed that metal ions work as charge carriers in the non-crystalline phase of the polymer host. Ionic diffusion occurs through the formation and dissociation of the coordination structure between cations and oxygen atoms in PEO (Ratner, 1988). The disadvantage of PEO is a very low metal ion transportation caused by the crystallization and trapping effects due to the strong coordination between the PEO backbone and metal ions (Capiglia, 1999; Zhang, 2014; Itoh, 2017).

Compared to SPEs, gel polymer electrolytes (GPEs) have higher ionic conductivity with good interfacial and mechanical properties due to the liquid phase and solid component. The electrolyte in the liquid state is immobilized in the polymeric matrix and forms the gel phase. GPEs could combine advantages from both liquid and solid components. GPEs can be found in the form of either the heterogeneous (phase-separated) or the homogeneous (uniform) gel. Heterogeneous GPEs are composed of a polymer network with interconnected pores filled with liquid electrolytes.

The metal ions in heterogeneous GPEs can diffuse in the swollen-gelled phase. Most of GPEs exhibit higher ionic conductivity in the order of 10^{-3} Scm^{-1} at room temperature. Consequently, GPEs are one of the potential polymer electrolytes for the battery application with enhanced efficiency and safety.

2.1.1 Rotational isomeric state (RIS) model of PVC

The mean-square unperturbed dimensions of vinyl polymers frequently are dependent on strongly on stereochemical composition, as noted in the innumerable instances mentioned in the book on the rotational isomeric state model (Flory, 1969; Mattice, 1994; Rehahn, 1997). The unperturbed dimensions have usually been calculated as a function of P_m , the probability for a meso (m) diad, using the presupposition of Bernoullian statistics. This method brings averaging of the mean-square unperturbed dimensions through various chains many different at each p_m , $0 < p_m < 1$, to take into account sufficient randomness of the stereochemical sequence.

The construction of metal catalysts allows for better control over the stereochemical sequence of vinyl polymers. This handle can consist the installation of a stereochemically pure isotactic and syndiotactic polymers, in which the only *diads* are *m* or *racemo* (*r*), respectively. It might likewise consist forced synthesis of chains in which the primary duplicate for the stereochemical series expand an array prolonged than a single diad, e.g., *mr*, *mmr*, etc. This potential ability in synthesis forces curiosity in conjectured behaviour of chains in which the stereochemical orders consist of reiterations of a small thread of diads. This attention will help to identify the sequence that tends to provide the newest features and to explicate an understanding of the origination of tendencies in family effects chains with methodically related repeat units.

Poly(vinyl chloride) is a renowned atactic polymer. For decades, stereochemical compositions have been dealt with in a limited range by performing the polymerization at different temperatures. Bovey reports that p_m can vary from 0.37 (for polymerization at -78°C) to 0.46 (for polymerization at 100°C) (Bovey, 1967). Most of the commercial materials are in this range. Pay attention to the use of vinyl chloride in the preparation of polymers with different properties from those of the usual *atactic* material, it's worth it to question which repeating stereochemical series,

apart from that of the pure isotactic and pure syndiotactic polymer, could perform variously than before atactic structure. An uncomplicated consideration for each a series is to calculate the mean square dimension for conventional atactic chains.

Determining of the mean-square unperturbed end-to end distance, $\langle r^2 \rangle_0$, use the classic rotational isomeric state model for the partition of configurations in chains unperturbed by long-range interactions. The values of $\langle r^2 \rangle_0$ are transformed to the characteristic ratio, C_n ,

$$C_n = \frac{\langle r^2 \rangle_0}{nl^2} \quad (2.1)$$

where n denotes the number of C-C bonds of length l .

Three rotational isomeric states are employed for such internal bond. First- and second-order interactions are employed in the 3×3 statistical weight matrices, U . In the description of the chain with m and r diads (Flory, 1974), the statistical weight matrix for the C^a-C bond is

$$U_p = \begin{bmatrix} 1 & 1 & 1 \\ 1 & 0 & 1 \\ 1 & 1 & 0 \end{bmatrix} \quad (2.2)$$

where C^a denotes the carbon atom bearing a chlorine atom. The matrix for the next bond, which accomplishes the diad, is either U_m or U_r ,

$$U_m = \begin{bmatrix} \eta^2 \omega_{xx} & \eta & \eta \tau \omega_x \\ \eta & \omega & \tau \omega_x \\ \tau \eta \omega_x & \tau \omega_x & \tau^2 \omega \omega_{xx} \end{bmatrix} \quad (2.3)$$

$$U_r = \begin{bmatrix} \eta^2 & \eta \omega_x & \eta \tau \omega_{xx} \\ \eta \omega_x & 1 & \tau \omega \\ \eta \tau \omega_{xx} & \tau \omega & \tau^2 \omega_x^2 \end{bmatrix} \quad (2.4)$$

depending on whether the *diad* is m or r . Rows and columns are indexed in the order $t, g+, g-$ (Flory, 1974), with columns indexing the states of the present bond and rows indexing the states of its ancestor.

Equitably, the chain can be described along with d, l pseudo-asymmetric centers and statistical weight matrices defined by

$$U_p = Q U d = U_l Q$$

$$U_m = U_{dd} Q = Q U_{ll}$$

$$Ur = U_{dl} = QU_{ld}Q$$

The statistical weights showing in the matrices are for first-order interactions in the t and $g+$ states (η and τ , respectively) and second-order interactions between two carbon atoms in the backbone, between a carbon atom and a chlorine atom, and between two chlorine atoms (ω , ω_X , and ω_{XX} , respectively).

The geometry and statistical weights are intimately related to those described recently by Smith et al. (Smith, 1995). The bond angles are 112° and 116° for $\angle C-C^a-C$ and $\angle C^a-C-C^a$, respectively. Within a dd (ll) *diad*, the torsion angles are -178° (178°), 61° (60°), -60° (-61°) at the C^a-C bond and 178° (-178°), 60° (61°), -61° (-60°) at the $C-C^a$ bond, both given in the sequence t , $g+$, $g-$. Within a dl (ld) *diad*, these torsion angles are 175° (-175°), 66° (62°), -62° (-66°) at the C^a-C bond and at the $C-C^a$ bond. The statistical weights were calculated as Boltzmann factors, using the energies $E_\eta = -0.9$, $E_\tau = -0.5$, $E_\omega = 3.0$, $E_{\omega_X} = 2.3$, and $E_{\omega_{XX}} = 4.0$, all expressed in kcal/mol. The temperature was 373 K. Calculations of C_n were performed using the program V2.RIS, for which the FORTRAN source code (Mattice, 1994).

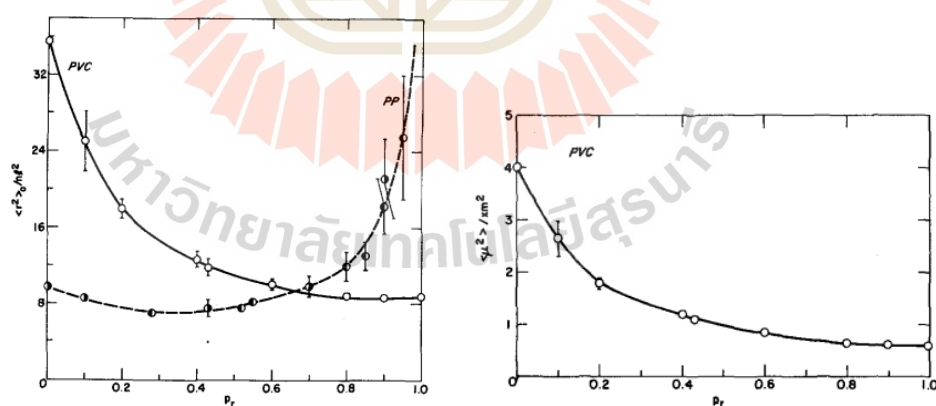


Figure 2.1 The characteristic ratios, ($C_n = \langle r^2 \rangle_0 / nl^2$), and dipole moment ratio, ($C_m = \langle m^2 \rangle_0 / nm^2$), for PVC chains with Bernoullian tacticity and a probability for a repeating diad p_r (equivalent to the probability of *meso* diad).

2.1.2 Rotational isomeric state (RIS) model of PVF

For example, the RIS model for vinyl- $[\text{CH}_2\text{-CH(X)}]_n$ - chains, where all bonds have 3-fold symmetry of their torsion potential with the nearest neighbor determined by a statistical weight matrix for consecutive C-C^α and $\text{C}^\alpha\text{-C}$ bonds. With the stereochemistry of pseudo-asymmetric centers, the statistical weight matrices for the $\text{C}^\alpha\text{-C}$ bond is

$$U_d = \begin{bmatrix} \eta & 1 & \tau \\ \eta & 1 & \tau\omega \\ \eta & \omega & \tau \end{bmatrix} \quad (2.5)$$

when the fluorine atom is attached to C^α with d configuration.

The statistical weight matrices for the C-C^α bonds depend on two successive pseudo-asymmetric centers as

$$U_{dd} = \begin{bmatrix} \eta\omega_{xx} & \tau\omega_x & 1 \\ \eta & \tau\omega_x & \omega \\ \eta\omega_x & \tau\omega\omega_{xx} & \omega_x \end{bmatrix} \quad (2.6)$$

$$U_{dl} = \begin{bmatrix} \eta & \omega_x & \tau\omega_{xx} \\ \eta\omega_x & 1 & \tau\omega \\ \eta\omega_{xx} & \omega & \tau\omega_x^2 \end{bmatrix} \quad (2.7)$$

For an l configuration, the statistical weight matrices for these bonds can be found by

$$U_l = QU_dQ, U_{ll} = QU_{dd}Q \text{ and } U_{ld} = QU_{dl}Q \quad (2.8)$$

where

$$Q = \begin{bmatrix} 1 & 0 & 0 \\ 0 & 0 & 1 \\ 0 & 1 & 0 \end{bmatrix}$$

In these statistical weight matrices, the rows and columns refer to the conformation of bonds $i-1$ and i , respectively. Three conformational states are t , $g+$, and $g-$, ordered in the matrices. The reference state corresponds to the conformation with $\text{CH}\dots\text{CH}_3$ arrangement. The first-order energy E_η is defined for the bond conformation with $\text{CH}\dots\text{F}$ interaction but no $\text{CH}\dots\text{CH}_3$ interaction, while a conformation resulting in both a $\text{CH}\dots\text{F}$ and $\text{CH}\dots\text{CH}_3$ interaction is another first-order energy E_τ . In addition, E_ω , E_{ω_x} and $E_{\omega_{xx}}$ are the energy of the second-order $\text{CH}_3\dots\text{CH}_3$,

$\text{CH}_3 \dots \text{F}$ and $\text{F} \dots \text{F}$ pentane-type interaction, respectively. For PVF, E_{wp} is the energy for $\text{F} \dots \text{F}$ interaction when the chain has W conformation.

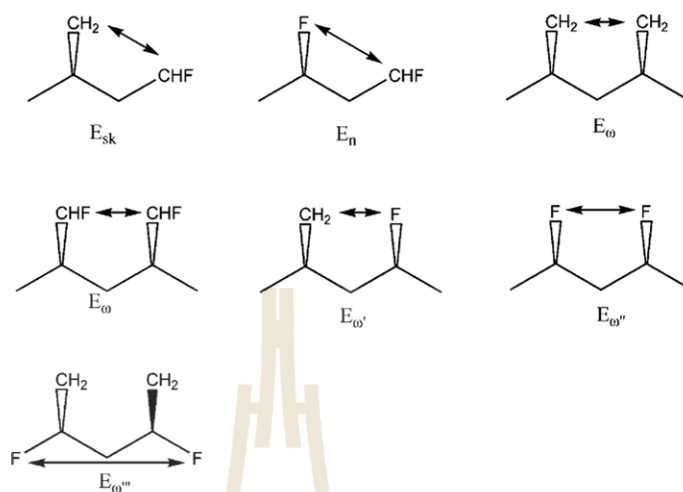


Figure 2.2 Characteristic interactions of PVF.

The main purpose of this work is to examine structures, dynamics and material properties of amorphous PVC and PVF at the bulk density by multiscale simulation technique. In general, this method consists of four steps: (i) determination for statistical weights for conformational statistics of PVC and PVF chains based on quantum chemistry calculation (ii) mapping of an atomistic PVC or PVF chains to the coarse-grained representation on the $2nd$ lattice, (iii) performing MC simulations on the $2nd$ lattice, and (iv) reverse mapping of selected snapshots from the $2nd$ lattice back to fully atomistic models. Many examples of this simulation have been performed during many years ago inclusive homogeneous polymers and their mixtures such as polyethylene, poly(ethylene oxide), polypropylene, polystyrene and polyvinyl alcohol (Cho, 1997; Doruker, 1997 and 1999; Haliloglu, 1998; Clancy, 2000; Jang, 2000; Vao-soongnern, 2000, 2001, 2004, 2006, 2010 and 2014; Akten, 2001; Xu, 2002 and 2003; Choi, 2004; Rane, 2004 and 2005; Dionne, 2005 and 2006; De la Rosa, 2002). In this work, we employ the coarse-grained model to investigate the structures and dynamics of bulk α PVC and α PVF melts. In addition, the fully atomistic models can be obtained from the reverse-mapping procedure to determine their material properties. The main focus is to validate the simulation method for the specific polymer with a comparison

to the prediction from theory and experimental results. This investigation is an extension of our recent published work on PVA and PS (Wichai, 2021; Kusinram, 2022).

2.2 Monte Carlo simulation : Effect of chain stiffness on the free surface of polymers

Most of these past studies have mostly limited to the surfaces of polymers with relatively flexible chains. It is of interest to see how the surface properties can be changed if polymer chains become more flexible or stiffer as chemical modification of polymers can give new molecules with different degrees of chain stiffness. For example, perfluoro-polymers usually exhibit stiffer chains compared to analog molecules such as polytetrafluoroethylene $-(CF_2CF_2)-$ vs polyethylene $-(CH_2CH_2)-$ (Smith, 1994).

The chain stiffness arising from barriers to bond rotation and structural constraints are closely related to the macroscopic properties of polymers. For computer simulation, the degree of local flexibility can be adjusted by manipulating the intramolecular energetics can affect the molecular and structural properties of polymer surfaces. In principle, the simulation of fully atomistic models should provide the most detailed information as one can consider the specific chemistry of polymer chains. Because of their long time and large length scales, polymer simulations at the atomistic level are normally restricted to rather small molecules with some degree of chain flexibility. Thus, one might question whether atomistic simulation to study polymer surfaces with different degrees of chain stiffness could be done properly. Sufficient equilibration of polymer systems should be confidentially ensured, for instance, the chain end-to-end vector of individual polymers should be fully uncorrelated with their initial orientation, and the mean square displacements for polymer chains should be larger than molecular dimension (Mansfield, 1990; Misra, 1995).

By resorting to coarse-grained (CG) models, the efficacy of polymer simulation can be improved. One approach is Monte Carlo (MC) simulations of CG models on the *2nd* lattice developed to investigate the free surface of polyethylene (PE) melts with different geometric confinements (Doruker, 1998; Baschnagel, 2000; Vao-soongnern,

2000 and 2001). The energetics of this simulation method are composed of the rotational isomeric state (RIS) model (Flory, 1969; Mattice, 1994) and the Lennard-Jones (LJ) energy function to describe the intra- and intermolecular interactions of polymer chains, respectively. Free surface models of PE melt (108 PE chains with the degree of polymerization = 50) can be effectively created and equilibrated by this MC simulation (Doruker, 1998). Subsequently, molecular, structural, and dynamic characteristics of the free surface of PE melts can be determined from these CG models. It is possible to extend this simulation method to incorporate the chain stiffness on polymer surfaces. The concept of the “polyethylene-like” model was recently proposed so that the effect of chain stiffness can be determined systematically on the free surfaces of polymer melts. Note that this MC method can be extended to generate the atomistic models as reported recently (Vao-soongnern, 2014; Wichai, 2021; Kusinram, 2022).

In this work, structural and molecular properties of the free surface of the polymer melt with different degrees of chain stiffness are investigated using *polyethylene-like* models. First, the important feature of modeling polymers with different chain stiffness is presented. The simulation method and the technique to generate polymer surfaces are described, followed by the results, discussion, and conclusion.

2.3 The effect of intermolecular interaction on polymer crystallization

Polymer crystallization is a relatively slow process, especially near the melting point, and often occurs by the kinetic-controlled mechanisms far from thermodynamic equilibrium (Yamamoto, 2009). Molecular simulations can be applied to rigorously monitor molecular mechanisms in these non-equilibrium states. Nevertheless, due to the very slow dynamics, computer simulation has long been beyond the scope of fully atomistic models to investigate polymer crystallization (Hu, 2005; Muthukumar, 2005; Luo, 2009). With new developments in calculation algorithms and the increasing power of computational resources, computer simulations can also be performed to examine the assumptions of theoretical models, predict experimental results, and suggest underlying microscopic details. Computer simulations have been used to understand

molecules in terms of issues including crystal formation, crystal-amorphous interfaces, temperature protocols, molecular weights, and bond stiffness (Ergoz, 1972; Mavrantza, 2001; Lavine, 2003; Gee, 2006; Koyama, 2008; Luo, 2011, 2013 and 2016; Piorkowska, 2013; Yi, 2013; Yamamoto, 2005 and 2014; Jabbari-Farouji, 2015; Nguyen, 2015; Ramos, 2015). Despite more advancements in computer hardware, realistic simulations of physical systems at the atomic scale are still difficult in practice. To solve this problem, molecular simulations of CG models have been developed to investigate polymer crystallization to cover a wider range of length and time scales (Fujiwara, 1997; Meyer, 2001 and 2002; Reith, 2001). For example, crystallization in dilute solution for polymers with varying chain rigidity, which has a strong influence on the folding kinetics of polymers in the crystal structure, has been studied by MC simulations (Chen, 1998).

The role of interaction potential energies or “*forcefield*” (FFs) for molecular models on the crystallization of PE melts has been studied by MD simulation (Yamamoto, 2013; Anwar, 2015; Luo, 2017; Xiao, 2017; Verho, 2018). It was found that FF parameters greatly influence the PE crystal growth rate, and several FF parameters have been proposed, such as the united atom (UA) model, which is widely used to study PE crystallization (Ramos, 2015). There are several reports on the polymer crystallization of a single long PE chain upon cooling from the melting temperature, (Kavassalis, 1993; Sundararajan, 1995; Fujiwara, 2001; Yamamoto, 2013). The pioneering investigation of these works using DREIDING UA FF (Mayo, 1990) was successful as it can promote the *trans* state in PE crystallization. For the original UA model with DREIDING FF, the LJ parameters of the CH₂ beads were treated by the averaged values from CH₄ and C parameters. However, it was reported a problem of too large fraction of the *trans* state with DREIDING-UA FF (Jabbari-Farouji, 2015). Several FF parameters were then proposed to improve the crystallization of PE by MD simulations of UA models, mostly for short alkanes (Rigby, 1987; Esselink, 1994; Paul, 1995; Harmandaris, 1998; Mavrantzas, 1998; Fujiwara, 1998 and 1999; Takeuchi, 1998; Koyama, 2002 and 2003; Waheed, 2002 and 2005; Ko, 2004; Yi, 2009 and 2011; Nicholson, 2016; Welch, 2017). In addition, simulations were also compared between UA and atomistic (AA) models to determine the chain folding of a single PE molecule (Li, 2010). The fraction of the *trans* state in PE crystal with the AA model was lower than in the UA model.

The folding behavior was impossible for UA FFs with $\sigma_{LJ} > \sigma$ (LJ diameter of CH_2) because the probability distribution of the torsion angle has no *gauche* minima. In addition, the atomistic united-atom representation of PE which was demonstrated, through Monte Carlo simulations, to provide very accurate predictions for the volumetric and size properties of PE chains under a wide variety of conditions, including temperature and average molecular weight (Karayiannis, 2002; Foteinopoulou, 2009; Anogiannakis, 2012).

Another lattice MC simulation of CG models has been proposed to investigate polymer crystallization from the melts (Baschnagel, 2000). Chains are represented by the rotational isomeric state (RIS) model to describe the short-range intramolecular interaction and the LJ potential energy to treat the long-range intermolecular interactions between CG beads (monomer units), respectively. This lattice-based MC method can be applied to simulate polymers with chemical details and the CG model can be reverse-mapped back to the fully atomistic structure (Wichai, 2021; Kusinram, 2022). Previously, this simulation technique has been employed to investigate PE crystallization in different situations such as nanofiber (Xu, 2002), nanoparticle (Vao-soongnern, 2004), cyclic vs linear chains (Jamornsuriya, 2022), mixed molecular weights (Vao-soongnern, 2023), and polymers with varied degrees of the chain stiffness (Sirirak, 2023). Generally, the long-range interaction among non-bonded units is obtained from the LJ interaction among ethylene units since each CG bead represents a repeating (CH_2CH_2) unit of PE. Because the LJ parameters for $-\text{CH}_2\text{CH}_2-$ as a portion of a long chain are unknown, it is suggested that the non-bonded LJ interaction parameters should be within the range of CH_2CH_2 but should not exceed those values for CH_3CH_3 . The LJ parameters determined from the viscosity data for $\text{CH}_2\text{CH}_2/\text{CH}_3\text{CH}_3$ molecules are $\sigma = 0.42/0.44$ nm and $\epsilon/k = 205/230$ K (Poling, 2002). Typically, two sets of LJ parameters were proposed by comparing bulk properties obtained from simulation to experimental data such as the cohesive energy *i.e.* set I ($\sigma = 0.44$ nm and $\epsilon/k = 185$ K) and set II: ($\sigma = 0.42$ nm and $\epsilon/k = 205$ K), used successfully to investigate structures and dynamics in the past simulations of PE melts (Cho, 1997).

Nevertheless, it was found that only the parameter set I ($\sigma = 0.44$ nm and $\epsilon/k = 185$ K) can be applied successfully to observe the crystallization upon cooling from

the melts while simulations with parameter set II give quite disordered structures with a low degree of chain orientation (a slightly different parameter set, $\sigma = 0.42$ nm and $\epsilon/k = 185$ K, was also applied and the structure formation can be observed clearly for PE crystallization). As the main difference in the LJ parameters between sets I and II is from the potential well depth (ϵ), the sensitivity of the intermolecular interaction on polymer crystallization from the molten state is explored here by MC simulation of CG *PE-like* models *i.e.* the same bead dimension ($\sigma = 0.44$ nm) but different potential well depth ($\epsilon/k = 125$ -205 K) for more repulsive and more attractive interactions compared to the normal PE chains.

2.4 Molecular dynamics (MD) simulation of detailed structures and ion transportation of polymerized ionic liquid/ionic liquid blends

PILs include charged groups with an ionic liquid structure in the main and/or side chains, which is weakly coordinated with opposite charges counterions. One of the major challenges for the application of polymers such as PIL as electrolytes is to create highly conductive while maintaining strong mechanical properties (Shaplov, 2018; Rochow, 2020; Yoshizawa-Fujita, 2021). Consequently, understanding the structures and dynamics of PILs and counter ions with their correlations is necessary in designing PIL-based materials with better performance. We employed molecular dynamics simulations to carry out ion mobilities and the molecular mechanisms of transport in blends of [poly(1-butyl-3-vinylimidazolium bis(trifluoromethanesulfonyl)imide): Pbvim-TFSI] electrolytes with [1-butyl-3-methylimidazolium bis(trifluoromethanesulfonyl)imide : Bmim-TFSI] ionic liquids.

2.4.1 Ionic conductivity in Experiment

The classical Nernst–Einstein (NE) equation relates the ionic conductivity to ion diffusion, D_i (Kremer, 2003):

$$\sigma = \frac{1}{kT} \sum_i n_i q_i^2 D_i \quad (2.9)$$

Where, n_i is the concentration and q_i is charge, of the free ions participation to conductivity.

In a clarified random walk estimation, indicating that the diffusion coefficient can be displayed over the average jump length λ_i and the rate of ion jumps $1/\tau_i$. It is

assumed that the ion diffusion reaches the Fickian regime after the first jump. We emphasize that $1/\tau_i$ is the obvious ion jump rate (Sangoro, 2011).

$$D_i \sim \lambda_i^2 / (6\tau_i) \quad (2.10)$$

2.4.1.1 Mechanisms of ionic conductivity in polymer electrolytes.

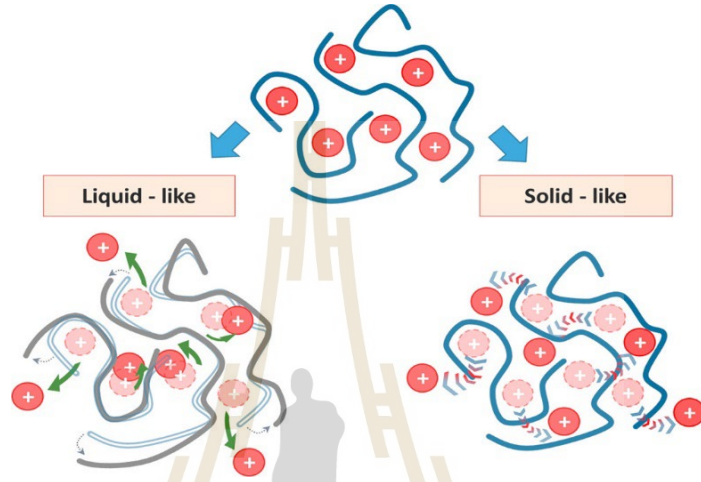


Figure 2.3 Schematic presentation of two possible mechanisms of ion transport in polymers: the liquid-like (lower left) requires the motion of the polymer segment and depends on the rate of segmental relaxation, whereas the solid-like (lower right) is based on ion jumps over an energy barrier in the frozen (on the time scale of ion jumps) polymer matrix (Bocharova, 2020).

2.4.1.1.1 Liquid-like Mechanism:

The first mechanism always reveals a Vogel–Fulcher–Tammann (VFT) temperature differentiation, following the temperature subordination of the structural relaxation and viscosity (Choi, 2014; Zhang, 2017; Kisliuk, 2019; Yao, 2019; Bocharova, 2020):

$$\sigma_i = \frac{A}{T} \exp\left[-\frac{E_a}{kT}\right] \quad (2.11)$$

Where, A refers to the pre-exponential factor, k is the rate constant, and E_a is the activation energy for conductivity.

Ion conductivity follows the VFT-like behavior at $T > T_g$ (Choi, 2014). Any interpolation of the polymers, and gathering of ions, lead the way an important improvement in T_g and decelerating of segmentary relaxation at ambient temperature.

As a consequence, using the liquid-like mechanism has fundamental restriction and unfeasible to produce the desired level of ionic conductivity in dry polymer electrolytes at ambient temperature. Powerful acceleration of polymer segmental dynamics can be brought to fruition by adding small molecular plasticizers.

2.4.1.1.2 Solid -like Mechanism:

This mechanism illustrates a vigorous decoupling of ion diffusion from structural relaxation in superionic systems. In this case, ion diffusion occurs in a principally frozen structure through the solid-like mechanism. Generally, ion jump motion and polymer chain relaxation and/or segmental motion together affect conductivity, so the ionic conductivity in SPEs is usually modeled by the VTF equations with non-linear relationship (Choi, 2014; Zhang, 2017; Kisluk, 2019; Yao, 2019; Bocharova, 2020):

$$\sigma_i = \sigma_0 T^{-\frac{1}{2}} \exp\left[-\frac{B}{T-T_0}\right] \quad (2.12)$$

where B is the pseudo-activation energy, σ_0 is the pre-exponential factor, and T_0 is the reference temperature. So, polymer electrolytes show an Arrhenius temperature dependence of conductivity at $T < T_g$ (Choi, 2014).

2.4.2 The charge screening on the viscoelastic properties and the conformation of polymerized ionic liquids (PILs) in ionic liquid (IL) solutions

Matsumoto et al. (Matsumoto, 2019), they conduct detailed rheological characterization of a model system containing a PIL [PC₄-TFSI: poly(1-butyl-3-vinylimidazolium bis(trifluoromethanesulfonyl)imide)] in a mixture of a salt-free solvent (DMF: dimethylformamide) and an ILs [Bmim-TFSI : 1-butyl-3-methylimidazolium bis(trifluoromethanesulfonyl)imide] solution, with low to high IL concentrations, while spanning dilute and semidilute polymer regimes.

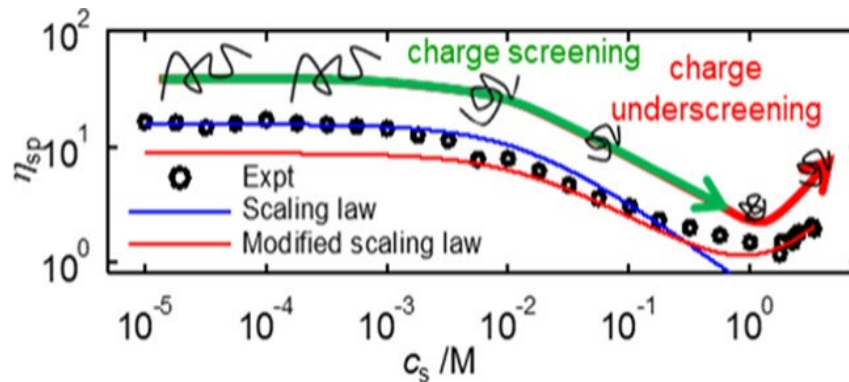


Figure 2.4 Specific viscosity as a function of the concentration of Bmim-TFSI for PC₄-TFSI solutions at $c_p = 4.0 \times 10^{-2}$ M. The values of η_{sp} via a bulk shear rheometer (ARES-G2; open circles), a microfluidic-based rheometer (m-VROC; open diamonds), and a gravity-driven capillary viscometer (Ubbelohde; filled circles) are compared. Blue solid and red dashed curves represent the scaling prediction of η_{sp} for semidilute unentangled (SUF) and DF* solutions, respectively.

They then studied the four different polymer concentrations ranging from $c_p = 8.0 \times 10^{-4}$ to 4.0×10^{-2} M, with the ionic liquid concentration $0 \text{ M} \leq c_s \leq 3.42 \text{ M}$. Specifically we identified three regions: (i) at low c_s , η_{sp} and λ , remained constant with increasing c_s ; (ii) at an intermediate c_s , η_{sp} and λ , decreased with increasing c_s ; (iii) at sufficiently high c_s , η_{sp} and λ , increased with increasing c_s . Regions (i) and (ii) were well described by the scaling laws of Dobrynin et al. (Dobrynin, 1995). for ordinary polyelectrolytes in a good solvent.

2.4.3 Molecular Dynamics (MD) Simulation of polymerized ionic liquids

Molecular dynamics (MD) simulation is the force field-constructed procession to investigate the trajectory of atomic movement followed by Newtonian equation of motion. The average values can be assessed using the statistical mechanic principles to link the microscopic trajectories to predict static and dynamic properties at the macroscopic level. The calculation for bond stretching and bending motion are quite taking very long time, as they have large force constants. Because the performance of current computer technology is not powerful enough, these two terms are generally fixed. Consequently, the properties of polymer usually depend on the other energetic terms: torsional energy and non-bond energies, as shown by:

$$E = E_{covalent} + E_{non-bond} \quad (2.13)$$

Where $E_{covalent} = E_{bond} + E_{angle} + E_{torsion} \quad (2.14)$

$$E_{non-bond} = E_{electrostatic} + E_{van\ der\ waals} \quad (2.15)$$

Molecular dynamic (MD) simulation is based on the statistical mechanic formalism that links the macroscopic properties of the bulk materials to their microscopic parameters. MD simulation generates a series of configurations as a function of “time”. Each of simulated system consists of the kinetic energy, potential energy, thermodynamic properties, and the structure at a particular state or ensemble. This is because MD can change each configuration both the structure and momentum under thermodynamic equilibrium. If one gets enough number of these “snapshots”, one can evaluate the macroscopic properties of the system of interest.

The main trust of MD simulation is to solve the Newtonian equation of motion for the system composed of N atoms that interact among themselves through the potential function called “force field”. The interacting force (F_i) on each particle which is a function of time can be obtained from the derivative of the potential function (force field) to the position of this particle as the equation

$$F_{r_i} = -\frac{\partial U}{\partial r_i} \quad (2.16)$$

where F_{r_i} is the force acting on the i th particle, U is the function of potential energy and r_i is the position of the i th particle.

The position and velocity of the particle at the next time step can be evaluated by extending the current position and velocity of the particle using Newtonian's equation of motion. This equation is originally written as $F_i = m_i a_i$ where the accelerator (a_i) for each particle can be calculated from the reaction force (F_i) and the mass of the particle according to the equation:

$$a_i = \frac{F_i}{m_i} \rightarrow \frac{d^2 r_i}{dt^2} = \frac{F_i}{m_i} \quad (2.17)$$

The solution of this second-order differential equation with time ($\frac{d^2 r_i}{dt^2}$) can be obtained by the integration of each particle throughout the time span as

$$\frac{\partial r_i}{\partial t} = \left(\frac{F_i}{m_i} \right) t + c_i \quad (2.18)$$

For the boundary condition, at $t = 0$, the initial velocity (u_i) will be a constant value of c_i and the velocity at time t is $\frac{\partial r_i}{\partial t} = a_i t + u_i$. If a is also constant, one can further integrate to result in the following relation

$$S_i = u_i t = \frac{1}{2} a_i t^2 + c_2 \quad (2.19)$$

as where c_2 is another constant that is related to the position at the present time. Hence, all the changes can be calculated from the initial velocity u_i and accelerator $a_i \frac{F_i}{m_i}$.

The format of the above equation is in accord with the approximation using Taylor's series expansion up to the second degree as the relation:

$$x(t + \Delta t) = x(t) + \left(\frac{dx}{dt}\right) \Delta t + \left(\frac{d^2x}{dt^2}\right) \frac{\Delta t^2}{2} + \dots \quad (2.20)$$

From this equation, if one knows the position (first term), the velocity (second term) and the accelerator (third term) at the time t , one can calculate the position and velocity for the time $t + \Delta t$ (in practice, the time step Δt is the time interval at which the particles change their position. Usually, we set Δt in the range of femtosecond). There are many numerical algorithms used for solving this integration function of motion such as Verlet, Leap-frog and Beeman. All of them are similar as they consist of looping and changing coordinate for every atom in the system. A set of atomic configurations for the MD run can be averaged in an appropriate ensemble to result in some parameters of interest such as the average distance between atom pair and the coordinations number of the reference atom.

2.4.4 Molecular Dynamics (MD) Simulation of Ionic conductivity

In addition, the ionic conductivity can be determined microscopically from the movement of ions obtained from the MD trajectory. The diffusion coefficient can be calculated as an ensemble average of the center-of-mass vector of a molecule or ion at the time t , $R(t)$, $6Dt = \langle |R(t) - R(0)|^2 \rangle$. An alternative way is to use the center-of-mass velocity autocorrelation function of each species. $3D = \int_0^\infty \langle v(t)v(0) \rangle dt$. The conductivity (at zero frequency) can be equated to $3Vk_B T \lambda = \int_0^\infty \langle j(t)j(0) \rangle dt$. Here, V is the volume, k_B is Boltzman constant, T is temperature. The flux of charge is given

by $j(t) = e \sum_{ions} q_i v_i(t)$ where e is the elementary charge and q_i is the formal charge of ion i . The Einstein equation equivalent to Kubo equation can also show by

$$6tVk_B T \lambda = e^2 \langle \sum_i \sum_j q_i q_j \times [R_i(t) - R_i(0)] [R_j(t) - R_j(0)] \rangle \quad (2.21)$$

The cross term ($i \neq j$) in this equation is for the correlation between the diffusion of two different ions.

In molecular dynamics simulations, this is suitable to describe the upon equation in the format of an impartial Einstein relation:

$$\sigma = \lim_{t \rightarrow \infty} \frac{e^2}{6tVk_B T} \langle \sum_i \sum_j q_i q_j \times [R_i(t) - R_i(0)] [R_j(t) - R_j(0)] \rangle \quad (2.22)$$

As discussed by McDaniel et al. (McDaniel, 2018). The conductivity can be split into five components: $\sigma = \sigma_+^s + \sigma_-^s + \sigma_+^d + \sigma_-^d + \sigma_{+,-}^d$ where the cation- self ($\sigma_+^s = q_+^2 D_+ N_+ / (Vk_B T)$), anion- self ($\sigma_-^s = q_-^2 D_- N_- / (Vk_B T)$), cation-distinct (σ_+^d), anion-distinct (σ_-^d), and cation/anion-distinct ($\sigma_{+,-}^d$) conductivities all contribute to the total conductivity.

If the ions all move independently, then the cross-terms are zero, and the Nernst-Einstein relationship applies (Demir, 2020):

$$\sigma_{NE} = \frac{1}{Vk_B T} (q_+^2 D_+ N_+ + q_-^2 D_- N_-) \quad (2.23)$$

Where D_+ (D_-) and N_+ (N_-) are the diffusion coefficient and the number of cations (anions), respectively.

From the cross-correlation term is small and hence may be neglected. As a result, we arrive at a modified Nernst-Einstein equation based exclusively on the free ions:

$$\sigma_{NE,modified} = \frac{1}{Vk_B T} (q_+^2 D_+ N_+ p_+ + q_-^2 D_- N_- p_-) \quad (2.24)$$

Where p_+ and p_- are fractions of cations and anions in the free state (Feng, 2019).

2.4.5 Ion Transport Mechanisms

Mixtures of polyILs with pure ILs compose a stimulating level matter with potential for desired property characteristics. Such materials share features in common with plasticizer-doped polymer electrolytes (Abraham, 1997; Song, 1999; Scott, 2002), wherein the additive (in this case, pure ILs) can serve as a means to accelerate the

polymer dynamics and whereupon enrich the conductivity. Nevertheless, when compared with traditional plasticizers, ionic liquid additives can also encourage mobile ions and increase the overall conductivity of the electrolyte. Furthermore, as a resultant of the decoupling phenomena considered above, such blends may also offer a wider parameter space to override the conductivity–mechanical strength trade-off.

Santosh and Venkat (Mogurampelly, 2018). They used atomistic molecular dynamics simulations to study ion mobilities and the molecular mechanisms of transport in blends of poly(1-butyl-3-vinylimidazolium hexafluorophosphate) electrolytes with 1-butyl-3-methyl-imidazolium hexafluorophosphate ionic liquids. At all temperatures, the diffusion coefficients of both were examined both BMIM⁺ and PF₆[−] ions diminish monotonically with expanding polyIL wt %. Such outcomes confirm the speculation underlying their research and illustrates that blending polyILs with pure ILs can actually bring about an elevation in the ion mobilities relative to polyILs. And between the various blends the decoupling consequence is most dominant in comparing pure ILs with the different blend complements and that the dissimilarity in the ion mobilities turns into less essential when comparing nonidentical blend ratios. From the simulation results for the true conductivity and the NE values as a function of the polyIL wt% and T/T_g . Interestingly, it is seen that while both the NE and the direct conductivities exhibit a “decoupling” from T/T_g , the degree of such effects becomes significantly reduced when compared to the ion mobilities. After that the ion transport mechanisms within the polyIL–IL blends were explored to offer molecular type enlightenments. Their outcomes propose that the intrachain interaction transport mechanism implying ion hopping along polymer chains is outstanding of all the transport events.

Xubo et al. (Luo, 2021). They study the ion-transport mechanism in poly(ethyl vinyl imidazolium) with different anions: Br[−], BF₄[−], PF₆[−], and Tf₂N[−] by MD simulations.

These results indicate that anion diffusivity (D_A) calculated with the Einstein relation from mean square displacements (MSDs) of the simulation trajectories, Br[−] has much lower diffusivity than the other anions, while the other three anions do not exhibit large differences at any of the temperatures. Generally, it is observed that Tf₂N[−] > BF₄[−] > PF₆[−] > Br[−]. For the distinct part of the van Hove function, $G_d(r,t)$, show

that the nontrivial peaks at $r = 0$ specify correlated motion, where it is possible for an anion to occupy the position of another anion as a replacement. The much higher peaks at $r = 0$ for Br^- , BF_4^- , and PF_6^- indicate the precise replacement, while the lower peaks for Tf_2N^- are probably due to its flexibility as the center of mass of Tf_2N^- has more freedom to fluctuate. And length of stringlike motion, indicate that they do not observe significantly more immobile ions in the Tf_2N^- system, the shorter strings are not due to less mobility. It can be due to its larger size and multiple conformations. It might be possible that poly(C_2Im) Tf_2N is more flexible such that the hopping of Tf_2N^- at $t = t^*$ may not exactly locate the position of the replaced ion at $t = 0$.



CHAPTER III

RESEARCH METHODOLOGY

3.1 A multiscale molecular simulations for structural and material properties of two polymer hosts for gel electrolytes of poly(vinyl chloride) : PVC and poly(vinyl fluoride) : PVF

Simulations to generate and equilibrate amorphous PVC and PVF structures were first done using the coarse-grained chains mapped on a high coordination lattice which was created by removing every other position from a diamond lattice, namely the 2nd nearest neighbor diamond (2nd) lattice, with a coordination number of $10i^2 + 2$ at shell i th. All the coarse-grained bonds have the same length of 2.5 Å and the occupied lattice sites is 20.75%. For this reason, the simulation proficiency is the extremely developed comparison with MD simulation of atomistic model. The most essential characteristic is that polymer chains on 2nd lattice can be conveniently transformed to fully atomistic models and effectively recovered the real chain conformation. Moreover, the stereochemical structure of coarse-grained polymer chain can also be retained on the 2nd lattice which permit us to study the effect of side chain tacticity on structural properties of vinyl polymers from the on-lattice models as well.

3.1.1 Rotational Isomeric State (RIS) Model

RIS analysis is useful in conformational characterization of polymer molecules. This method is based on statistical thermodynamics to determine the average properties of ensemble derived from various different conformation according to its energetics. RIS model employs a small segment, usually dimer, to calculate for statistical weight matrices for each polymer conformation and then employ matrix multiplication scheme to determine the average conformational dependent properties. In the RIS scheme, the conformational partition function may be written as

$$Z = \sum_{\phi_1} \dots \sum_{\phi_n} e^{[-E(\phi_1 \dots \phi_n)/RT]} \quad (3.1)$$

For most polymer chains, this is a bad estimate because the state of a bond is influenced by the states of its neighbors. This is due to the pentane effect or the second-order interaction, named after the smallest molecule in which the phenomenon occurs. When taking into account the dependency of the nearest neighbor, the weight participatory with a given conformation is

$$\prod_i e^{[-E(\phi_{i-1}, \phi_i)RT]} \quad (3.2)$$

where $E_i(\phi_i)$ single bond energy, independent of the states of all other bonds. The statistical weight of the conformational state for each bond pair is given by

$$u_i(\phi_{i-1}, \phi_i) = e^{[-E(\phi_{i-1}, \phi_i)RT]} \quad (3.3)$$

The partition function can then be expressed as the sum over all rotational states of the product of these weights. That is

$$Z = \sum_{\phi_1} \dots \sum_{\phi_n} \prod_i u_i(\phi_{i-1}, \phi_i) \quad (3.4)$$

In matrix form, this can be rewritten as

$$Z = \prod_i U_i \quad (3.5)$$

where U_i is the statistical weight matrice of bond i .

It is constructive to consider the relative conformational energies for the model compounds of a polymer chain to be the sum of conformation-dependent interaction depending on single torsions (first-order) and consecutive pairs of torsions (second-order). Such RIS analysis is useful in understanding more conformational-dependent

interactions in these molecules. The quantities of interest in this work are the $\langle r^2 \rangle_0$, the $\langle r^2 \rangle_0 / nl^2$, $\langle s^2 \rangle_0 / nl^2$, and the fraction of bond conformer, all were tested to verify the characteristics of the polymer. Some of the useful mathematical formulas based on the original framework of the RIS model are listed below.

For example, the for the chain is obtained by evaluating the following matrix multiplication scheme.

$$\langle r^2 \rangle_0 = Z^{-1} G_1 \langle G_2 \rangle \dots \langle G_{n-1} \rangle G_n \quad (3.6)$$

where Z is the conformational partition function.

U is the statistical weight matrices in the form as shown in Eq. (3.5).

$\langle \dots \rangle$ is the ensemble average for all possible conformations.

$$\langle G_i \rangle = \begin{bmatrix} U & (U \otimes I^T) \| T \| & 0 \\ 0 & (U \otimes I^T) \| T \| & U \otimes I \\ 0 & 0 & U \end{bmatrix}_i \quad (3.7)$$

G_i is the super generator matrix, I denotes to the identity matrix and \otimes denotes to the direct product. If U_i is of dimensions $\mathbf{V}_{i-1} \times \mathbf{V}_i$ and I_A is of dimensions 4×4 , the direct product, in the sequence $U_i \otimes I_A$, is of dimensions $4\mathbf{V}_{i-1} \times 4\mathbf{V}_i$, with the form

$$U_i \otimes I_A = \begin{bmatrix} u_{11} I_A & u_{12} I_A & \dots \\ u_{21} I_A & u_{22} I_A & \dots \\ \vdots & \vdots & \ddots \end{bmatrix} \quad (3.8)$$

T is the transformation matrix of the form

$$T_i = \begin{bmatrix} -\cos \theta & \sin \theta & 0 \\ -\sin \theta \cos \varphi & -\cos \theta \cos \varphi & -\sin \varphi \\ -\sin \theta \sin \varphi & -\cos \theta \sin \varphi & \cos \varphi \end{bmatrix} \quad (3.9)$$

where θ and φ denote the bond angle and the torsion angle, respectively.

Properties depend on other conformational such as $\langle s^2 \rangle_0 / nl^2$, and the fraction of bond conformer are calculated in the same way by changing only the super generator matrix for each of these properties.

3.1.2 RIS model of vinyl polymers

For example, the RIS model for vinyl- $[\text{CH}_2\text{-CH(X)}]_n$ - chains, where all bonds are subject to a torsion potential 3-fold asymmetry with the nearest neighbor interdependence. Determined by a statistical weight matrix for successive bonds of C^α and $\text{C}^\alpha\text{-C}$. Describing the stereochemistry with dl pseudo-asymmetric centers, the statistical weight matrix for the $\text{C}^\alpha\text{-C}$ and $\text{C}^\alpha\text{-C}$ bond are

$$U_d = \begin{bmatrix} \eta & 1 & \tau \\ \eta & 1 & \tau\omega \\ \eta & \omega & \tau \end{bmatrix} \quad (3.10)$$

when the methyl group is attached to C^α to produce a d pseudo-asymmetric center. The statistical weight matrices for the C-C^α bonds depend on the stereochemistry at two successive pseudo-asymmetric centers,

$$U_{dd} = \begin{bmatrix} \eta\omega_{xx} & \tau\omega_x & 1 \\ \eta & \tau\omega_x & \omega \\ \eta\omega_x & \tau\omega\omega_{xx} & \omega_x \end{bmatrix} \quad (3.11)$$

$$U_{dl} = \begin{bmatrix} \eta & \omega_x & \tau\omega_{xx} \\ \eta\omega_x & 1 & \tau\omega \\ \eta\omega_{xx} & \omega & \tau\omega_x^2 \end{bmatrix} \quad (3.12)$$

For an l pseudo-asymmetric center, the statistical weight matrices for these bonds become

$$U_l = QU_dQ, U_{ll} = QU_{dd}Q \text{ and } U_{ld} = QU_{dl}Q \quad (3.13)$$

$$\text{where } Q = \begin{bmatrix} 1 & 0 & 0 \\ 0 & 0 & 1 \\ 0 & 1 & 0 \end{bmatrix}$$

In these matrices, the states of bonds $i-1$ and i are denoted by the rows and columns, respectively, with t , g^+ , and g^- conformation. The *gauche* $\text{CH}\dots\text{CH}_3$ conformer is the reference state. The first-order energy E_η is a bond conformation with $\text{CH}\dots\text{X}$ in *gauche* interaction but not for $\text{CH}\dots\text{CH}_3$, while the other first-order energy, E_τ is a

conformation with both CH...X and CH...CH₃ in *gauche* interaction. E_ω is the second-order energy for CH₃...CH₃ “pentane” effect. E_{ω_x} and $E_{\omega_{xx}}$ are the second-order energies for CH₃...X and X...X interaction, respectively. In this work, the calculated conformational energies of small molecules, dichloroethane (DCE) and difluoroethane (DFE) respectively to represent PVC and PVF chains, based on *ab initio* electronic structure calculation at HF/6-311++G**//MP2/6-311++G** are reported in Table 4.1.1 and the RIS energies are determined for PVC and PVF chains are reported in Table 4.1.2 and 4.1.3 as: $E_\tau = -2.09$, $E_\eta = -3.76$, $E_\omega = 7.52$, $E_{\omega'} = 5.85$, $E_{\omega''} = 20.06$ kJ/mol $E_\tau = 3.51$, $E_\eta = -1.84$, $E_\omega = 7.19$, $E_{\omega'} = 2.51$, $E_{\omega''} = 13.63$ kJ/mol, respectively.

3.1.3 RIS parameters by quantum chemistry calculation

In an effort to quantify better the conformational energetics of vinyl polymers, *ab initio* electronic structure calculations will be performed to calculate geometries and conformational energetics for numerous stereoisomers of dimers. The parameterization of RIS model which more accurately conformational energies of model molecules can be obtained.

For a molecule in any particular conformation, one writes down the electronic Hamiltonian after the Born-Oppenheimer approximation as

$$H = \frac{-\hbar^2}{8\pi^2m} \sum_p \nabla_p^2 - \sum_A \sum_p e^2 Z_A r_{Ap}^{-1} + \sum_{p<q} \sum e^2 r_{pq}^{-1} \quad (3.14)$$

The total energy of the system is obtained as the sum of electronic energy and the nuclear repulsion energy. The electronic energy is the expectation value $\langle \psi | H | \psi \rangle$ where ψ is the wave function for the system obtained from the solution of the time-independent Schrodinger equation. For a closed shell system with $2n$ electrons, one can write ψ in the form

$$\psi = N \sum_p (-1)^p P \{ \psi_1(1)\alpha(1)\psi_1(2) \dots \psi_n(2n)\beta(2n) \} \quad (3.15)$$

where y_i are molecular orbitals and P is a permutation of the electron numbers a and b represent the spin of the electron involved.

Now the Hamiltonian can be divided into one- and two-electron parts. In terms of atomic units we have

$$H = H_1 + H_2 \quad (3.16)$$

where $H_1 = \sum_p H^{core}(p)$ with $H^{core}(p) = -\frac{1}{2} \nabla_p^2 - \sum_A Z_A r_{pA}^{-1}$ is the one-electron Hamiltonian corresponding to the motion of an electron in the field of the bare nuclei and $H_2 = \sum_{p<q} \sum r_{pq}^{-1}$. Then we get the total electronic energy as

$$E = 2 \sum_i^n H_{ii} + \sum_i^n \sum_j^n (2J_{ij} - K_{ij}) \quad (3.17)$$

where

$$\begin{aligned} H_{ii} &= \int \psi_i^*(1) H^{core} \psi_i(1) d\tau_1 \\ J_{ij} &= \int \int \psi_i^*(1) \psi_j^*(2) \frac{1}{r_{12}} \psi_i(1) \psi_j(2) d\tau_1 d\tau_2 \quad (\text{Coulomb integral}) \\ K_{ij} &= \int \int \psi_i^*(1) \psi_j^*(2) \frac{1}{r_{12}} \psi_j(1) \psi_i(2) d\tau_1 d\tau_2 \quad (\text{Exchange integral}) \end{aligned}$$

The optimal value of E is the energy that issues in the lowest energy for that particular conformation of the molecule. Thus, one can apply the variable essential and be able to adjust the molecular orbital until the energy decreases. In veritable operate, we demonstrate a molecular orbital as a linear combination of atomic orbitals (LCAO) as $\psi_i = \sum_\mu C_{\mu i} \varphi_\mu$. Furthermore, the properties of orthonormality imply that $\sum_{\mu\nu} C_{\mu i}^* C_{\nu j} S_{\mu\nu} = \delta_{ij}$ where $S_{\mu\nu} = \int \varphi_\mu(1) \varphi_\nu(1) d\tau_1$ and the density matrix is defined as $P_{\mu\nu} = 2 \sum_i^{occ} C_{\mu i}^* C_{\nu i}$. Eventually, the whole energy of the molecule can be indicated as

$$E = \sum_{\mu\nu} P_{\mu\nu} H_{\mu\nu} + \frac{1}{2} \sum_{\mu\nu\lambda\sigma} P_{\mu\nu} P_{\lambda\sigma} \left[(\mu\nu|\lambda\sigma) - \frac{1}{2} (\mu\lambda|\nu\sigma) \right] \quad (3.18)$$

where

$$\begin{aligned} H_{\mu\nu} &= \int \varphi_\mu^*(1) H^{core} \varphi_\nu(1) d\tau_1 \\ (\mu\nu|\lambda\sigma) &= \int \int \varphi_\mu^*(1) \varphi_\nu^*(2) \frac{1}{r_{12}} \varphi_\lambda(1) \varphi_\sigma(2) d\tau_1 d\tau_2 \end{aligned}$$

Now the variational principle can be used to minimize the energy; than one ends up with the equations

$$\sum_v (F_{\mu v} - \varepsilon_i S_{\mu v}) C_{vi} = 0 \quad (3.19)$$

where

$$F_{\mu v} = H_{\mu v} + \sum_{\lambda \sigma} P_{\lambda \sigma} \left[(\mu v | \lambda \sigma) - \frac{1}{2} (\mu \lambda | v \sigma) \right]$$

This equation was first set forth by Roothaan and is known as Roothaan equation. The series of coefficients must be regularly resolved in order to acquire the final eigenfunctions and the energy.

The SCF process relates to the selection of atomic orbitals from which the density matrices are calculated by employing some arbitrary value of C_{vi} . Then one solves the above equation to get new values of C_{vi} which will again be used in the above equation. This is repeated until the value of C_{vi} are self-consistent. This is known as Roothaan-Hartree-Fock procedure. In this work, we will use Gaussian09 computer program, which passed the above procedure self-consistently. Both use a combination of Gaussian functions as the input atomic functions. The only other input is the geometry of the molecule in particular configuration. The program will then observe the best energy for that situation.

For ab initio calculations, various geometries of low energy conformers of the stereoisomers of vinyl polymer dimers along with rotational energy barriers between the low-energy conformers were determined at the self-consistent-field (SCF) level using a 6-311++G** basis set, a 6-31G split-valence basis set plus polarization functions on all atoms. The geometry of all conformers is determined by fully optimizing the molecular geometries using the ab initio quantum chemistry package Gaussian03 which performs full geometry optimizations. The Hartree-Fock or SCF calculations exclude contributions from electron correlation. For conformational energy studies, the most significant participator to electron correlation effects is the dispersion energy which can be that can be calculated sufficiently through the use of second-order Moller-Plesset perturbation theory (MP2). Therefore, the SCF optimized geometries was used to calculate the MP2 level calculations of electron correlation effects. The single-point MP2 calculations were also operated using Gaussian03. The conformational geometries and energies of the difluoropentane/ dichloropentane conformers are determined.

For semi-empirical calculation, statistical weight matrices were estimated from the conformational energy map of representative small segments of polymer chain by AM1 calculation using HyperChem7. The procedure is as following

- Select a section of PVF and PVC of which conformations depend on two neighboring backbone bond rotation angles were selected. The atom coordinates are adjusted to minimize the energy while the torsion angle is constant.
- The conformational energies for each of these fragments are calculated as a function of the rotation angles and torsion are rotated from 0o to 360° (10° for each step).
- The conformational energy maps are generated and statistical weights are assessed for each of the nine pair-wise dependent rotational states, for example

$$U_{\phi_i, \phi_j} = \frac{\sum_{\phi_i} \sum_{\phi_j} \exp [-V(\phi_i, \phi_j)/RT]}{\sum_{10^\circ}^{360^\circ} \sum_{10^\circ}^{360^\circ} \exp [-V(\phi_i, \phi_j)/RT]} \quad (3.20)$$

where $V(\phi_i, \phi_j)$ is the conformational energy (kcal/mole) at torsional angles ϕ_i and ϕ_j , R is the gas constant, and T is the absolute temperature.

- The RIS estimation for polymer molecules is usually based on the first- and second-order interactions for three rotational isomeric states i.e. trans (t), gauche⁺ (g⁺), and gauche⁻ (g⁻). Then, all the statistical weight matrices assigned to the skeletal bonds are 3x3 dimension.

3.1.4 Monte Carlo Simulation of polymer

In the 1990s, the research group at Akron designed a new high coordination lattice that is appropriate to simulate a real polymer chain at the bulk. This method succeeds in studying the dynamic and static properties of simple structured polymers such as polyethylene, polyoxyethylene, and polypropylene. The lattice simulation techniques for real specific polymers with the characteristics can be described by three steps.

Step 1. Mapping: A fully atomistic model of an amorphous polymer in continuous space is mapped at bulk density onto a coarse-grained representation on a suitable chosen high coordination lattice. The mapping produces a coarse-grained representation of the real chain, so diminishing the number of fundamental particles

in the posterior simulation on the lattice will be computationally effective, even when the system is bulk density.

Step 2. Dynamics/Equilibration: The system develops through time by simulation on the high coordination lattice. Monte Carlo simulation is used with Metropolis criteria for the acceptance of the bead moves. The move must have a change that retains the local conformational characteristics of the real atomistic chains derived in Step 1.

Step 3. Reverse Mapping: The final process gives a fully atomistic explanation of the system in continuous space from randomly chosen points in the trajectory. The reverse mapping must restore chain atoms (and bonds) that were perfunctorily eliminated from the delineation of the system during the mapping in Step 1.

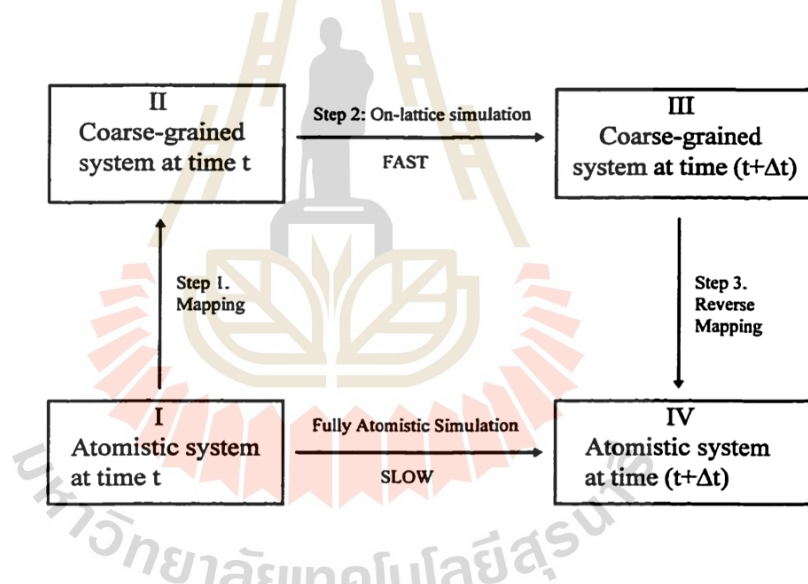


Figure 3.1 Schematic representation of three numbered steps in a MC simulation on a high coordination lattice that replaces a simulation of the fully atomistic system in a continuous space.

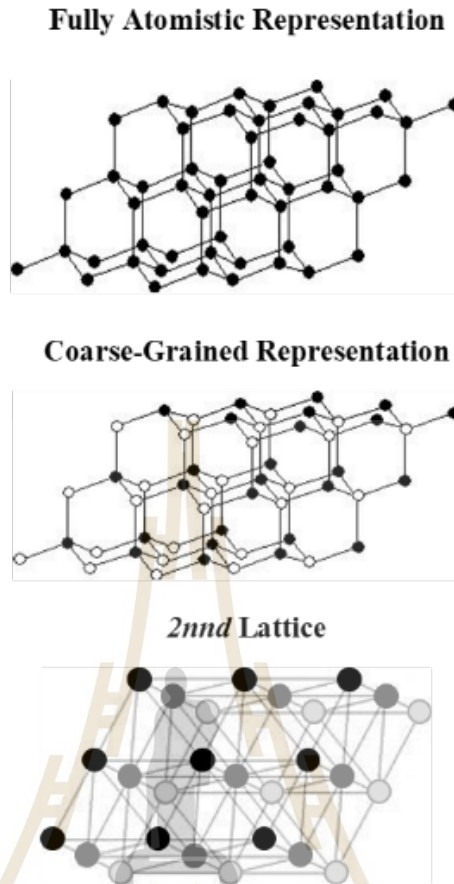


Figure 3.2 Graphical demonstration of how a tetrahedral lattice can be converted into a *2nd* lattice.

For vinyl polymer, the relations between the *2nd* lattice and the underlying diamond lattice can be illustrated as following. The rotational isomeric states of the two C–C bonds to bead j can be assigned obviously, given the vectors from bead i to bead j , and from bead j to bead k . These assignments can be showed in a 12x12 matrix. The 12x12 matrix is used to associate the reverse mapped C–C bonds in positive z direction from each *2nd* bead. This 12x12 matrix can be abbreviated to sixteen 3x3 blocks as follows,

$$\begin{bmatrix} A & B & A & B \\ B & A & B & A \\ A & B & A & B \\ B & A & B & A \end{bmatrix} \quad \text{and} \quad A = \begin{bmatrix} a & b & c \\ c & a & b \\ b & c & a \end{bmatrix} \quad B = \begin{bmatrix} b & c & d \\ c & d & b \\ d & b & c \end{bmatrix} \quad (3.21)$$

where a is tt or g^+g^+ , d is rev or g^-g^- . In all sixteen blocks, b and c are selected from tg^+tg^- , g^+t , g^-t , g^+g^- , g^-g^+ , and col , where col denotes an unphysical collapse.

The long-range interaction involves both long-range intramolecular interaction that separated by more than four bonds and the non-bonded intermolecular interaction. The long-range interactions are gotten from a discretized form of the Lennard-Jones (LJ) potential, in which the second virial coefficient (B_2) for polymers are assessed similar to a nonideal gas using the Mayer f function according to the imperfect gas theory as follows:

$$B_2 = \frac{1}{2} \int \{ \exp[-\beta u(r)] - 1 \} d\mathbf{r} = \frac{1}{2} \int f d\mathbf{r} \quad (3.22)$$

where, $\beta = 1/kT$; k is the Boltzmann constant and f is called the Mayer function. B_2 in the lattice space can be obtained by dividing the integral for each sub-shell as:

$$\begin{aligned} B_2 &= -\frac{1}{2} \left[-\int d\mathbf{r} + \sum_{1st} \int_{cell} f d\mathbf{r} + \sum_{2nd} \int_{cell} f d\mathbf{r} + \sum_{3rd} \int_{cell} f d\mathbf{r} + \dots \right] \\ &= \frac{V_c}{2} \left[1 - \sum_{1st} \langle f \rangle_{1st} - \sum_{2nd} \langle f \rangle_{2nd} - \sum_{3rd} \langle f \rangle_{3rd} - \dots \right] \end{aligned} \quad (3.23)$$

where $\int_{cell} d\mathbf{r}$ is the shell volume V_c of the 2^{nd} lattice. The shell averaged $\langle f \rangle$ can be determined by

$$\langle f \rangle = \int_{cell} f d\mathbf{r} / \int_{cell} d\mathbf{r} \quad (3.24)$$

To determine $\langle f \rangle$, the center of the one monomer is fixed at the origin while the others are allowed to be at any lattice sites. Therefore, Eq. (3.23) is transformed to

$$B_2 = \frac{V_c}{2} [1 - z_1 \bar{f}_{1st} - z_2 \bar{f}_{2nd} - z_3 \bar{f}_{3rd} - \dots] \quad (3.25)$$

where, z_i is the coordination number of the i th shell and the shell interaction parameter, u_i , for the i th neighbor can be equated as

$$\exp(-\beta u_i) - 1 = \bar{f}_{ith} \quad (3.26)$$

In these simulations, the Lennard-Jones (LJ) potential energy function is employed as follows:

$$u = \begin{cases} \infty & r < 2.5 \text{ \AA} \\ u_{\text{LJ}} = 4\epsilon \left[\left(\frac{\sigma}{r} \right)^{12} - \left(\frac{\sigma}{r} \right)^6 \right] & r \geq 2.5 \text{ \AA} \end{cases} \quad (3.27)$$

Here, the LJ-potential parameters for chloroethane ($\epsilon/k_B = 300.0$ K, $\sigma = 4.898$ Å) and fluoroethane ($\epsilon/k_B = 253.3$ K, $\sigma = 4.268$ Å) was used to estimate the interaction at the simulated temperature of 600 K (Poling, 2002) and only the first shell parameters for PVC (21.968, 1.575, -1.369 kJ/mol) and PVF (17.369, 0.330, and -0.776 kJ/mol) were employed to speed up the calculation.

3.1.5 Moves in the Simulation

Two types of moves were recommended into the simulation. One type is a series of moving single beads in which every bead has a chance to move to one of the nearest vacant neighbors within the constraints of the bond length and energy. The movement of a single bead on the 2nd lattice can move the position of either two or three consecutive carbon atoms on the underlying fully atomistic diamond lattice. For the purpose of improvement computational efficiency, a set of multiple bead pivot moves is executed.

Two to six bead pivot moves are applicable in the simulation. For every Monte Carlo Step (MCS), single bead moves and again multiple bead pivot moves are operated randomly. Every bead is tried once, on average, both in single bead moves and pivot moves, respectively. Moves to cause double to occupy and collapses were forbidden. The moves are accepted or rejected according to the Metropolis criterion.

3.1.6 System Description

MC simulations on 2nd lattice were based on coarse-grained chains with 46 monomer $[\text{CH}_2\text{CHX}]$ beads. The bulk systems were composed of 12 chains in the box of $16 \times 16 \times 16$ lattice units (equal to $4 \times 4 \times 4$ nm) equivalent to the density of 1.38 and 1.45 g/cm^3 for PVC and PVF systems which are close to their experimental densities (Lee, 1992; Ludovice, 1992). The simulation temperature was above their melting temperature at 600 K for *atactic* chains with trajectories of 10,000,000 MCS after equilibration.

3.1.7 Fully atomistic models

Reverse mapping of coarse-grained (CG) models from 2nd lattice to atomistic representation in the continuous area can be done by defining the location of central backbone atoms that are demonstrated on the diamond lattice underlying the 2nd lattice. After structural relaxation by MC simulation of CG models, all bonds and all the missing atoms will be restored. The coordinates of the carbon, fluoride and hydrogen atoms in polymer chains were generated after reverse mapped back onto the diamond lattice. The side group (X) configuration can be also uniquely in accordance with the description of the RIS model. The atomic structure can then be adjusted off-lattice by reducing the energy of the selected snapshot. This procedure is performed using Xenoview (<http://www.vemmer.org>) with PCFF force field until the gradient is less than 0.1 kcal/(mol Å). The steepest descents method is used if the gradient is greater than 1000 kcal/(mol Å), and the conjugate gradient is used in other ways. In addition, short NVT molecular dynamics (< 1 ns) was run to further relax the atomistic structures. To regularize these atomistic models, some molecular and material features of amorphous polymer structures will be defined and compared with experimental data including conformational statistics and solubility parameter factors.

3.2 Monte Carlo simulation : Effect of chain stiffness on the free surface of polymers

3.2.1 Rotational Isomeric State (RIS) Model

The RIS model (Flory, 1969; Mattice, 1994) is an effective method to calculate quickly by computer the conformational-dependent properties of a single polymer chain based on its molecular structure (bond length, bond angles, and torsion potential energetics) in the matrix multiplication formalism. The calculation is the exact result for the specific model, as imposed by the molecular geometry and the intramolecular interaction energies. From the RIS formalism, the statistical weight matrix of polyethylene-like model can be defined by:

$$U = \begin{bmatrix} 1 & \sigma' & \sigma' \\ 1 & \sigma' & \sigma'\omega' \\ 1 & \sigma'\omega' & \sigma' \end{bmatrix} \quad (3.28)$$

where the statistical weights of the first-, $\sigma = \exp(-E_\sigma/RT)$, and the second-order, $\omega = \exp(-E_\omega/RT)$, interaction parameters are multiplied by the chain stiffness parameter (k) as $\sigma' = k\sigma$ and $\omega' = k\omega$ where the energy parameters of the unperturbed polyethylene are $E_\sigma = 2100$ and $E_\omega = 8400$ J/mol, respectively (Misra, 1995). For this 3x3 matrix, the rows and columns are the conformations of ($i-1$)th and i th bonds, respectively, with the index of t , g^+ and g^- states (*trans*, *gauche*⁺ and *gauche*⁻ conformation with the torsion angles of 180°, +60° and -60°, respectively).

The conformational partition function (Z) which is the sum over all rotational states of the product of these weights can be determined using the above statistical weight matrices.

$$Z = \prod_i U_i \quad (3.29)$$

The probability of bond i at the rotational isomeric state, η , can be derived by dividing Z into the sum of the statistical weights of all conformations where this bond is in the η state.

$$p_{\eta,i} = \frac{Z_{\eta,i}}{Z} = \frac{U_1 U_2 \dots U_{i-1} U'_{\eta,i} U_{i+1} \dots U_n}{Z} \quad (3.30)$$

where U_i is the statistical weight matrices in the form as shown in Eq (3.30) and $U'_{\eta,i}$ is similar to U_i with the statistical weights of two rows except for the state η of bond i are zero.

The characteristics ratio defined as the proportion of the unperturbed mean square end-to-end distance, $\langle r^2 \rangle_0$, relative to that of the fully flexible chain (nl^2) can be used to describe the chain stiffness at the molecular level.

$$C_\infty = \lim_{n \rightarrow \infty} \frac{\langle r^2 \rangle_0}{nl^2} \quad (3.31)$$

where n and l are the number of internal bonds and the bond length, respectively.

For a particular conformation, the squared end-to-end distance of a polymer chain can be obtained by the matrix multiplication.

$$r^2 = G_1 G_2 \dots G_{n-1} G_n \quad (3.32)$$

The internal G_i matrices have 5x5 dimensions which are in the 3x3 block format.

$$G_i = \begin{bmatrix} 1 & 2l^T T & l^2 \\ 0 & T & l \\ 0 & 0 & 1 \end{bmatrix}, 1 < i < \quad (3.33)$$

Here, l is the bond vector, l^T is its tranpose and T is the transformation matrix defined by

$$l = \begin{bmatrix} l \\ 0 \\ 0 \end{bmatrix} \text{ and } l^T = [l \quad 0 \quad 0]$$

$$T_i = \begin{bmatrix} -\cos\theta & \sin\theta & 0 \\ -\sin\theta\cos\phi & -\cos\theta\cos\phi & -\sin\phi \\ -\sin\theta\sin\phi & -\cos\theta\sin\phi & \cos\phi \end{bmatrix}$$

where θ and ϕ denote the bond angle and the torsion angle, respectively. G_1 and G_n are given by the top row and the last column of G_i , respectively.

The unperturbed mean square end-to-end distance, $\langle r^2 \rangle_0$, is the ensemble average value of all possible conformation and can be calculated as a serial product of $\langle G_i \rangle$ matrices.

$$\langle r^2 \rangle_0 = Z^{-1} G_1 \langle G_2 \rangle \dots \langle G_{n-1} \rangle G_n \quad (3.34)$$

where the super-generator matrix $\langle G_i \rangle$ for the bond vector is determined by

$$\langle G_i \rangle = \begin{bmatrix} U & (U \otimes I^T) \parallel T \parallel & 0 \\ 0 & (U \otimes I^T) \parallel T \parallel & U \otimes I \\ 0 & 0 & U \end{bmatrix}_i$$

where I is the identity matrix and \otimes is denoted the direct product. U_i is of dimensions 3×3 for polyethylene and I_A is of dimensions 4×4 , the direct product, $U_i \otimes I_A$, is of dimensions 12×12 , with the form

$$U_i \otimes I_A = \begin{bmatrix} u_{11}I_A & u_{12}I_A & \cdots \\ u_{21}I_A & u_{22}I_A & \cdots \\ \vdots & \vdots & \ddots \end{bmatrix}$$

The chain stiffness can be checked at the bond and chain scale using the probability of the *trans* state and the characteristics ratio in Eq. (3.30) and (3.34), respectively. The bond probabilities and the characteristic ratios at 473 K with different chain stiffness parameters ($k = 0.0$ to 2.0) calculated by the RIS model and those averaged from MC simulations are presented in Table 3.1 Note that the fractions of

trans determined by the RIS model of a single chain are relatively smaller than those averaged from MC trajectories of polymer surfaces with multiple chains (in the next section).

The probability of *trans* conformation (and the characteristics ratio) of the *polyethylene-like* model is systematically increased from the most flexible chain 2.192 (0.333) to the most rigid chain 8.702 (0.683). The range of the chain stiffness parameter ($0.0 \leq k \leq 2.0$) is suitable in the lattice MC simulation used in this work so that structural relaxation and equilibration can be satisfied to observe different characteristics of polymer surfaces.

Table 3.1 The characteristics ratio and probability of the conformational states with different chain stiffness parameters at 473 K.

k	C_∞	P_t	P_g^+, P_g^-	$*P_t$	$*P_g^+, P_g^-$
0.0	2.192	0.333	0.333	0.393 ± 0.006	0.303 ± 0.007
0.5	4.490	0.494	0.253	0.525 ± 0.006	0.237 ± 0.006
1.0	6.282	0.579	0.211	0.616 ± 0.006	0.192 ± 0.005
1.5	7.548	0.636	0.182	0.687 ± 0.005	0.156 ± 0.005
2.0	8.702	0.683	0.159	0.756 ± 0.005	0.122 ± 0.005

*determined from MC simulation.

3.2.2 Monte Carlo simulation

MC simulation of *polyethylene-like* models has been proposed and applied to study polymer-blend nanofilm (Sirirak, 2023), random copolymer surface (Wichai, 2021), and polymer crystallization (Sirirak, 2023). In this work, the *polyethylene-like* model is used to mimic the characteristics of chain stiffness (Sirirak, 2023). Polymers are coarse-grained, as one monomer unit to one CG bead, and mapped onto the *2nd* lattice where the conformation of C-C bonds can be defined implicitly from the underlying diamond lattice (Baschnagel, 2000). The *on-lattice* intra- and intermolecular interaction of *polyethylene-like* chains are treated by the refined RIS model (Flory, 1969; Mattice, 1994) and the discretized version of LJ potential energy, respectively

(Cho, 1997). The statistical weight matrix for *polyethylene-like* chains (U_{PE}) can be transformed to the lattice version (U_{2nd}) as (Baschnagel, 2000):

$$U_{PE} = \begin{bmatrix} 1 & \sigma' & \sigma' \\ 1 & \sigma' & \sigma'\omega' \\ 1 & \sigma'\omega' & \sigma' \end{bmatrix} \rightarrow U_{2nd} = \begin{bmatrix} 1 & 4\sigma' & 2\sigma'\sigma'(1+\omega') \\ 1 & 4a & 2b\sigma'(1+\omega') \\ 1 & 4b & 2c(1+\omega') \end{bmatrix} \quad (3.35)$$

The first- ($\sigma' = k\sigma$) and the second-order ($\omega' = k\omega$) interaction parameters for *polyethylene-like* chains are defined by Eq. (3.28), with $a = \sigma'\omega'^{1/8}$, $b = \sigma'\omega'^{1/4}$ and $c = \sigma'^2\omega'^{1/2}$. For *polyethylene-like* models used in this work, polymers can be considered as stiffer chains ($k = 1.5$ and 2.0) or more flexible ($k = 0.0$ and 0.5) than the normal PE ($k = 1.0$).

Non-bonded intermolecular interaction between two CG beads can be treated by the Lennard-Jones (LJ) potential energy with $\sigma = 0.44$ nm and $\epsilon/k = 185$ K for ethylene (Poling, 2000). The first three shell of intermolecular energies on the *2nd* lattice (with cut-off radius = 0.75 nm) at 473 K are $u_1 = 15.048$, $u_2 = 0.620$ and $u_3 = -0.625$ kJ/mol, respectively.

The starting configurations of chains on the lattice were based on the self-avoiding walks in the simulation box. After that, intra- and intermolecular energies were included. Single-bead move was used to displace the CG beads to the empty position in the lattice. Each single-bead move corresponds to the displacement of two or three carbon atoms in the fully atomistic representation of the chain (Baschnagel, 2000). The acceptance of each bead move is governed by total (RIS + LJ) energy change according to the Metropolis rule. Monte Carlo Step (MCS) is assigned as a set of bead movements that are randomly tried once, by average.

3.2.3 Free surface formation

The technique to create the free surface of polymer melts is explained in our recent publications (Vao-soongnern, 2021; Wichai, 2021; Sirirak, 2023). In this work, all the systems were created as free-standing thin films with two polymer-vacuum surfaces made of 56 *polyethylene-like* chains with 50 repeating units. The starting box dimension of 25×25×25 units was first used to create and equilibrate the bulk structures. Then, the periodic box in the z direction was extended 3 times to 75 units so that the periodic structures could not interact with their parent chains. Free-standing

thin films can be obtained to represent the model for the polymer-vacuum surface of polymer melts.

All simulations were performed at 473 K which was higher than the melting (T_m) and glass transition temperature (T_g) of normal ($k = 1.0$) polyethylene to facilitate comparison with the results to previous reports (Doruker, 1998; Vao-soongnern, 1999 and 2001). In addition, all *polyethylene-like* chains with different chain stiffness parameters are in the molten state at 473 K (Sirirak, 2023). As T_g is related to the temperature at which the local segment of polymer chains starts to move motion, it is expected that T_g should be increased for stiffer chains. Nevertheless, the main focus of this work is to study the molecular and structural properties of the free surface of polymer melts. The study about glass transition temperature for polymers with different chain stiffness is also interesting and would be investigated in the future.

3.3 The effect of intermolecular interaction on polymer crystallization

For all simulations, there were 38 chains of *PE-like* molecules with 24 monomer units in each system. These CG chains were created so that one bead was represented by one ethylene (CH_2CH_2) unit and then mapped to the second nearest neighbor diamond ($2nd$) lattice, a distorted cubic lattice ($\alpha = \beta = \gamma = 60^\circ$) derived from removing every other position on the underlying diamond lattice. The $2nd$ lattice has a coordination number of 12, similar to the closest packing of uniform hard spheres, and is suitable for mapping the CG model of several polymers (Baschnagel, 2000; Xu, 2002; Vao-soongnern, 2004 and 2023; Wichai, 2021; Jamornsuriya, 2022; Kusinram, 2022; Sirirak, 2023). All CG chains were put in the simulation box with a length of 16 units (equivalent to 4.0 nm). The bead occupancy (total number of CG beads divided by box volume) in the $2nd$ lattice was fixed to 0.225 (comparable to the density = 0.95 g/cm³) which is close to the density of crystalline PE (Xu, 2001).

For CG *PE-like* models, the RIS model (Mattice, 1994) and the LJ potential energy were adopted to describe the intra- and intermolecular interactions in bulk polymers, respectively (Cho, 1997). The original RIS statistical weight matrix of the PE chain (U_{PE}) is formulated to the CG model on the $2nd$ lattice (U_{2nd}) according to (Baschnagel, 2000):

$$U_{PE} = \begin{bmatrix} 1 & \sigma & \sigma \\ 1 & \sigma & \sigma\omega \\ 1 & \sigma\omega & \sigma \end{bmatrix} \rightarrow U_{2nd} = \begin{bmatrix} 1 & 4\sigma & 2\sigma\sigma(1+\omega) \\ 1 & 4a & 2b\sigma(1+\omega) \\ 1 & 4b & 2c(1+\omega) \end{bmatrix} \quad (3.36)$$

Here, two statistical weights are defined as $\sigma = \sigma_0 \exp(-E_\sigma/k_B T)$ and $\omega = \omega_0 \exp(-E_\omega/k_B T)$ with $E_\sigma, E_\omega = 2100, 8400$ J/mol (Abe, 1965), respectively, and $a = \sigma\omega^{1/8}$, $b = \sigma\omega^{1/4}$ and $c = \sigma^2\omega^{1/2}$ and k_B is Boltzmann's constant,

To investigate the influence of intermolecular interaction between polymer chains, the original non-bonded interaction LJ parameters for the CG model of PE beads ($\sigma = 0.44$ nm and $\varepsilon/k = 185$ K) were varied in the range of ($125 \text{ K} \leq \varepsilon/k \leq 205 \text{ K}$) with the same bead diameter ($\sigma = 0.44$ nm). For *PE-like* models with ($125 \text{ K} \leq \varepsilon/k < 185 \text{ K}$) or ($185 \text{ K} < \varepsilon/k \leq 205 \text{ K}$), CG beads in polymer chains can be regarded as more repulsive or more attractive interaction than those in the normal PE ($\sigma = 0.44$ nm and $\varepsilon/k = 185$ K). In this work, five *PE-like* chains with different intermolecular interaction parameters ($\sigma = 0.44$ nm and $\varepsilon/k = 125, 145, 165, 185$, and 205 denoted by E125, E145, E165, E185, and E205, respectively) were used for comparison.

The starting configurations of the CG model of *PE-like* chains in the periodic box were created via self-avoiding random walks. After that, the intra- and intermolecular energetics were applied in the simulation. *PE-like* chains were randomly displaced on the *2nd* lattice by the single-bead movement to the vacant lattice sites. The Metropolis criteria were adopted to accept or reject the moves from the changes in total energetics in every bead displacement. On average, one Monte Carlo Step (MCS) is counted when every bead randomly tries to change its position. The single bead move on the *2nd* lattice corresponds roughly to the random local configuration changes that happen in a real polymer system due to jumps from one minimum of the torsion potential to the next one. Thus, the MCS in this dynamic MC simulation can be potentially mapped to the real time such as done previously with MD simulation [70]. The structure formation at an early stage was monitored with stepwise cooling from the molten state for the total 100 million MCS trajectories, ($473 \text{ K} \rightarrow 400 \text{ K} \rightarrow 350 \text{ K} \rightarrow 298 \text{ K}$ with 10 million MCS in each step except the final one with 70 million MCS). Data analysis was done for structures saved every 10,000 MCS from simulation trajectories. The crystallization temperature (298 K) was significantly higher

than T_g of normal PE (ca. 150 K) such that the crystallization can be observed within reasonable simulation time.

All simulations were performed at the same density (0.95 g/cm^3) with the same chain length (24 CG beads) and chain number (38 chains) in all systems so that the effect of intermolecular interaction on crystallization can be better realized although the actual densities should be depend on the intermolecular interaction. Three independent runs were repeated. The chain length of 24 monomers is slightly larger than the box dimension of 16 units so that the ordered structure can be formed as a single domain with all chains oriented in the same direction. Although the densification is produced by cooling, the neglect of densification should mostly to delay the onset of crystallization in the simulation. Like the setup in our recent publication (Jamornsuriya, 2022; Sirirak, 2023; Vao-soongnern, 2023), the systems were stepwise cooled from 473K (well above the melting temperature) to 298 K which is about 70 K below melting temperature of this normal PE model ($\sigma = 0.44 \text{ nm}$ and $\epsilon/kT = 185 \text{ K}$). Although the actual trajectories in each run are different, the overall characteristics are more or less the same. Thus, only one representative trajectory with 100 million MCS is presented in this work.

3.4 Molecular dynamics (MD) simulation of detailed structures and ion transportation of polymerized ionic liquid/ionic liquid blends

3.4.1 Experimental Methods

3.4.1.1 Materials

1-vinylimidazol, 1-butyl-3-methylimidazolium bis(trifluoromethanesulfonyl)imide (Bmim-TFSI) and lithium bis(trifluoromethanesulfonyl)imide (Li-TFSI) were purchased from Tokyo Chemical Industry Co. Ltd. 1-bromobutane, methanol, dimethylformamide (DMF), acetone, silver nitrate (AgNO_3), toluene and 2,2'-azobis(isobutyronitrile) (AIBN) were purchased from FUJIFILM Wako Pure Chemical Corporation.

3.4.1.2 Synthesis of Poly (1-butyl-3-vinylimidazolium bromide)

1-vinylimidazole (157.2 g, 1.67 mol) and 1-bromobutane (256 g, 1.87 mol) were dissolved in methanol (150 mL) and refluxed at 65 °C for 3 days. Methanol and unreacted 1-bromobutane are removed from the products under vacuum. Purity of the product was ascertained with ^1H NMR. The product 1-butyl-3-vinylimidazolium bromide (356.5 g, 1.54 mol) and AIBN (7.66 g, 0.0467 mol) as initiator were dissolved in water (200 mL) and polymerized at 60 °C for 18 h. The polymer was dialyzed against water for 1 week using a dialysis tube. During the dialysis, the water was refreshed daily. The resultant solution was dried via a freeze-drying method and poly (1-butyl-3-vinylimidazolium bromide) was obtained in a powder form (62.5 g, 17.5 % yield).

3.4.1.3 Synthesis of Poly (1-butyl-3-vinylimidazolium bis(trifluoromethanesulfonylimide))

Poly (1-butyl-3-vinylimidazolium bromide) (24.9 g, 0.108 mol) was dissolved in water (600 mL). Li-TFSI (37.7 g, 0.131 mol) was dissolved in water (220 mL). While stirring the poly (1-butyl-3-vinylimidazolium bromide) solution, the Li-TFSI solution was dropped into the stirring solution. After dropping, the mixed solution was stirred at room temperature for 3 days. The precipitation was filtered and washed with water. AgNO_3 aqueous water was dropped into the filtrate. 41.6 g of poly (1-butyl-3-vinylimidazolium bis(trifluoromethane-sulfonylimide)) was obtained (89.2 % yield). The white liquid of Bvim-TFSI was obtained and confirmed the structure by the NMR method (NMR JNM ECS-400, JEOL Ltd., Tokyo, Japan). Figure 3.4.1 shows the ^1H -NMR result of Bvim-TFSI in CDCl_3 solvent. The board and sharp peak at each position shown the unreacted monomer molecules were completely removed from the polymer product.

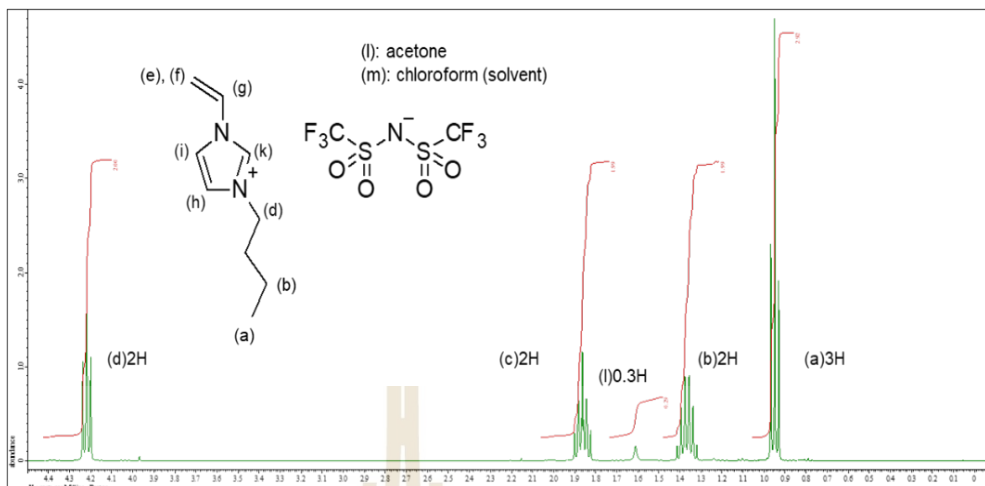


Figure 3.3 NMR spectra of Bvim-TFSI.

3.4.1.4 Synthesis of blend systems: [Pbvim-TFSI]-[Bmim-TFSI]

For Low polymer concentrations (from 10 wt% to 30 wt%): Suitable amounts of poly (1-butyl-3-vinylimidazolium bis(trifluoromethanesulfonylimide)) was added to Bmim-TFSI and the polymer was completely dissolved.

For High polymer concentrations (from 40 wt% to 95 wt%): Suitable amounts of poly (1-butyl-3-vinylimidazolium bis(trifluoromethanesulfonylimide)) and Bmim-TFSI were dissolved in acetone and mixed. Acetone was removed from the mixed solution under vacuum.

3.4.1.5 Characterization

3.4.1.5.1 Differential Scanning Calorimetry (DSC)

The glass transition temperature (T_g) of Pbvim-TFSI with various Bmim-TFSI concentrations was determined by DSC using a DSC 8230 (Rikaku Instruments Inc., Tokyo, Japan). The sample films were prepared around 10-20 mg in the aluminum pan. The pans were hermetically sealed and drying in the vacuum before DSC measurement. Samples were conditioned at a temperature range of -120 °C to 100 °C for three cycles with heating and cooling rates of 10 K/min.

3.4.1.5.2 Ionic Conductivity Measurement: Broadband Dielectric Spectroscopy (BDS)

The ionic conductivity was determined by Novocontrol high-resolution alpha-A dielectric analyzer (Novocontrol Technologies GmbH & Co. KG, Montabaur, Germany) with a frequency range from 1.0×10^{-1} to 1.0×10^6 Hz. The sample liquids were dried in vacuum and then they bring into a sample cell of diameter 14 mm. and spacer 0.17 mm. thickness at 100 °C overnight. The conductivity values were measured under nitrogen conditions with temperatures ranging from -100 °C to 180 °C, the temperature ranges were controlled using a Cryogenic temperature controller (Model 331 cryogenic temperature controller, Lake Shore Cryotronics Inc., Ohio, USA).

3.4.2 Molecular dynamics simulation

3.4.2.1 Simulation details

Molecular dynamics simulations were performed using the open-source GROMACS 2020.1 package (Abraham, 2020). The OPLS-AA force field and non-bond parameters of poly (1-butyl-3-vinylimidazolium bis(trifluoromethanesulfonyl)imide): Pbvim-TFSI were directly obtained from (Jorgensen, 1996; Doherty, 2017; Keith, 2017; Mogurampelly, 2017). The optimized structures of Pbvim⁺ with 15 monomers were generated using PolyPargen web server (Yabe, 2019). The structure and the force field parameters of ionic liquid (1-butyl-3-methyl-imidazolium bistriflimide): Bmim-TFSI were directly obtained from Acevedo and co-workers' works (Acevedo, 2018).

For constructing the polyIL material, 20 atomistic polymer chains (15 monomers each) created from the above equilibration procedure are packed into a simulation box (using the cubic cell with periodic boundary conditions) with corresponding number of TFSI⁻ anions and Bmim⁺ cations (Zhang, 2020), (as listed in Table 3.2). The initial box length is 10 nm.

Table 3.2 Composition Details of PolyIL–IL Blend Electrolytes with Varying ILs Loadings.

$C_{\text{Bmim-TFSI}}$	PolyILs			ILs	
	Bvim ⁺	Pbvim ⁺	TFSI ⁻	Bmim ⁺	TFSI ⁻
0.0	300	20	300	0	0
0.2	300	20	300	60	60
0.4	300	20	300	120	120
0.6	300	20	300	180	180
0.8	300	20	300	240	240
1.0	0	0	0	300	300

Equations of motion in MD simulations were integrated using the leapfrog algorithm with a time step of 1 fs. Temperature was controlled using a V-rescale thermostat with a relaxation time of 1 ps. A Parrinello-Rahman barostat (coupling time 1 ps with an isothermal compressibility of $4.5 \times 10^{-5} \text{ bar}^{-1}$) was employed for constant pressure simulations. Electrostatic interactions were calculated using particle mesh Ewald with a real-space cutoff of 1.3 nm. Lennard-Jones interactions were truncated at 1.3 nm, with long-range corrections for both potential and pressure applied. Neighbor lists were updated every 10-time steps using a list cutoff radius of 1.3 nm (Zhang, 2020). Bond constraints were solved using the Linear Constraint Solver (LINCS) algorithm (Khongvit, 2020).

3.4.2.2 Simulation procedure

Such a pre-equilibrium procedure was inspired by the 25-step decompression. And then a multi-step equilibration procedure was used to prepare the equilibrated configuration for the production run follow as: The first step, using 0.1 ns NVT simulation at 1000 K and 0.1 ns. The second step, using 0.1 NPT simulation at 600 K and 100 bar. The third step, 0.1 NPT simulation at 600 K and 1 bar, all 3 steps use 10 steps. The equilibrated system was finally step to an NPT production run for 110 ns for in-depth analyses (Zhang, 2020). And All images were created using VMD open-source software (Humphrey, 1996). This process resulted in an equilibrated structure with box size and density for each system reported in Table 3.3.

Table 3.3 Box size, density (ρ), radius of gyration (R_g), and average end to end distance (R_{ee}) of PolyIL–IL Blend Electrolytes with Varying ILs Loadings.

$C_{\text{Bmim-TFSI}}$	Box size (nm ³)	ρ (g/cm ³)	R_g (nm)	R_e (nm)
0.0	5.41 ³	1.375	0.357	0.706
0.2	5.78 ³	1.343	0.334	0.646
0.4	6.09 ³	1.329	0.318	0.605
0.6	6.37 ³	1.312	0.308	0.580
0.8	6.65 ³	1.300	0.301	0.559
1.0	5.60 ³	1.200	0.257	0.417

3.4.2.1 Quantification Measures

3.4.2.1.1 Validated method for equilibrium: potential, density and radius of gyration (R_g)

Polymer conformation was investigated in terms of the radius of gyration (R_g) and the average end-to-end distance (R_{ee}). The R_g is calculated as follows:

$$R_g = \left(\frac{\sum_i \|r_i\|^2 m_i}{\sum_i m_i} \right)^{\frac{1}{2}} \quad (3.37)$$

where m_i is the mass of atom i and r_i is the position of atom i with respect to the center of mass of the molecule (Khongvit, 2020).

3.4.2.1.2 Polymer dynamics

3.4.2.1.2.1 The mean squared displacement (MSD) and Diffusion coefficient (D)

The dynamics of polymer chains were studied both in terms of translational and orientational mobility. Translational dynamics were analyzed through a time-dependent diffusion coefficient (D), derived from the mean squared displacement (MSD) using the Einstein relation (Allen, 1987);

$$\lim_{t \rightarrow \infty} \langle \|r_i(t) - r_i(0)\|^2 \rangle = 6Dt \quad (3.38)$$

where $r_i(t)$ and $r_i(0)$ are the positions of the particle at time 0 and t , respectively. The term in the bracket $\langle \dots \rangle$ represents the MSD of the particle.

For the anion (TFSI⁻), the nitrogen atom is used as the reference to calculate the MSD, whereas, for cation 1-butyl-3- methyl-imidazolium (BmIm⁺), the nitrogen atom that connects the butyl functional group was used to calculate the MSD. Polycation diffusivities are not facile to achieve for longer polymer chains (Zhang, 2020). Therefore, in the current study, we overpass the diffusivity of polycations in the polyIL system.

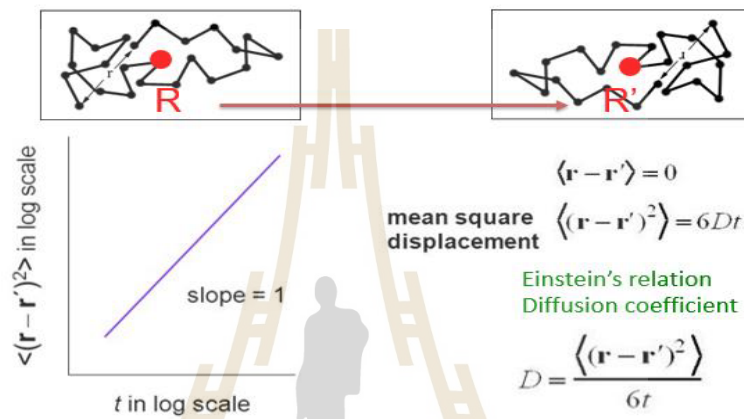


Figure 3.4 The definition of the mean squared displacement (MSD) and Diffusion coefficient (D).

3.4.2.1.2.2 The Orientational autocorrelation functions (ACF)

ACF of PolyIL-IL blends were analyzed through the autocorrelation function (the second Legendre polynomial) of a vector connecting two next-nearest atoms in the backbone of the polymer chains (1-3 vector). The autocorrelation function is calculated through (Khongvit, 2020).

$$P_2(t) = \left\langle \frac{\mathbf{v}(t+t_0) \cdot \mathbf{v}(t_0)}{|\mathbf{v}(t+t_0)| |\mathbf{v}(t_0)|} \right\rangle \quad (3.39)$$

where \mathbf{v} is the 1-3 vector and the bracket $\langle \dots \rangle$ denotes an average over different time origins t_0 as well as for the 1-3 vectors belonging to the same chain. This function measures the decorrelation of the vector at time $(t + t_0)$ with reference to its position at time t_0 .

We forecasted the local characteristic relaxation times of polymer chains by fitting the Kohlrausch Williams-Watts (KWW) stretched-exponential function (Graham, 1970).

$$f(t) = A \exp(-(t/\tau_{KWW})^\beta) \quad (3.40)$$

where the prefactor A denotes the initial, very fast relaxation (e.g., bond and angle vibrations) and is smaller than unity. The τ_{KWW} stands for the KWW relaxation time and gives an estimation of the characteristic decorrelation time for the 1-3 vector. The stretching exponent β describes deviations from the single-exponential behavior, that is, the behavior typical for a system with only one relaxation time (where $\beta = 0.82$).

3.4.2.1.3 Transference number

The transference number amounts the current transported by the identity of attention (in our case, the anion) relative to the whole current. While a number of definitions of transference number exist, in the current factor, we employ the definition that only depends on ion mobilities and the number of mobile species (Mogurampelly, 2018):

$$t_- = \frac{N_{TFSI^-} D_{TFSI^-}}{N_{TFSI^-} D_{TFSI^-} + N_{BMIM^+} D_{BMIM^+}} \quad (3.41)$$

In pure polyLLs, the cations can be approximated as almost immobile at the temperatures probed in our simulations.

3.4.2.1.4 Glass transition temperature (T_g)

T_g is one of the most essential characteristics of polymers as it describes the plastic normality of these materials at their serve temperature. Glass transition temperature is determined as the temperature at which the specific volume (V_{specific}) of the polymer undergoes a sudden transformation throughout the cooling down procedure (Zhang, 2007; Khongvit, 2016). The T_g determination for each system was started with the final structure obtained from the production run. We use cooling rate $= 1 \times 10^{10}$ K/s and the system density was calculated from the last 1ns from 2ns of NPT trajectory (Mogurampelly, 2017).

Data points corresponding to the glassy and rubbery regimes were separately fitted to two linear regression equations. The point of intersection was then used to denote the T_g .

3.4.2.1.5 Radial Distribution Functions and Coordination Number (RDF&CN)

The structural properties of the monomeric IL, polyIL systems and polyIL-IL blends were evaluated by calculating the pair distribution functions using were identified by calculating the Radial Distribution Functions function (Zhang, 2020),

$$g_{ij}(r) = \frac{V}{4\pi r^2 N_i N_j} \langle \sum_i^{N_i} \sum_j^{N_j} \delta(r - r_{ij}) \rangle \quad (3.42)$$

Where N_i and N_j are the number of atoms of ion species i and j . V is the volume of simulation box, and δ is the Dirac delta function.

3.4.2.1.6 Ideal ionic conductivity

The ionic conductivity of the IL ions, σ , can be determined from

$$\sigma = \lim_{t \rightarrow \infty} \frac{e^2}{6tVk_B T} \langle \sum_i \sum_j q_i q_j \times [R_i(t) - R_i(0)] [R_j(t) - R_j(0)] \rangle \quad (3.43)$$

Where q_i is charge of ion i , e is electronic charge, V is volume of the simulation box, k_B is Boltzmann's constant, T is the absolute temperature, and $\langle \dots \rangle$ represents the ensemble average (Mogurampelly, 2018).

From the cross-correlation term is small and hence may be neglected. As a result, we arrive at a modified Nernst-Einstein equation based exclusively on the free ions (Feng, 2019):

$$\sigma_{NE,modified} = \frac{1}{Vk_B T} (q_+^2 D_+ N_+ p_+ + q_-^2 D_- N_- p_-) \quad (3.44)$$

Where D_+ (D_-) and N_+ (N_-) are the diffusion coefficient and the number of cations (anions), respectively, p_+ and p_- are fractions of cations and anions in the free state.

CHAPTER IV

RESULTS AND DISCUSSION

4.1 Multiscale molecular simulations of two polymer hosts for gel electrolytes: poly(vinyl chloride) and poly(vinyl fluoride)

This section aims to develop a multiscale molecular simulation to generate and equilibrate amorphous structures of poly(vinyl chloride), PVC, and poly(vinyl fluoride), PVF. Then these models are validated by comparing molecular and material properties results with experimental data.

4.1.1 Conformational Energy

The first part of the method of multiscale molecular simulation is to construct the rotational isomeric state (RIS) model derived from *ab initio* electronic structure calculation which can be used to predict the conformational statistics of PVF, in comparison with PVC. The first step is to determine the conformational energies of the representative molecule for PVC and PVF i.e. 2,4-dichloropentane (DCP) and 2,4-difluoropentane (DFP), respectively, through *ab initio* electronic structure calculations. Figures 4.1 and 4.2 present the description of the first (η and τ) and the second (ω , ω_x and ω_{xx}) order interaction used in the RIS model of PVC and PVF.

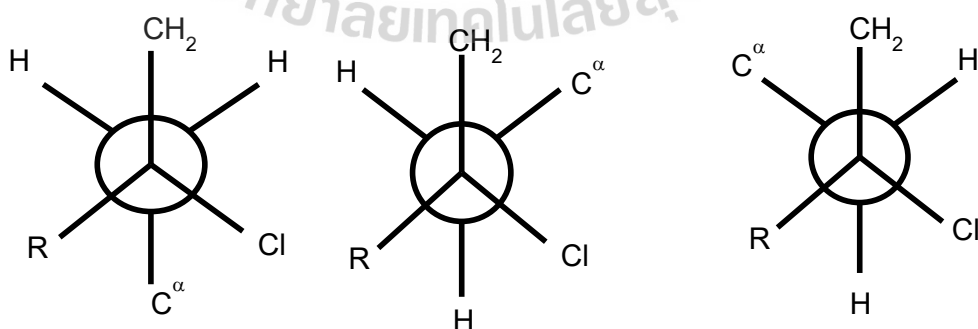


Figure 4.1.1 Newman projections of the t , g^+ and g^- conformations of the $C-CH_2CH(Cl)-C$ and $C-CH_2CH(F)-C$ three-bond sequences.

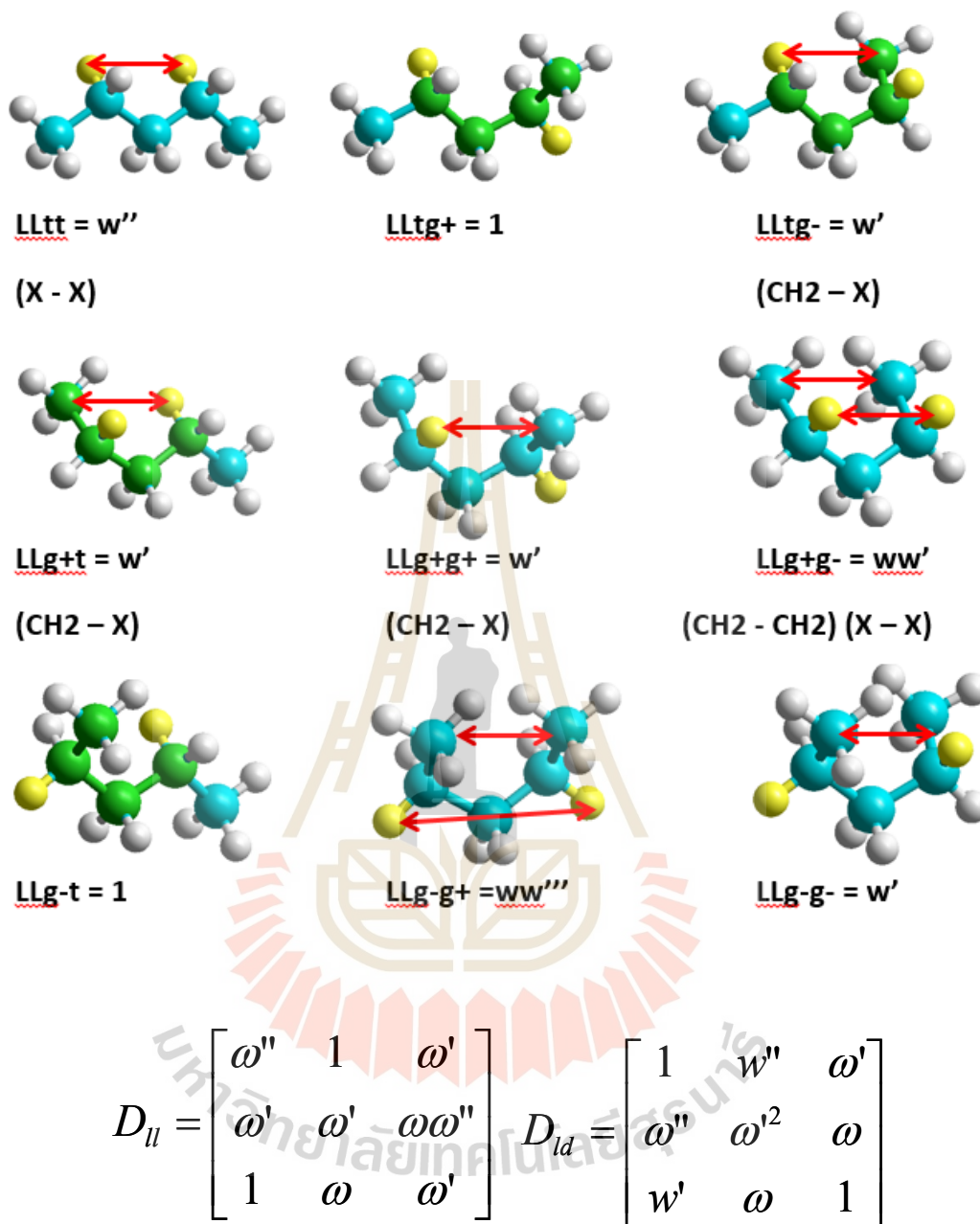


Figure 4.1.2 The representative conformation and statistical weight matrices of the second order interaction for PVC and PVC chains with the LL configuration of 2,4-dichloropentane (DCP) and 2,4-difluoropentane (DFP).

In this work, the calculated conformational energies of small molecules, dichloroethane (DCE) and difluoroethane (DFE), based on *ab initio* electronic structure calculation at HF/6-311++G**//MP2/6-311++G** are reported in Table 4.1.1, the conformational energies for DCP, obtained with a 6-311++G** basis set with electron correlation effects considered at the MP2 level, yield a value of $E_\eta = -3.76$ kcal/mol and $E_\eta = -1.84$ kcal/mol for PVC and PVF, denoting the energy of the racemic *tt* conformer relative to the meso *tg* conformer. In summary, the RIS statistical weight parameters derived from the conformational energy of DCP dimer based on quantum chemistry calculation for PVC are $E_\eta = -3.76$, $E_\tau = -2.09$ kJ/mol for first-order interaction and $E_\omega = 7.52$, $E_{\omega_x} = 5.85$, $E_{\omega_{xx}} = 20.06$ kJ/mol for second-order interaction and for PVF are $E_\eta = -1.84$, $E_\tau = 3.51$ kJ/mol for first-order interaction and $E_\omega = 7.19$, $E_{\omega_x} = 2.51$, $E_{\omega_{xx}} = 13.63$ kJ/mol for second-order interaction. PVF has an unusual small value for E_ω , which is probably due to a small size of the fluorine atom, but $E_{\omega'}$ is large, presumably because it arises in conformations where two C-F dipoles are parallel, and hence interact repulsively. For comparison, various RIS models for PVC and PVF are listed in Table 4.1.2 and Table 4.1.3 including the one from this work.

Table 4.1.1 Conformational energies of 2,4-dichloroethane (DCE) and 2,4-difluoroethane (DFE), (kJ/mol).

DCE and DFE Structures	HF/6-311++G**		MP2/6-311++G**	
	E_{rel} of DCE	E_{rel} of DFE	E_{rel} of DCE	E_{rel} of DFE
LDg ⁻ g ⁻	10.847	12.960	7.751	9.899
LDg ⁺ g ⁻	20.421	20.277	17.163	17.534
LDtg ⁻	14.419	7.887	12.044	7.004
LDtt	0.000	0.000	0.000	0.000
LDtg ⁺	24.980	17.951	19.683	15.299
LLg ⁻ g ⁺	23.208	14.873	21.074	11.717
LLtg ⁻	12.553	7.072	10.000	5.248
LLtg ⁺	4.898	5.976	2.957	4.615
LLtt	23.171	14.530	20.667	13.695

Table 4.1.2 Statistical weights parameter of various RIS models for PVC.

RIS energetics	PVC Flory/Mark ^[a] (kJ/mol)	PVC Boyd ^[b] (kJ/mol)	PVC Yoon ^[c] (kJ/mol)	PVC This work (kJ/mol)
E_{η}	-3.554	-1.210	-3.766	-4.870
E_{τ}	1.977	0.790	-2.092	-3.700
E_{ω}	8.524	10.600	12.552	14.000
$E_{\omega'}$	6.550	6.630	9.623	8.000
$E_{\omega''}$	8.524	9.580	20.083	19.700

[a] Mark, 1972; [b] Boyd, 1981 ; [c] Smith, 1995.

Table 4.1.3 Statistical weights parameter of various RIS models for PVF.

RIS energetics	PVF Saiz ^[d] (kJ/mol)	PVF Jilin ^[e] (kJ/mol)	PVF This work (kJ/mol)
E_{η}	-2.570	-1.841	-1.840
E_{τ}	-0.613	3.511	-2.761
E_{ω}	7.220	6.600	6.601
$E_{\omega'}$	1.424	2.514	2.510
$E_{\omega''}$	6.543	13.633	13.634

[d] Carballeira, 1989; [e] Zhang, 2005.

The RIS models with the first- and second-order interactions were constructed based on quantum chemistry calculation and were then employed to calculate the average mean-square unperturbed dimensions of PVC and PVF chains with the probability of *meso diad*, P_m in the range of 0.0 - 1.0. From Figure 4.1.3, the average dimension of PVC chain is more dramatically decreased than that of PVF chain which is slightly decreased as a function of fraction of *meso* diads. The calculation gives results in good consistence with experimental data as shown in Table 4.1.4. The model for PVF predicts C_n to reach 5.0 at ambient temperature for P_m near 0.5. No experimental test of this prediction seems to be available. Both PCF and PVC have $E_\eta < 0$ in part because the halogen atom, being smaller than a methyl group, can more easily participate in a *syn* interaction with a methylene group. The value of the energy for this first-order interaction is one of the most differences between the RIS models for PVC by Flory and Williams vs. Boyd and Kesner. The two models predict similar unperturbed dimensions (C_n around 11-12) at ambient temperature for polymers with stereochemical compositions typical of this polymer, $P_m = 0.43$, in reasonable agreement with experiment. Note that different results are seen between these two proposed RIS models in this work based on AM1 and MP2/6-311++G** calculation with those reported by Mark (1972) and Yoon (1995) for PVC models and Saiz (Carballeira, 1989), Jilin (Zhang, 2005) for PVF models. These findings suggest that it is possible to employ the *ab initio* quantum chemistry calculation to obtain better RIS models to describe the dimension of PVC and PVF chains.

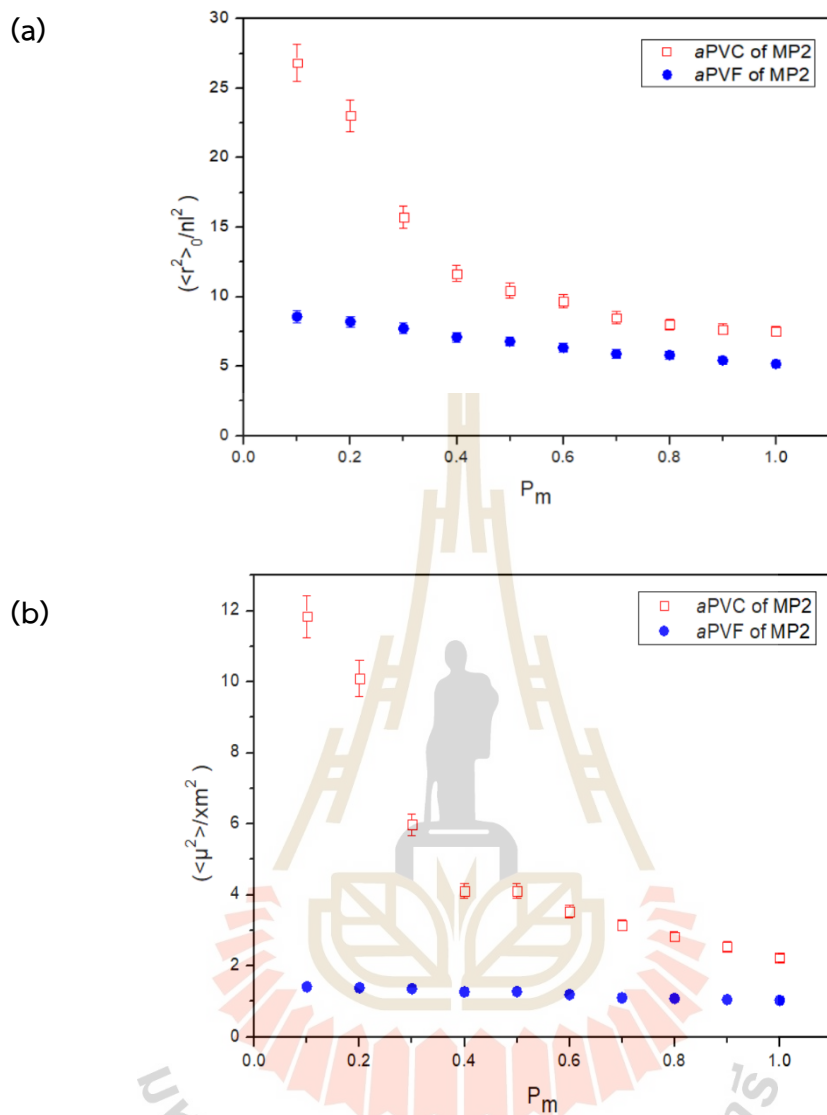


Figure 4.1.3 (a) Characteristics ratio and (b) dipole moment ratio for PVC and PVF chains based on statistical weight matrices determined in this work.

Table 4.1.4 Comparison of the characteristic ratio of PVC and PVF determined by experiment and RIS calculation.

PVC : Characteristic Ratio and dipole moment at 25 °C, ($P_m = 0.43$) ($\langle r^2 \rangle_0 / nl^2$)				
Marks	Boyd	AM1	This work	Experiment ($P_m = 0.43$)
C_n 12.6	10.2	8.7	$C_n = 11.7$	$13^a, 8 \pm 1^b$
-	-	-	$C_m = 4.1$	1.4^c D
PVF : Characteristic Ratio and dipole moment ratio at 323/423 K				
Saiz	Tonelli (50/150°C)	This work	Experiment ($P_m = 0.5$)	
C_n 7.7/6.5	8.1/6.5	$C_n = 8.1/6.8$	6.0^d	
C_m 1.52/1.37	1.46/1.30	$C_m = 1.37/1.28$	1.2^d D	

a. Nakajima, 1966; b. Mark, 1972; c. Kivelson, 1960; d. Carballeira, 1989.

4.1.2 Structural relaxation

Equilibration of coarse-grained PVC and PVF at their bulk melts can be justified by the orientation autocorrelation functions (OACF) of the end-to-end vectors, $\langle \vec{R}(t) \cdot \vec{R}(0) \rangle$. As presented in Figure 4.1.4(a), chain relaxation can be decayed to zero within 3×10^4 and 3×10^5 MCS, for PVC and PVF systems, respectively. The decay rate for the rotational motion is faster for PVF than PVC chains about one order of magnitude. For translational motion, the mean-square displacements (MSD) of the chain center-of-mass and at the individual monomer also exhibit similar behavior to the OACF as shown in Figure 4.1.4(b) and 4.1.4(c). For PVF chains, as the intermolecular interaction between CG beads is weaker, their dynamics become faster. In addition, the monomers near chain ends tend to exhibit faster dynamics than those in the inner position. In Figure 4.1.5, the representative snapshots for the coarse-grained models before the reverse-mapping and the fully atomistic structures after energy minimization are illustrated.

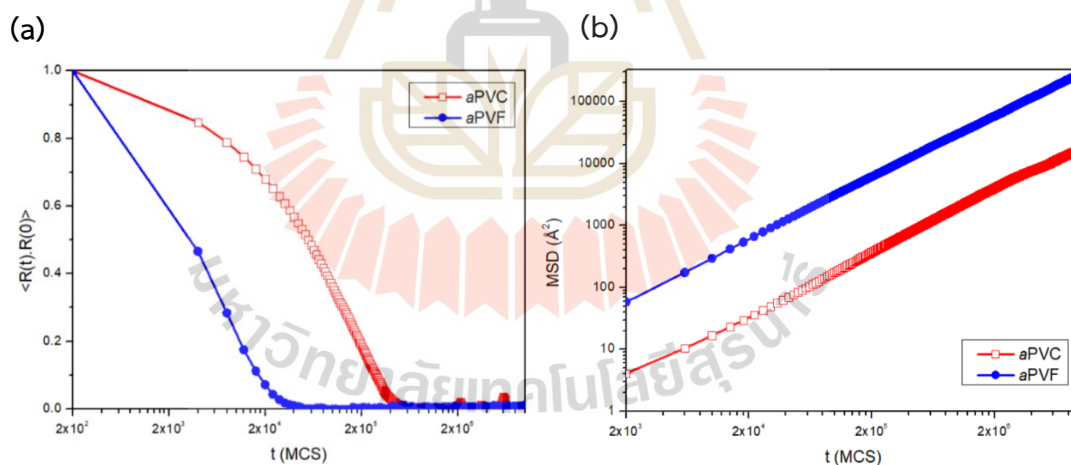


Figure 4.1.4 (a) Orientation autocorrelation function (OACF) of the end-to-end vectors (b) the mean-square displacement (MSD) for the chain center of mass and (c) the MSDs of the individual monomer from MC simulation of bulk PVC and PVF at 600 K.

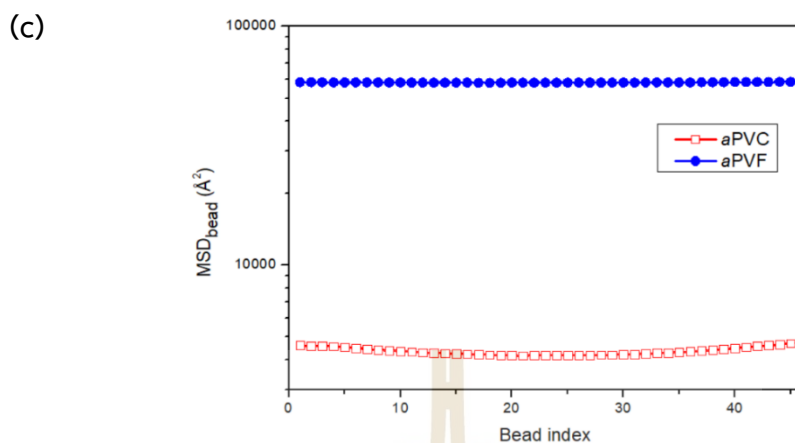


Figure 4.1.4 (a) Orientation autocorrelation function (OACF) of the end-to-end vectors (b) the mean-square displacement (MSD) for the chain center of mass and (c) the MSDs of the individual monomer from MC simulation of bulk PVC and PVF at 600 K (continued).

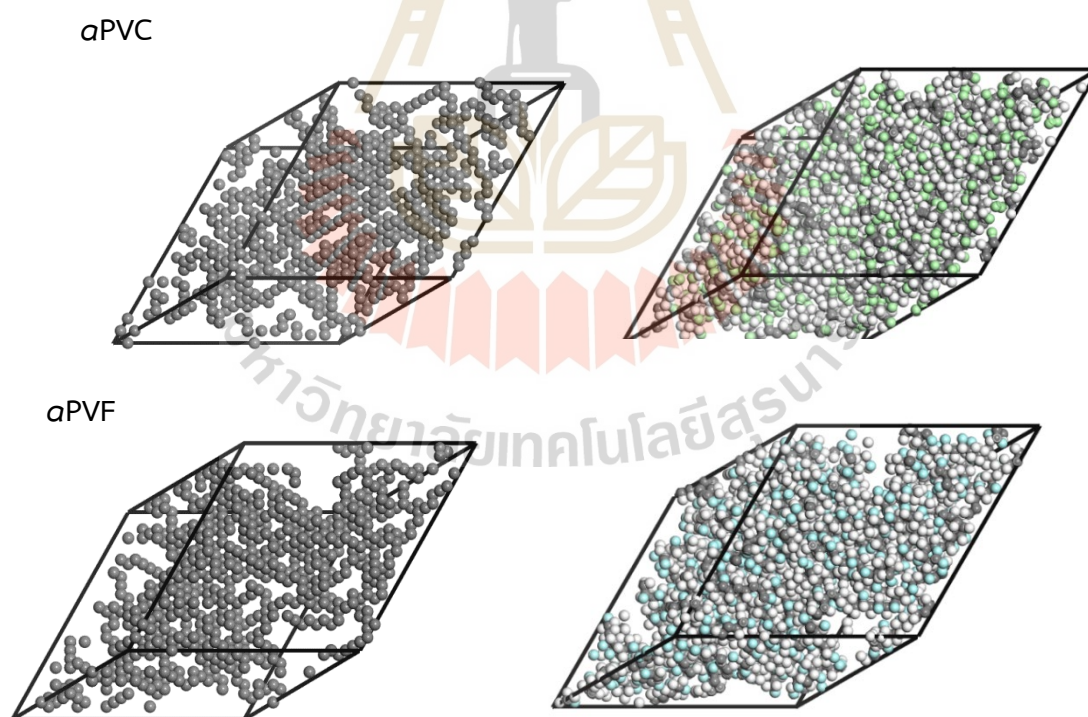


Figure 4.1.5 Example of the snapshot of coarse-grained and fully atomistic models of atactic PVC (above) and PVF (below) at their bulk densities.

4.1.3 Molecular dimension

The mean square radius of gyration ($\langle R_g^2 \rangle$), the mean square radius of end-to-end distance ($\langle R^2 \rangle$) and the characteristic ratio ($C_n = \langle R^2 \rangle / nl^2$) for PVC and PVF chains are presented in Table 4.1.5. The $\langle R^2 \rangle / \langle R_g^2 \rangle$ ratio both for PVC and PVF chains are close to 6.0 in consistent with the theoretical random flight model at long-chain limit (Flory, 1969; Mattice, 1994). Reported experimental results and RIS calculation at the probability of *meso* diads = 0.5 in the long chain limit give the characteristic ratio (C_n) of 13.0 for *α*PVC (Nakajima, 1966) and 6.0 for *α*PVF (Carballeira, 1989). As this simulation is based on relatively short chains ($n = 46$ monomers), smaller magnitudes of C_n are expected. Molecular dimension ($\langle R_g^2 \rangle$ and $\langle R^2 \rangle$) and the chain stiffness (C_n) tend to be larger for *α*PVC than those of *α*PVF. However, their magnitudes are within the range of large standard deviation which may not be statistically different. For chain dynamics, the diffusion coefficient for *α*PVF is significantly larger than *α*PVC. Thus, both intramolecular (molecular dimension) and intermolecular interaction should be possible factors to govern the chain dynamics such that PVC exhibit slower dynamics because of larger chain dimension and stronger intermolecular interaction.

Table 4.1.5 Molecular dimension and chain mobility.

Chain	$\langle R^2 \rangle$ (nm ²)	$\langle R_g^2 \rangle$ (nm ²)	$\langle R^2 \rangle / \langle R_g^2 \rangle$	C_n	D (nm ² / 10 ⁷ MCS)	Relative D
<i>α</i> PVC	9.21±6.77	1.58±0.68	5.84	4.37±3.20	2.84E-03	0.06
<i>α</i> PVF	9.09±6.65	1.50±0.63	6.07	4.31±3.15	4.93E-02	1.00

4.1.4 Conformational statistics

Figure 4.1.6 presents the torsional angle distribution of backbone C-C bonds before and after energy minimization in the conformational states at $g^+(60^\circ)$, $t(180^\circ)$ and $g^-(300^\circ)$. During geometry optimization, these torsional angles can be displaced from the lattice sites and the distribution of conformational states becomes continuous in three different kinds of dihedral angles along the backbone as presented in Figure 4.1.6 for both CG and fully atomistic models. The statistics for each conformation state determined from the integral areas of the fully

atomistic model are presented in Table 4.1.6 together with results from the RIS *a-priori probabilities*.

The conformation of atomistic models of *a*PVC and *a*PVF generated by this multiscale simulation are almost equally distributed in the g^+ and g^- state, while the RIS model gives the fraction of g^+ conformation substantially larger than g^- state. This finding may be related to the non-bonded interaction of fluorine/chlorine atoms which are not explicitly included in the RIS model. Due to the smaller size of fluorine atoms, the repulsion occurring at the *gauche* conformation is weaker than that of the chlorine atoms in PVC, thus the *trans* fraction becomes larger with a lower amount of the *gauche* fraction for the PVF chain.

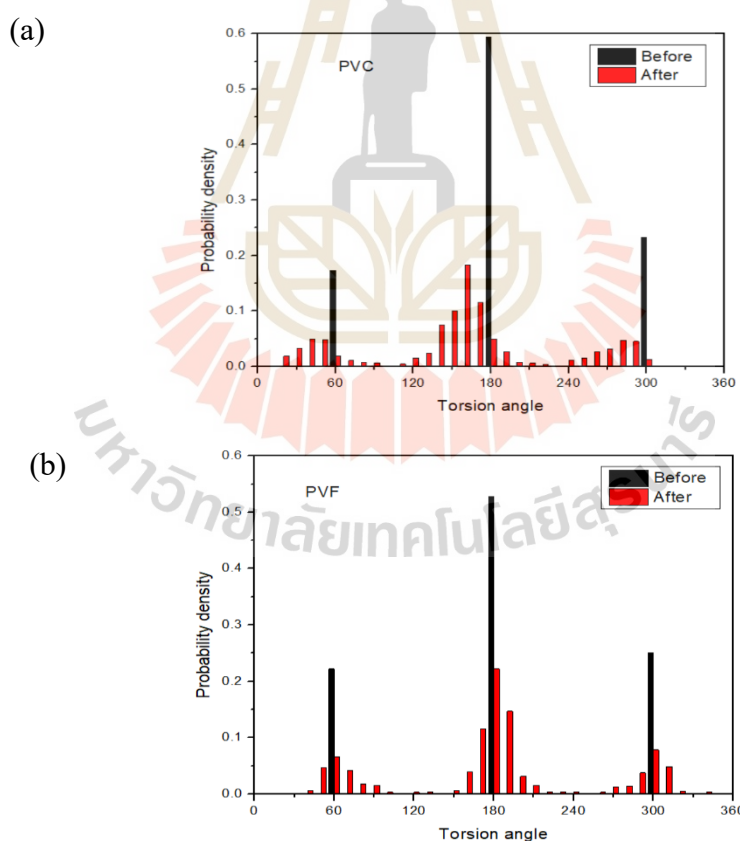


Figure 4.1.6 Distribution of the backbone torsional angles for amorphous (a) *a*PVC and (b) *a*PVF bulks from the reverse-mapping structures before and after energy minimization.

Table 4.1.6 Torsional angle distribution of PVC and PVF models.

Tacticity of polymer chains	Coarse-grained model (MC simulation)			Fully atomistic model (before/after minimization)		
	g^+	t	g^-	g^+	t	g^-
<i>a</i> PVC	0.19	0.60	0.19	0.17/0.20	0.59/0.61	0.23/0.19
<i>a</i> PVF	0.24	0.53	0.24	0.22/0.23	0.53/0.52	0.25/0.25

4.1.5 Cohesive energy and solubility parameter

One manner to rectify the simulated structures is to compare the calculated cohesive energy and solubility parameters with experimental data. The cohesive energy can be assigned from the energy difference between polymer molecules in the bulk compared to their isolated state. The Hildebrand solubility parameter (δ) can be determined from the cohesive energy density (CED) as (Theodorou, 1985):

$$\delta = (CED)^{1/2} = \left[\frac{\Delta E_v}{V_1} \right] \quad (4.1.1)$$

where V_1 is the molar volume and ΔE_v is equivalent to the cohesive energy, U_{coh} and equal to the difference of the total energy of the bulk structures (U_{tot}) with the parent chains with no periodic boundary condition (U_{par}). The experimental solubilities of *a*PVC and *a*PVF are around 19.2 - 22.1 and 14.6 - 16.3 J^{1/2}/cm^{3/2} (Brandrup, 2004). The calculated cohesive energies are $(2.41 \times 10^8) \pm (2.23 \times 10^5)$ and $(1.32 \times 10^8) \pm (3.76 \times 10^5)$ J/cm³. The calculated solubility of fully atomistic *a*PVC and *a*PVF models are 15.54 ± 0.0070 and 11.49 ± 0.016 J^{1/2}/cm^{3/2} which are close to the experimental data. Simulation data have high level of confidence as the standard deviations are of small magnitude, the atomistic structure of the amorphous model should be reasonable to represent the real system. The calculated solubility of *a*PVC is larger than *a*PVF implying the more cohesive structure due to the attractive interaction due to chlorine atoms and larger magnitude of dipole moment for C-Cl bonds. Note that the calculated solubility parameter is generally governed by the optimized structure

of the polymer model and the quality of the forcefield used in the calculation, especially the non-bonded interaction terms.

4.1.6 Coarse-grained structures

The pair correlation function (PCFs), $g_{AA}(i)$ of coarse-grained polymer models can be determined from the probability to find the A bead from another A bead at a distance r . For lattice simulation, $g_{AA}(i)$ at the i th shell can be defined as:

$$g_{AA}(i) = \frac{1}{(10i^2+2)V_A n_s} \sum n_{AA}(i), \quad (4.1.2)$$

where V_A is the volume fraction of A beads, n_s is the number of structures, and $n_{AA}(i)$ is the number of A beads in the i th shell from another A in different chains. At higher shell, $g_{AA}(i)$ approaches 1 for random arrangement. Figure 4.1.7 presents the local intermolecular PCFs.

Since in the first three shells of the non-bond intermolecular interaction parameter for PVC and PVF systems at the simulated temperatures (600 K) are (28.461, 2.547, -1.325 kJ/mol) and (17.369, 0.330, and -0.776 kJ/mol) , respectively. The PCFs are quite small (the magnitude < 1.0) in the first two shells due to the repulsive interaction of non-bonded energy parameters. The first maximum at the third shell is due to the attractive interaction. Interestingly, the magnitudes of PCFs for PVF tend to be larger than those of PVC system at all shells indicating the better packed structure probably due to smaller size of fluorine atom and weaker intermolecular interaction.

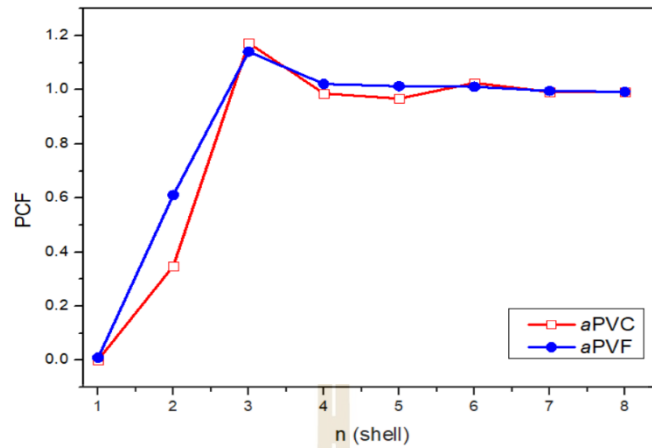


Figure 4.1.7 The intermolecular pair correlation function from MC simulation of the coarse-grained PVC and PVF bulk structures at 600 K.

4.1.7 Radial distribution function

The radial distribution function (RDF) of fully atomistic systems can be determined using a similar definition to the PCF for coarse-grained models on the lattice but in the continuous space. The relationship of each given atom pair AB is averaged out to calculate the RDF by

$$g_{AB}(r) = \frac{\langle n_{AB}(r) \rangle}{4\pi r^2 \Delta r \rho_{AB}} \quad (4.1.3)$$

where $\langle n_{AB}(r) \rangle$ is the average number of AB atom pairs in the spherical shell between the distance r and $r + \Delta r$ (with shell volume = $4\pi r^2 \Delta r$) and ρ_{AB} is the number density of AB atom pairs. According to this definition, RDF gives the probability of finding the separated atom pairs at the distance r , normalized by the probability for a uniform distribution with equal density. The intermolecular RDF gives information about molecular packing and the atomic distribution in the amorphous structure.

In Figure 4.1.8(a), the total RDF of all carbon pairs is presented along with the intermolecular correlations between methine and methylene carbons in Figure 4.1.8(b). It is necessary to confirm whether the generated structures of fully atomistic models are amorphous. The first and second peaks are seen clearly at $r = 6.0$ and $r = 12.0$ Å are due to the atomic pair without bond connectivity. The weaker third peak is around

18.0 Å and then the RDF of PVC approach 1.0, followed by PVC : C-C, methine-Cl, methylene-Cl and Cl-Cl at 33.4, 32.4, 34.2 and 28.1 Å, respectively. For PVF of RDF also reaches 1.0, followed by C-C, methine-F, methylene-F and F-F at 34.5, 35.2, 37.7 and 34.5 Å. Therefore, overall RDF of both polymers, implying that no long-range order exists beyond this distance and the generated atomistic structure is in the amorphous state. In addition, the intermolecular RDFs for halogen atoms in PVC (Cl...Cl) and PVF (F...F) are presented in Figure 4.1.8(c). Due to stronger interaction, the first peak for Cl...Cl correlation is seen at 4 Å and the second peak with higher amplitude is observed at 8 Å. However, there is no clear sign of RDF peak for F...F correlation in PVF probably due to smaller atomic size and weaker intermolecular interaction. Although the size of fluorine atom is smaller, chlorine atoms seem to stay closer to each other. Thus, the intermolecular interaction between PVC chains should be stronger in consistence of larger magnitude of solubility parameter.

(a)

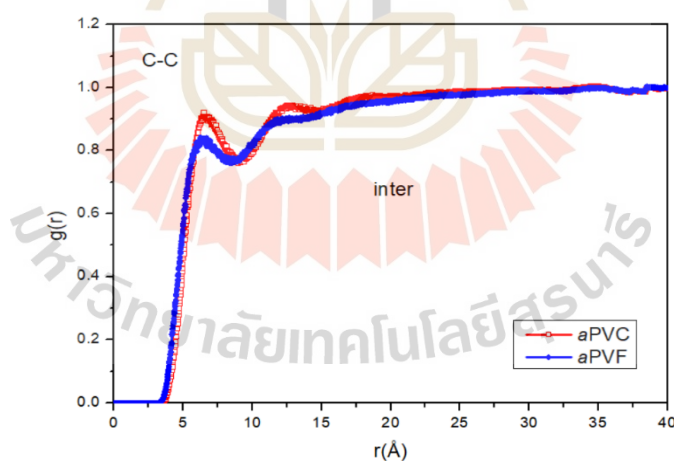
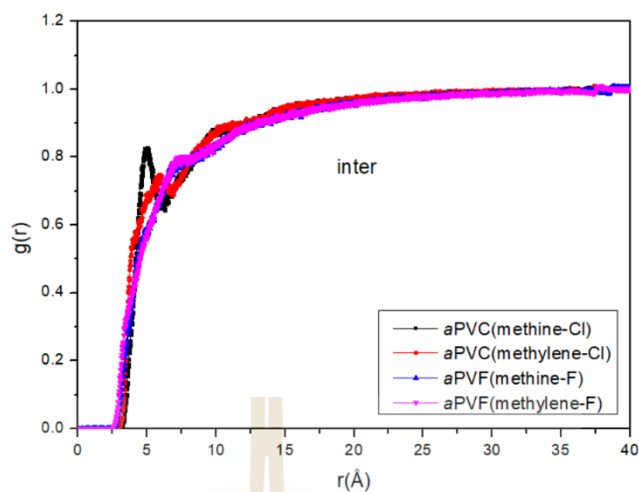


Figure 4.1.8 (a) intermolecular RDF of all carbon backbone atoms (b) intermolecular RDF of methine (CH) and methylene (CH₂) carbons and (c) Intermolecular RDFs of Cl...Cl, and F...F atom pairs from the fully atomistic models of amorphous structures.

(b)



(c)

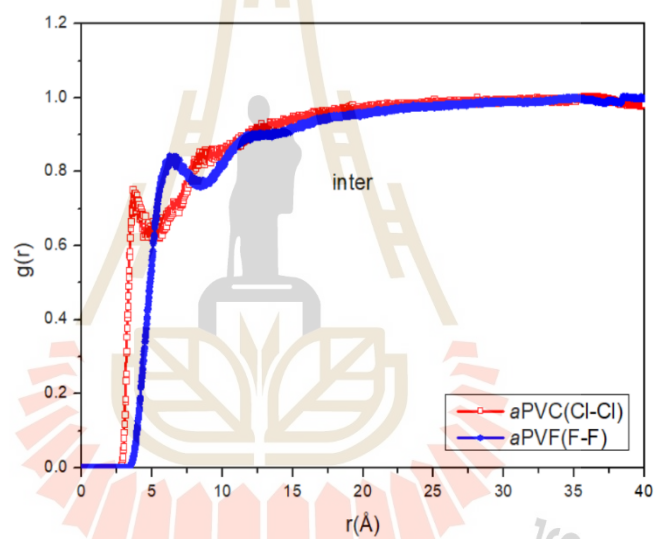


Figure 4.1.8 (a) intermolecular RDF of all carbon backbone atoms (b) intermolecular RDF of methine (CH) and methylene (CH₂) carbons and (c) Intermolecular RDFs of Cl...Cl, and F...F atom pairs from the fully atomistic models of amorphous structures (continued).

4.2 Monte Carlo simulation : Effect of chain stiffness on the free surface of polymers

Because the application of PVC and PVF as the host for gel electrolytes is in the form of polymer surface interacting with ionic liquids, surface properties of these polymers need to be characterized. As seen in the previous section, PVC and PVF have much different chain stiffness in terms of the characteristic ratio. Molecular understanding of surface properties of polymers with different chain stiffness should be important toward material design to give better properties of polymer gel electrolytes to exhibit higher ionic conductivity. Thus, the main aim of this section is to focus on investigation of the effect of chain stiffness on structural and molecular properties of the free surface of polymers. To treat the chain stiffness as the general characteristics, *polyethylene-like* models with varying statistical weight matrices but the same intermolecular interaction parameters are employed to simulate polymers as the free surface.

4.2.1 Equilibration

After coarse-graining PE-like model and mapping onto the 2nd lattice, the bulk structures were equilibrated using the Monte Carlo algorithm with the single bead move and the acceptance criteria was based on the Metropolis rule. The structures need around 10^7 MCS for equilibration. Data analysis was done from snapshots recorded every 10^4 MCS from the subsequent 10^7 MCS trajectories. System equilibration can be asserted by the mean square displacements (MSD) of polymer chains to exceed their molecular dimension and the normalized orientation autocorrelation functions of the chain end-to-end vector (OACF) $< 1/e$. As seen in Figure 4.2.1, the equilibration of all structures should be satisfied within 10^7 MCS for the chain stiffness parameters in the range of $0.0 < k < 2.0$. In addition, the local dynamics of monomer units can be represented by the MSDs of individual CG beads. As shown in Figure 4.2.1(c), monomers in the stiffer chains move slower. Moreover, the local dynamics of monomers are increased significantly for CG beads near the chain ends.

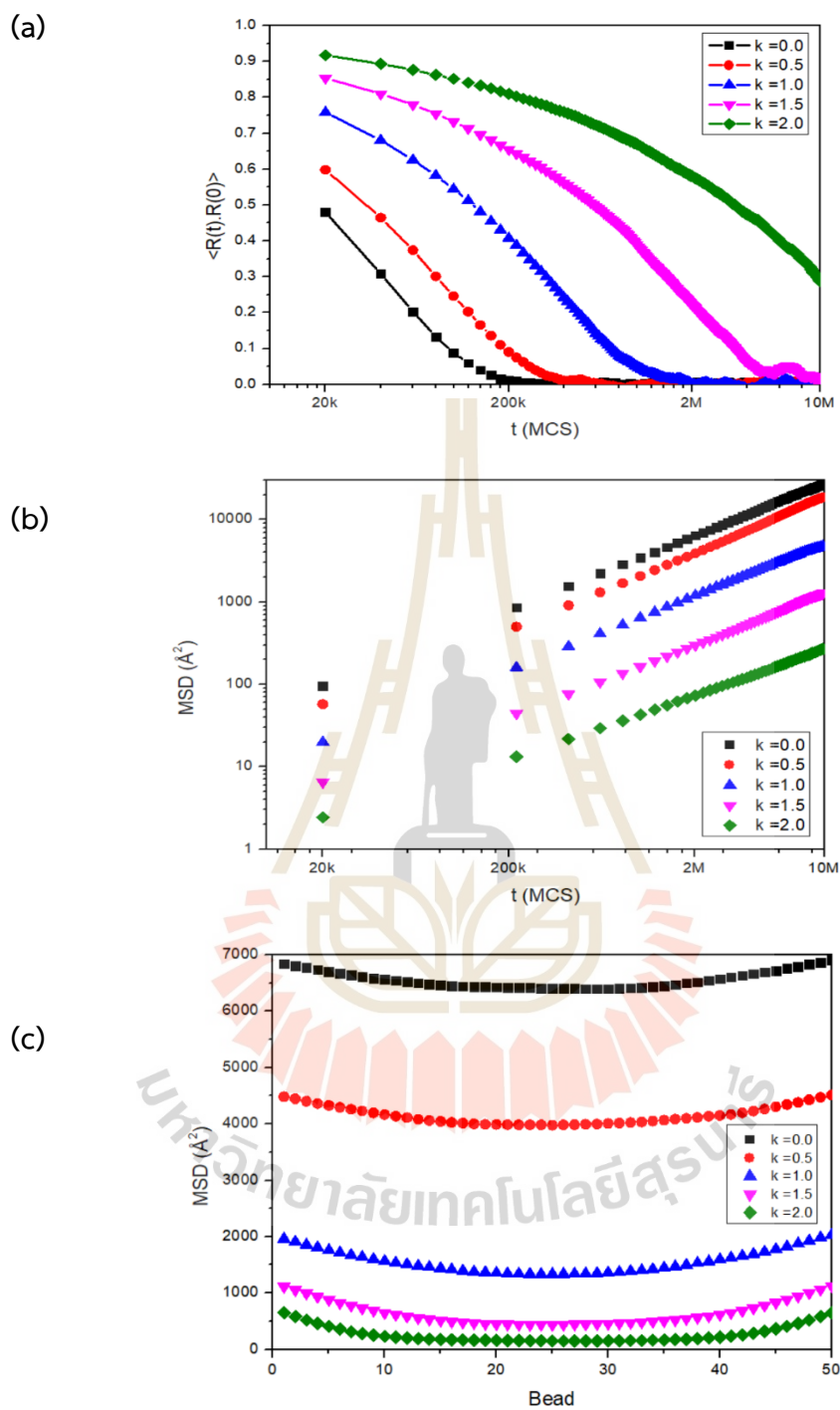


Figure 4.2.1 (a) the OACFs of the chain end-to-end vectors, (b) the MSDs of the chain center of mass, and (c) the MSDs of the individual monomer of polyethylene-like models.

4.2.2 Density profiles

Figure 4.2.2 illustrates the representative snapshots for the free surfaces of polyethylene-like models with different chain stiffness parameters (k). In this work, more flexible, normal and more rigid chains are represented by $k = 0.0, 1.0$ and 2.0 , respectively. By visual inspection and data for chain conformation in Table 3.2.1, polymers have a larger amount of *gauche* conformation and become denser structures for more flexible chains. In contrast, more rigid chains adopt more *trans* conformation, and the overall structures become less densely packed, especially at the surface where some chains can be exposed more to the vacuum side. The roughness of the free surface in a specific snapshot is defined as $R = (\langle z_p^2 \rangle - \langle z_p \rangle^2)^{1/2}$, where the averages of z_p and z_p^2 are taken over all x and y lattice sites across the periodic surface. At any x and y sites, z_p indicates the z coordinate (an integer number) of the outermost bead position of the free surface from the vacuum side. The $\langle R \rangle$ values in Table 4.2.1 indicate the averages over different snapshots separated by 100,000 MCS. The roughness of the free surfaces generally increases when the stiffness parameter is higher. Thus, the broadening of the surface regions observed in the density profiles is also a result of the increased surface roughness.

Density profiles were calculated by counting monomer beads in each divided layer with a thickness of 0.2 nm and then averaged for all trajectories versus the displacement from the center of film structures (Z). Figure 4.2.3 displays density profiles of melt-vacuum surfaces of polymers with different chain stiffness. In general, bulk densities are relatively constant and then sharply decayed near the surfaces. For more flexible chains, there is a larger amount of *gauche* conformation with denser structures. As a result, the bulk densities become higher accompanied by narrower surface thickness.

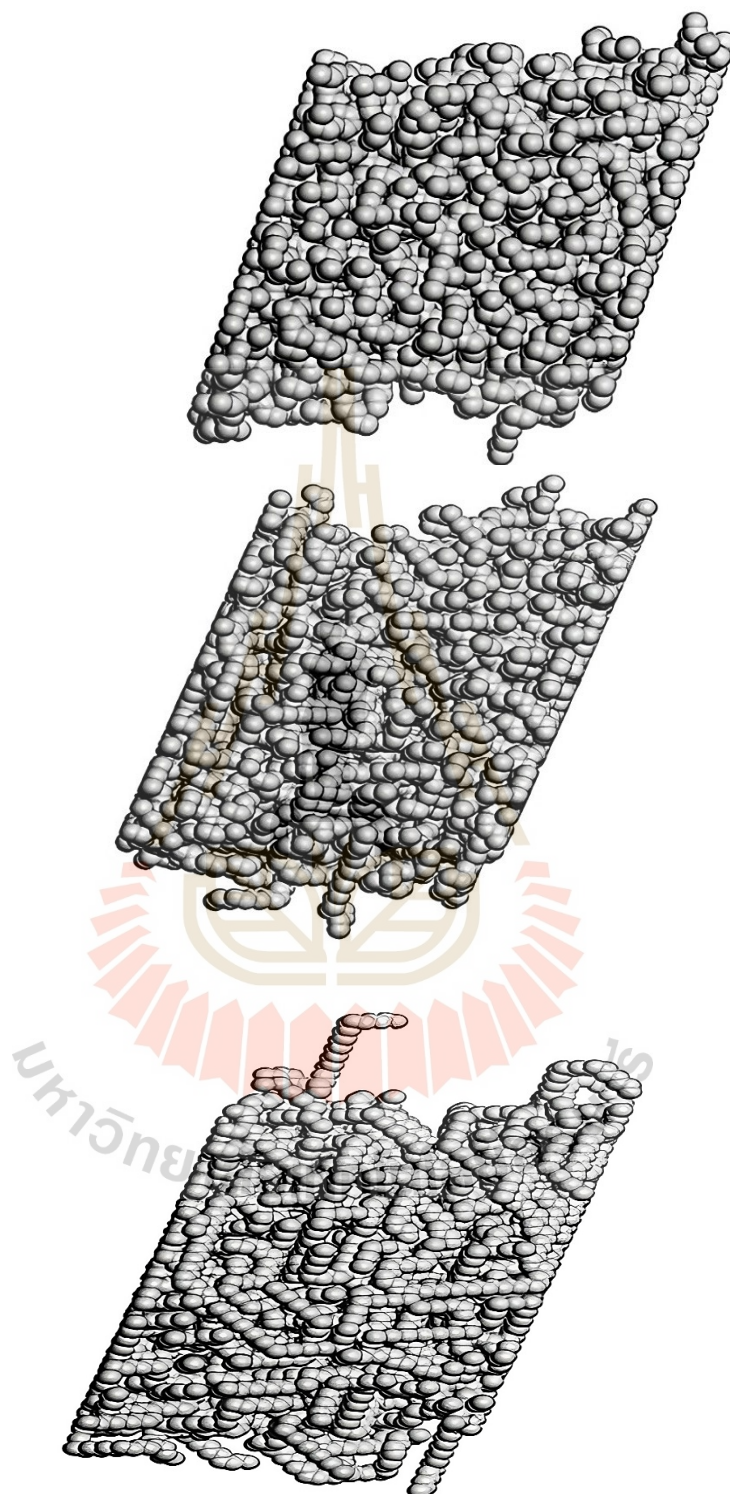


Figure 4.2.2 Representative structures of the free surfaces of polymer melt with different degrees of chain stiffness, $k = 0.0$ (top), 1.0 (middle), and 2.0 (bottom).

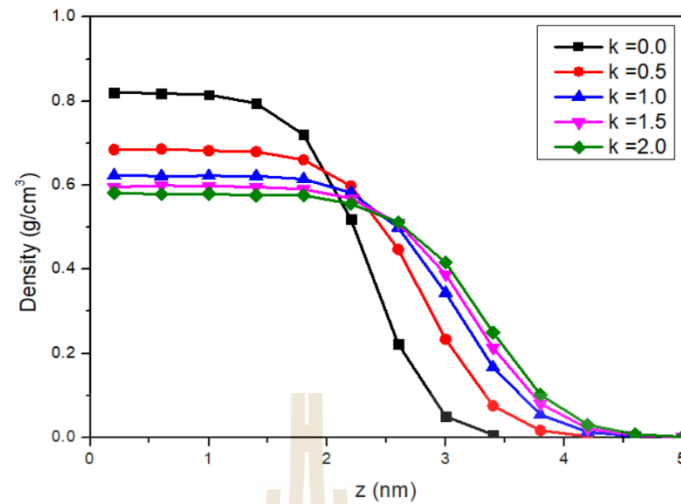


Figure 4.2.3 Density profiles of melt-vacuum surfaces of polymer with different chain stiffness as a function of the displacement from the center of structures.

Table 4.2.1 Parameters of Polymer Surfaces.

Chain stiffness parameter (<i>k</i>)	Surface roughness parameter ($\langle R \rangle$) in lattice units	Bulk density (ρ_{bulk}) (g/cm ³)	Gibbs surface (<i>z</i>) nm	Surface thickness (<i>t</i>) nm	Surface width (<i>w</i>) nm
0.0	4.15 ± 0.55	0.819	2.336	6.781	1.058
0.5	4.46 ± 0.60	0.686	2.787	7.885	1.226
1.0	5.74 ± 0.39	0.625	3.058	8.654	1.336
1.5	6.06 ± 0.41	0.607	3.968	8.783	1.353
2.0	6.67 ± 0.47	0.600	4.017	8.938	1.405

*Surface thickness (*t*) is defined as $t = 2z_{1\%}$ where $z_{1\%}$ is the normal distance of the films at 1% of the ρ_{bulk} and is provided as a characteristic size to represent the outer boundary of the films.

To quantitatively analyze polymer surfaces and their relation to the chain stiffness, the theoretical equation originally proposed to describe the interface of immiscible blends is applied (Helfand, 1972).

$$\rho(Z) = \frac{\rho_{bulk}}{2} \left[1 - \tanh \left[\frac{2(Z-z)}{w} \right] \right] \quad (4.2.1)$$

where ρ_{bulk} is the bulk density, Z is the displacement from the center of structures, z is the position where the density is about one-half of bulk density and w is the surface width. The density profiles for these polymer surfaces can be captured very well by this functional form and the fitting parameters are presented in Table 4.2.1. In this work, the Gibbs dividing planes are defined from the density profiles and can be estimated at the z position where $\rho = \rho_{bulk}/2$. The surface thicknesses (t) of the different systems can be estimated from $t = 2z_{1\%}$ where $z_{1\%}$ is defined as the normal distance of the surfaces at 1% of ρ_{bulk} (Doruker, 1998). From Table 4.2.1, it is seen that the surface thickness is larger than the chain dimension by about 3 to 5 times the radius of gyration of polymer chains so that each simulated system can have the bulk region with constant density.

The strength of chain stiffness in polymer surfaces can affect the density profiles, bulk densities, and surface thickness. For stiffer chains, the bulk densities are lower as the structures become less densely packed. The bulk densities are relatively constant and increased proportional to the chain stiffness parameter. Consequently, the surface width (w) and the locations of Gibbs dividing planes used to represent the thickness of surface profiles are inversely proportional to the chain stiffness parameter. The surface thickness changes significantly with the chain stiffness. This outcome is commonly an indication of the adjustment in polymer compressibility as a function of chain stiffness and suggests that the surface thickness, as predicted theoretically by the mean-field approach, is directly correlated to the efficacy of the structure to tolerate density fluctuations. Thus, stiffer chains exhibit thicker surface thickness implying that their surface densities should have larger fluctuations.

Apart from the density profiles, the distribution of polymer chains can be determined by the spatial distribution of their chain center of mass. The chain distributions and their cumulative profiles are shown in Figure 4.2.4. The peak for each profile in Figure 4.2.4(a) on the liquid side of the melt-vacuum surface appears at a distance corresponding approximately to the chain dimension. For more flexible polymers ($k = 0.0$ and 0.5), their magnitudes seem to be higher in the surface region while this distribution has no systematic difference in the bulk region ($Z < 1.5$ nm), except the most flexible chain exhibits the largest amplitude. Compared to more

flexible chains, stiffer polymers have less efficiency for chain packing. Thus, the surface becomes broader, and chains can stay at larger distances with increasing chain stiffness. The chain distribution can be systematically distinguished for the cumulative distribution as shown in Figure 4.2.4(b). The cumulative profiles at the same Z position are clearly different only for more flexible chains but almost indistinguishable for stiffer chains. The center of mass density is quite small near the surface as chains do not preferably to be confined close to an essentially impenetrable surface and have pancake-like shapes. Similar findings were also reported in Kumar, 1998 for the off-lattice MC simulation of bead-spring homopolymer models.

To compare the distribution of monomers at different positions in chains, the normalized middle- and end-monomer densities are presented in Figure 4.2.5. The monomer density profiles are normalized by the total monomer density in that bin, so that the distribution near the surface can be observed clearly. This is also typical in the sense that the end beads become more abundant closer to the vacuum. In general, both middle- and end-monomer densities have almost equal magnitude in the bulk region. However, near the surface, the end-monomer profiles are increased exponentially whereas the middle-monomer densities are decreased. This outcome is justified as a competition between the enthalpic (preferably not to have any segments to stay on the vacuum side) and the entropic effects (end-monomers in the free surface constitute smaller entropy loss than middle-monomers) (Kumar, 1994). For more flexible chains, both end- and middle-monomer profiles exhibit steeper curves. As more flexible chains can be packed denser with sharper surfaces, the monomer profiles for end- and middle-beads of more flexible chains exhibit steeper curves accordingly. For stiffer chains, the structures become less dense, and end/middle monomers tend to be placed more in the surface/bulk region (but no significant difference for chains with $k = 1.0 - 2.0$).

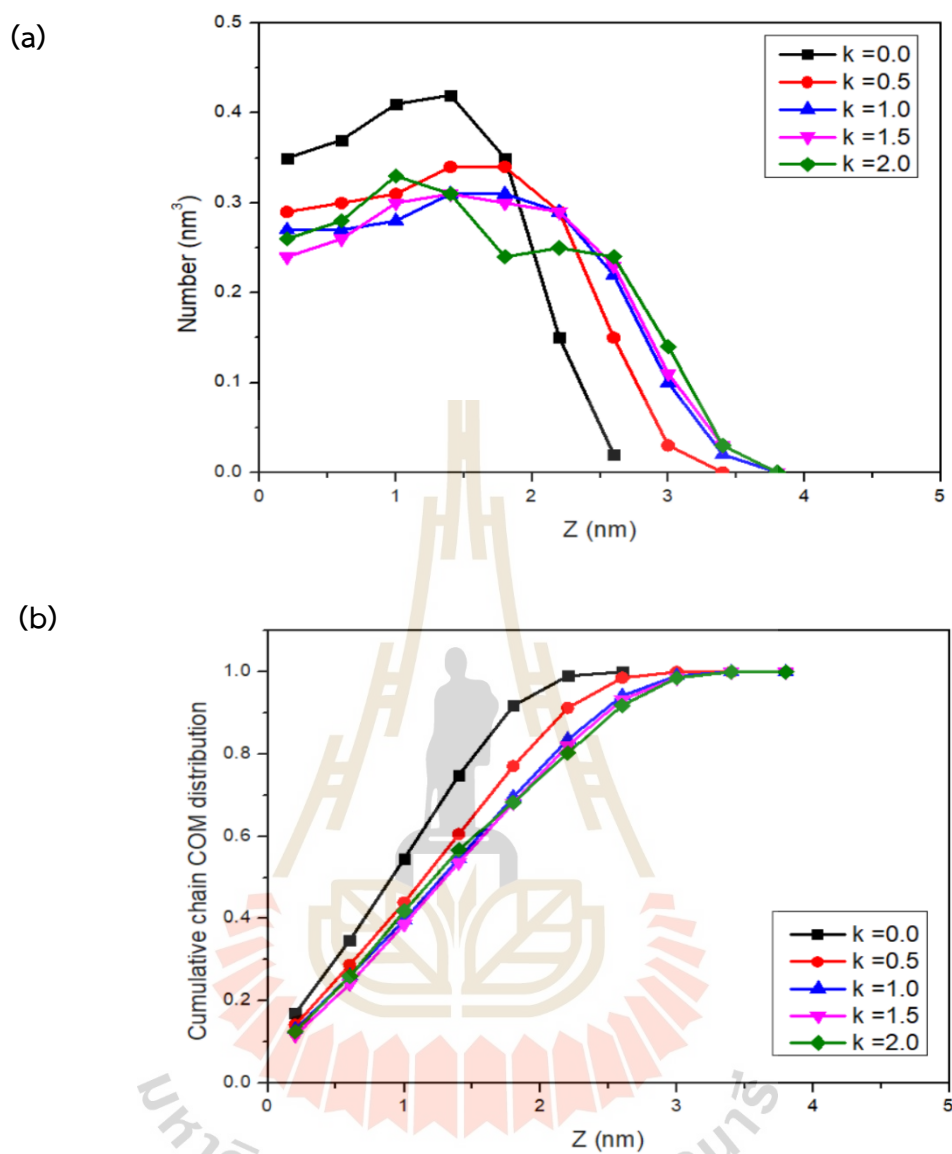


Figure 4.2.4 (a) Distribution of chain center of mass and (b) the corresponding cumulative profiles of polymer surfaces.

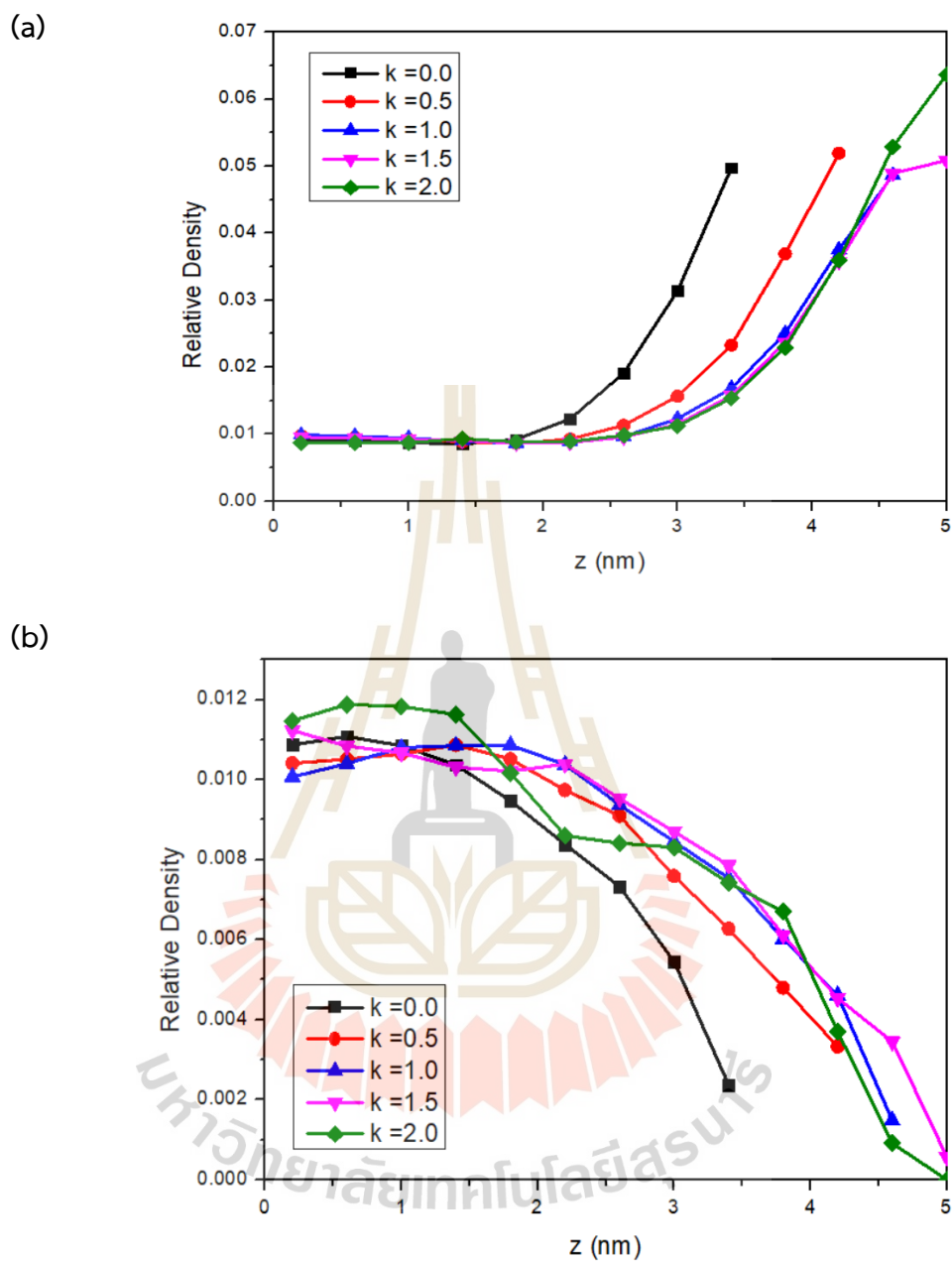


Figure 4.2.5 (a) Relative end-monomer and (b) middle-monomer densities of the free surface of polymer melts at different positions in the structures.

4.2.3 Bond orientation

The bond order parameter (S_b) is determined to evaluate the orientation of bonds in polymer surfaces as defined by

$$S = \frac{\langle 3\cos^2 \theta - 1 \rangle}{2} \quad (4.2.2)$$

where θ is the angle between a bond vector to the reference vector (the z axis) and $\langle \dots \rangle$ is the ensemble average. Thus, bonds tend to have parallel, random, and perpendicular orientations to the surface when $S_b = -0.5$, 0.0 and 1.0, respectively. As seen in Figure 4.2.6, both middle- and end-bonds exhibit random orientation in the bulk region. However, the opposite behavior is observed near the surface in that the end/middle bonds tend to be aligned in the normal/parallel direction to the surface. For stiffer chains, both end- and middle-bonds tend to have slightly more anisotropic orientation near the surface but no significant difference in the bulk region (except for data at $k = 2.0$ that chains have a greater fraction of *trans* conformation, especially for the middle-bonds which tend to have more anisotropy).

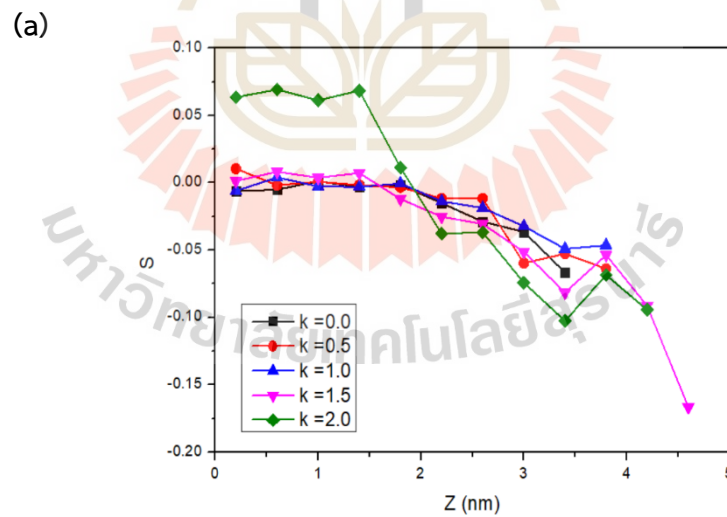


Figure 4.2.6 The order parameter of (a) middle-bonds and (b) end-bonds of the free surface of polymer melts.

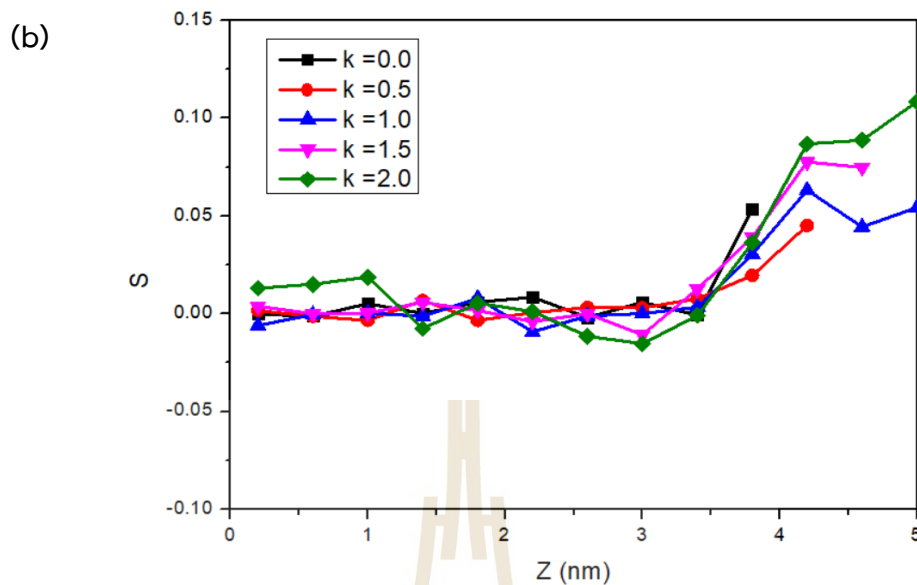


Figure 4.2.6 The order parameter of (a) middle-bonds and (b) end-bonds of the free surface of polymer melts (continued).

4.2.4 Molecular properties

To determine the distortion of molecular dimension for polymers with different degrees of chain stiffness, the mean square end-to-end vector, $\langle r^2 \rangle^{1/2}$, and the mean square radius of gyration, $\langle s^2 \rangle^{1/2}$ and three principal axes ($L_1 > L_2 > L_3$) derived from the radius of the gyration tensor were calculated and presented in Table 4.2.2. The size of more flexible chains is smaller as the polymer can adopt a greater amount of gauche conformation. As predicted theoretically by the freely jointed chain model at the long chain limit, the $\langle r^2 \rangle / \langle s^2 \rangle$ ratio should be 6.00. Simulation data give larger $\langle r^2 \rangle / \langle s^2 \rangle$ ratio in the range of 6.3 – 6.5 close to the prediction by the RIS model of $\langle r^2 \rangle / \langle s^2 \rangle = 6.5$ for normal polyethylene at the same chain length used in our simulation (Flory, 1969; Mattice, 1994).

In addition, polymer coils can be viewed as an equivalent ellipsoid defined by three principal axes ($L_1 > L_2 > L_3$). According to the freely jointed chain model, the $L_1^2 : L_2^2 : L_3^2$ ratio is theoretically equal to 11.7: 2.7: 1 (Solc, 1971). As presented in Table 4.2.2, the magnitudes of this ratio from the simulation are generally smaller for more flexible chains as they can form a compact shape due to a larger fraction of gauche

conformation. The overall shape of the polymer chain can be evaluated using the definition of acylindricity ($c = L_2^2 - L_3^2$) and asphericity ($b = L_1^2 - (L_2^2 + L_3^2)/2$) to represent the deviation from cylindrical ($c = 0.0$) and spherical shapes ($b = 0.0$). The acylindricity (asphericity) has noticeably changed from 0.098 (0.465) and 0.046 (0.230) for $k = 0.0$ and 2.0, respectively. These results suggest that the chain shape is more changed monotonically toward ellipsoid for more flexible chains.

To investigate the anisotropic change in molecular dimension relative to the surface, the XY (parallel) and the Z (perpendicular) components of the mean-squared radius of gyration are determined and depicted in Figure 4.2.7(a) and (b), respectively. The magnitudes of both quantities become larger for stiffer chains where the parallel (perpendicular) components are steadily increased (decreased) and then lower (higher) in the bulk and surface region, respectively. These results are due to chain flattening as polymers are forced to lie near the surface. As a function of the distance from the film center of mass, polymer chains are elongated/shrunk in the parallel/perpendicular direction, respectively, and have pancake-like shapes near the surfaces. The maxima in Figure 4.2.7(a) and the minima in Figure 4.2.7(b) are from the distortion of polymer chains that are confined near an essentially impenetrable surface.

In addition, the change of polymer dimension within the same chain at different positions on the surface can be monitored by the determination of the magnitude of L_1 and L_3 principal axes (normalized by the square radius of gyration). As presented in Figure 4.2.7(c), the magnitudes of both principal axes are larger for more flexible chains as they tend to distort more toward the oblate ellipsoid. The L_1 (L_3) eigenvalues are noticeably decreased (increased) near the surface.

Table 4.2.2 Chain dimension and shape parameters.

Chains	$\langle r^2 \rangle$ (nm ²)	$\langle s^2 \rangle$ (nm ²)	$\langle r^2 \rangle / \langle s^2 \rangle$	$\langle L_1^2 \rangle : \langle L_2^2 \rangle : \langle L_3^2 \rangle$	$\langle c \rangle / \langle s^2 \rangle$	$\langle b \rangle / \langle s^2 \rangle$
k = 0.0	8.29 ± 5.98	1.31 ± 0.54	6.34	9.35:2.59:1.00	0.098	0.465
k = 0.5	9.74 ± 7.13	1.55 ± 0.66	6.25	9.41:2.64:1.00	0.080	0.390
k = 1.0	11.85 ± 8.73	1.87 ± 0.81	6.32	10.15:2.74:1.00	0.066	0.328
k = 1.5	14.46 ± 10.89	2.27 ± 1.01	6.37	11.30:2.90:1.00	0.055	0.275
k = 2.0	17.89 ± 13.34	2.77 ± 1.22	6.46	12.16:3.07:1.00	0.046	0.230

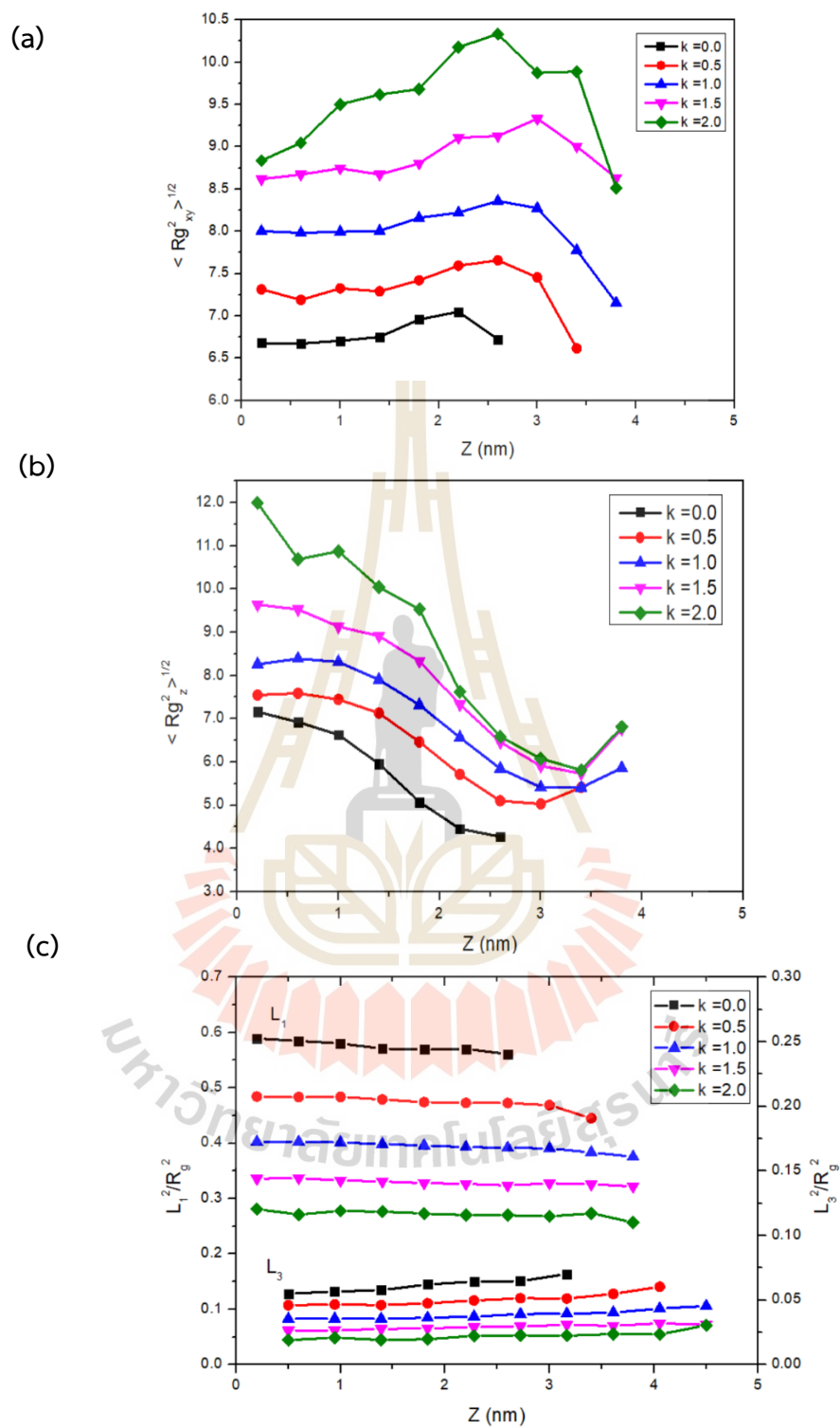
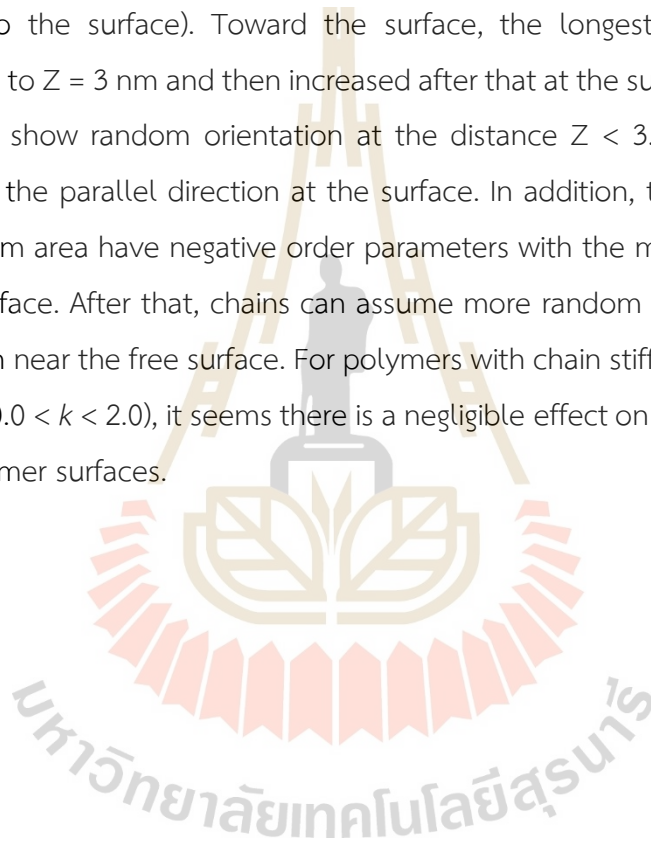


Figure 4.2.7 The components of the mean-squared radius of gyration in (a) the parallel (XY) and (b) the perpendicular (Z) direction to the surface and (c) the first and the third principal axes of polymer molecules.

4.2.5 Molecular orientation

Based on a similar definition to the bond order parameter. The molecular orientation can be evaluated by the calculation for the order parameter of L_1 and L_3 principal axes as the chain vectors. Figure 4.2.8 presents the orientation of L_1 and L_3 vectors relative to the surface. In the bulk region, both molecular axes are randomly oriented ($S = 0$) for most chains regardless of different degrees of chain stiffness (except for very rigid chains with $k = 2.0$, which have noticeable anisotropy in parallel orientation to the surface). Toward the surface, the longest vectors tend to be decreased up to $Z = 3$ nm and then increased after that at the surface. For the shortest vectors, they show random orientation at the distance $Z < 3.5$ nm and then have anisotropy in the parallel direction at the surface. In addition, the molecular vectors on the vacuum area have negative order parameters with the minimum position near the Gibbs surface. After that, chains can assume more random alignment at the low-density region near the free surface. For polymers with chain stiffness parameters used in this work ($0.0 < k < 2.0$), it seems there is a negligible effect on molecular orientation in these polymer surfaces.



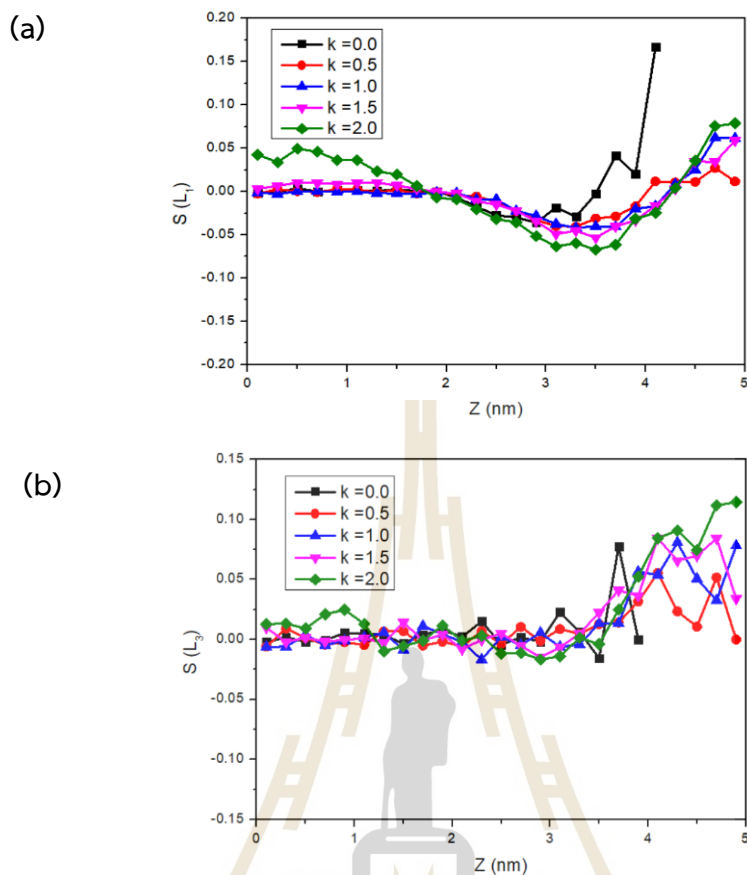


Figure 4.2.8 The chain order parameter of (a) the first and (b) the third principal axes of polymer chains.

4.2.6 Energetics

The intra- and intermolecular energies are presented in Figure 4.2.9 to compare quantitatively the energetics of polymer surfaces. For intramolecular energies in the bulk region, their magnitudes are higher for the more flexible chains due to more *gauche* conformation. In the surface region, intramolecular energies tend to be lower implying that chains have less amount of *gauche* conformation compared to those in the bulk region. For intermolecular energies, their magnitudes in the bulk region tend to be more negative (as the third shell energy is an attractive interaction with a minus sign, $u_3 = -0.625$ kJ/mol) for more flexible chains which are related to better chain packing. The situation is different in the surface region in that more flexible gain higher intermolecular energies because of the least efficient chain packing.

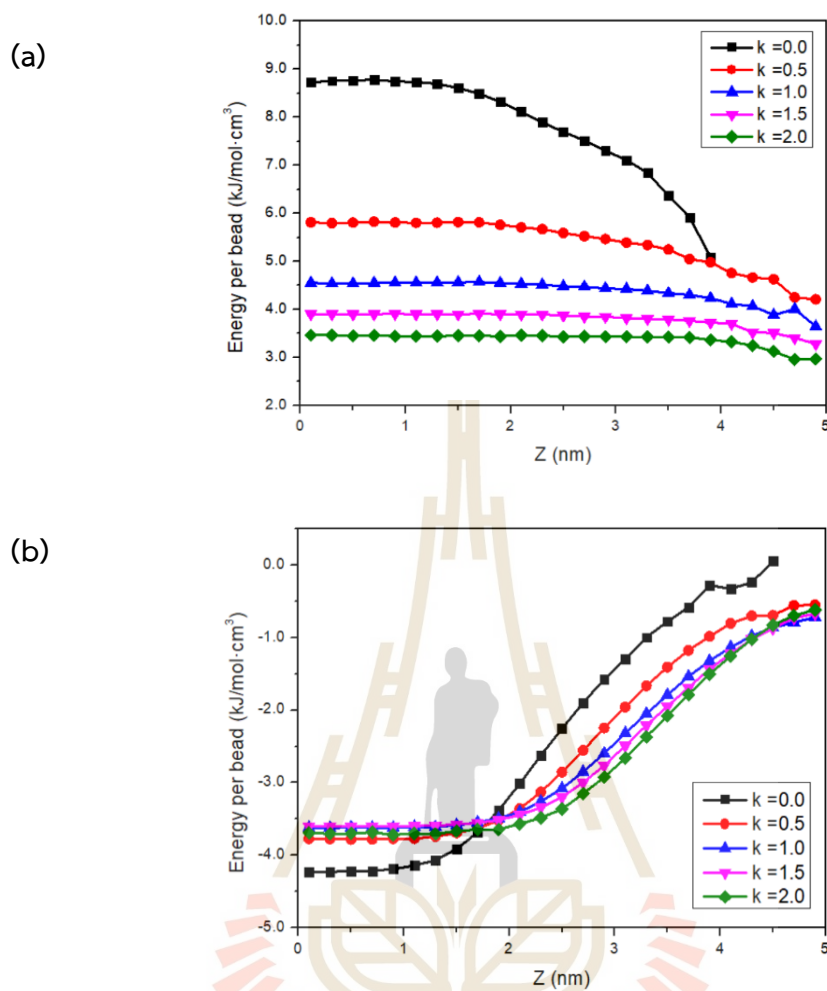


Figure 4.2.9 The profiles of (a) intramolecular and (b) intermolecular energies at different positions in polymer surfaces.

4.3 The effect of intermolecular interaction on polymer crystallization

The ionic conductivity of polymer electrolytes can be related to the ion diffusion in polymer matrices. In general, ions diffuse faster in the amorphous phase. Thus, the ability to control the crystallization characteristics should be important to control the amount of crystalline portion in polymeric materials. One possibility is to add the functional group or modify chain structures to manipulate the intermolecular between chains such as perfluoro-poly(ethylene oxide): $-\text{[CH}_2\text{CH}_2\text{O]}-$ vs $-\text{[CF}_2\text{CF}_2\text{O]}-$ and vinyl polymer $-\text{[CH}_2\text{CHCl]}-$ vs. $-\text{[CH}_2\text{CHF]}-$. Thus, this section will focus on the effect of the intermolecular interaction on polymer crystallization from the molten state investigated by MC simulation. To generalize the effect of different intermolecular interaction, the *PE-like* models were proposed using the same bead dimension ($\sigma = 0.44$ nm) but different potential well depth ($\epsilon/k = 125 - 205$) for more repulsive and more attractive interactions compared to the normal PE chains ($\epsilon/k = 185$).

4.3.1 Equilibration

Figure 4.3.1 presents the change in the intra- and intermolecular energies for *PE-like* models with different intermolecular interactions at 0-10 million MCS (473 K), 10-20 million MCS (400 K), 20-30 million MCS (350 K) and 30-100 million MCS (298 K). With the same CG bead dimension ($\sigma = 0.44$ nm), *PE-like* chains can be considered more attractive ($\epsilon/kT > 185$ K) or more repulsive interaction ($\epsilon/kT < 185$ K) than that of normal PE ($\epsilon/kT = 185$ K). The average values of intramolecular (intermolecular) energies during 50-100 million MCS (298 K) for E125, E145, E165, E185, and E205 are 2760.28+203.90 (-2528.08+44.29), 2132.73+231.70 (-3560.97+55.04), 1891.98+189.44 (-4681.03+50.37), 2155.75+151.38 (-5986.06+52.35) and 2513.75+133.23 (-7130.34+40.28) kJ/mol, respectively. In general, at lower temperatures, chains gain a larger fraction of the *trans* state (see Figure 4.3.4). As the conformational energy of the *trans* state is lower than the *gauche* state, the intramolecular energies become lower. In addition, the intermolecular energies become smaller as polymers can stay closer to other chains. Polymers with more repulsive interaction can have larger intramolecular energies (with larger fluctuation as indicated by the standard deviation) because their bonds tend to adopt more *gauche* conformation (with a higher degree of conformational interconversion).

For polymers with more attractive interaction (E205), chains can have a larger intramolecular energy implying a smaller amount of *trans* conformation. Note that chains in the E165 system have the lowest intramolecular energy. Thus, chains with a slightly more repulsive interaction than that of normal PE seem to have a larger amount of *trans* conformation. For the intermolecular energies, there is a systematic decrease as a function of intermolecular interaction parameters (ϵ) implying that the CG beads can stay closer to others for beads with more attractive interaction and the formed structures at lower temperatures tend to be more densely packed.

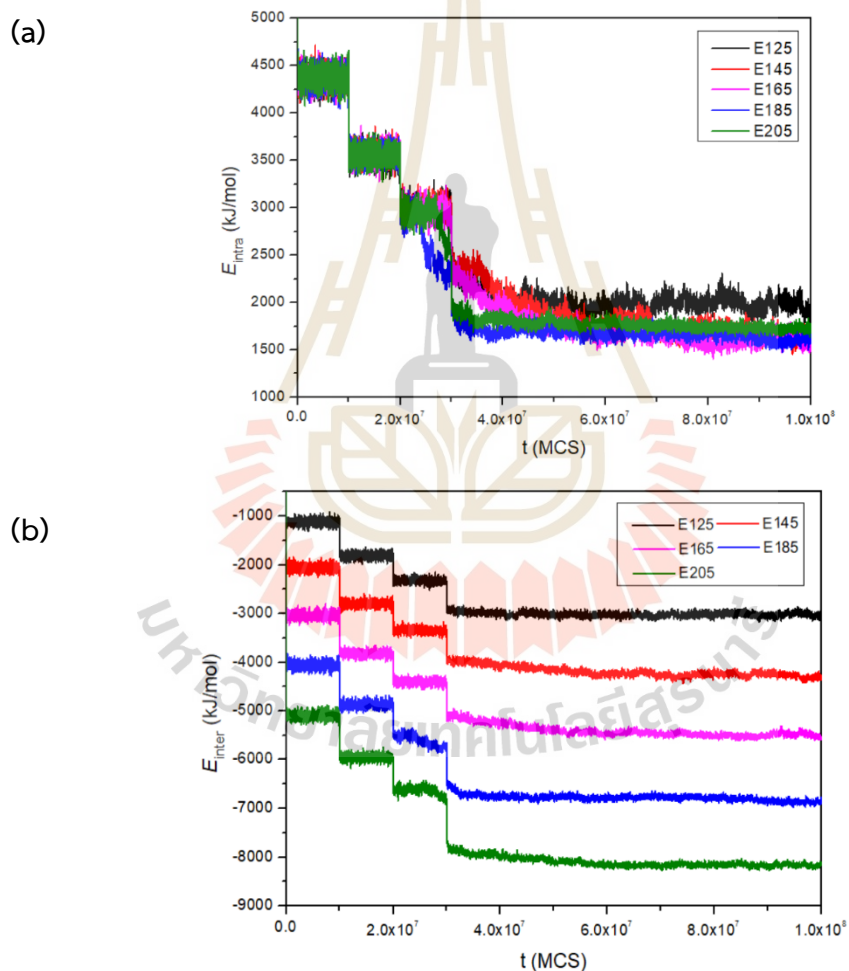


Figure 4.3.1 (a) Intramolecular energies (E_{intra}) and (b) intermolecular energies (E_{inter}), of *PE-like* chains with different intermolecular interactions.

Chain relaxation was determined using the orientational auto-correlation function (OACF) of the normalized end-to-end vector, $\langle \mathbf{R}(t) \cdot \mathbf{R}(0) \rangle / (\mathbf{R}^2)$ and the mean square displacement (MSD) for the chain center of mass, $g_{cm}(t) = \langle [\mathbf{R}_{cm}(t) - \mathbf{R}_{cm}(0)]^2 \rangle$ where the end-to-end vector and the center of the mass of chains at time t is denoted by $\mathbf{R}(t)$ and $\mathbf{R}_{cm}(t)$, respectively. As seen in Figure 4.3.2(a), the OACFs at 298 K suggest that the more repulsive chains exhibit faster relaxation in the rotational mode as the structures are less dense with more space for chain reorientation.

For the translational motion, according to the dynamics predicted by the Rouse model for ideal chains, the MSDs should exhibit the Fickian diffusive characteristics ($t^{1.0}$). Usually, the MSDs can show a sub-Fickian regime, t^n ($n < 1.0$) for $t < \tau_R$ where τ_R is the Rouse time or the relaxation time of the chain end-to-end vector. After that, the MSDs can exhibit the Fickian behavior at longer time. It was reported that MC simulation of CG PE melts on the $2nnd$ lattice at 473 K exhibited the Rouse dynamics (Baschnagel, 2000). Here, the dynamics at 298 K for PE-like chains with different intermolecular interactions are explored. From the MSDs data at 298 K shown in Figure 4.3.2(b), the scaling numbers in the sub-Fickian regime and at the long-time limit are proportional to $t^{0.79}/t^{0.74}/t^{0.65}/t^{0.43}/t^{0.30}$ and $t^{0.93}/t^{0.82}/t^{0.75}/t^{0.68}/t^{0.65}$, respectively, for chains in E125/E145/E165/E185/E205 systems. Generally, the scaling numbers are larger for chains with more repulsive interaction. The scaling numbers for all cases are less than 1.0. Thus, the non-Fickian characteristics are observed at both sub-diffusive regimes and the long-time limit at 298 K indicating the effect of intermolecular interaction with their neighboring CG beads.

The monomer dynamics at 298 K can be quantified in terms of the MSDs of individual CG beads as depicted in Figure 4.3.2(c). In general, monomer beads with more repulsive interaction have faster dynamics. Furthermore, the magnitudes of monomer MSDs are increased significantly for the monomers near the chain ends. As discussed previously, this MC method with the current CG polyethylene model gives dynamic characteristics comparable to data obtained from MD simulations of fully atomistic models or experiments with real polymers (Doruker, 1998; Baschnagel, 2000).

Note that chain dynamics are very slow at 298 K because polymers adopt almost all *trans* conformation, and the local chain packing becomes denser. The non-Fickian behavior from the scaling analysis of the MSDs may be caused by the influence of the interaction from nearby chains or a short simulation run with 100 million MCS trajectories. Longer simulation runs should be possible to completely relax the systems, but at the present, it is still impractical based on this MC simulation due to the formidable computational time. Nevertheless, the data presented here are still useful to see the general characteristics of an initial stage of polymer crystallization from the melts.

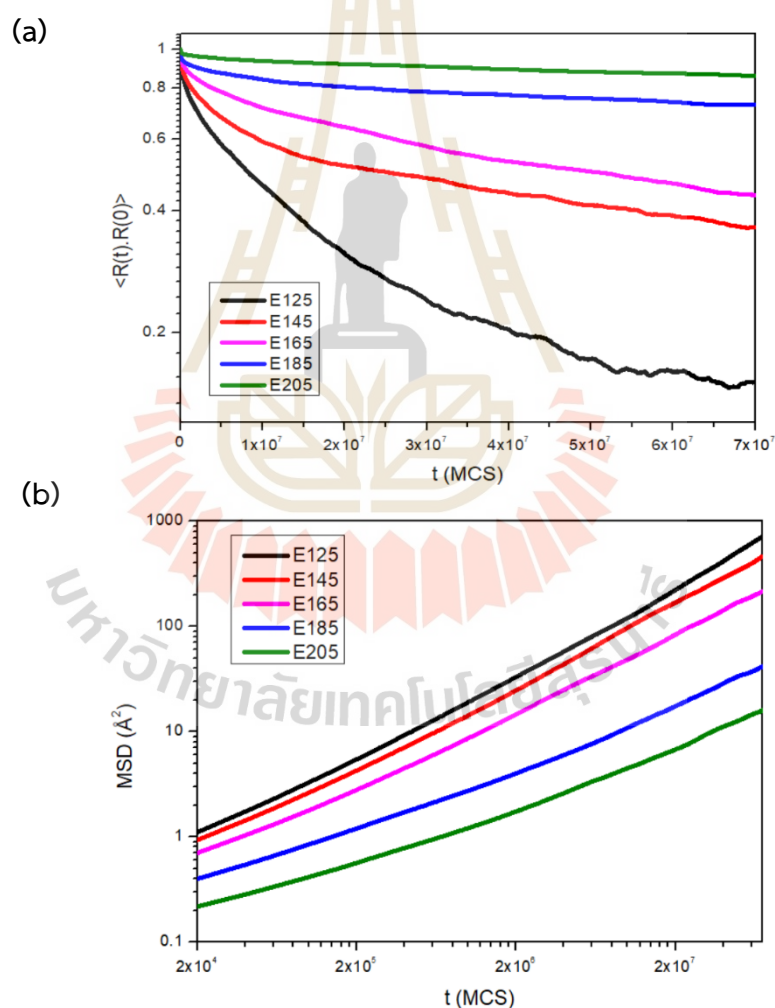


Figure 4.3.2 (a) The OACFs of the chain end-to-end vectors (b) the MSDs of the chain center of mass and (c) the MSDs of individual CG beads of PE-like models with different intermolecular interactions at 298 K.

(c)

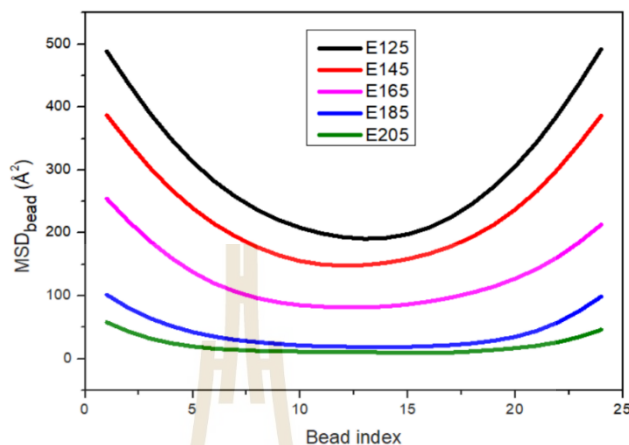
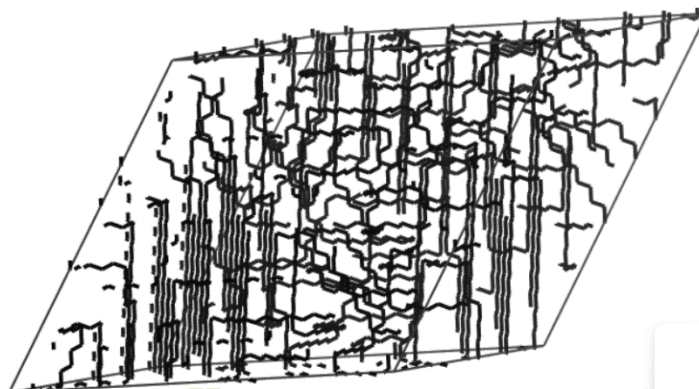


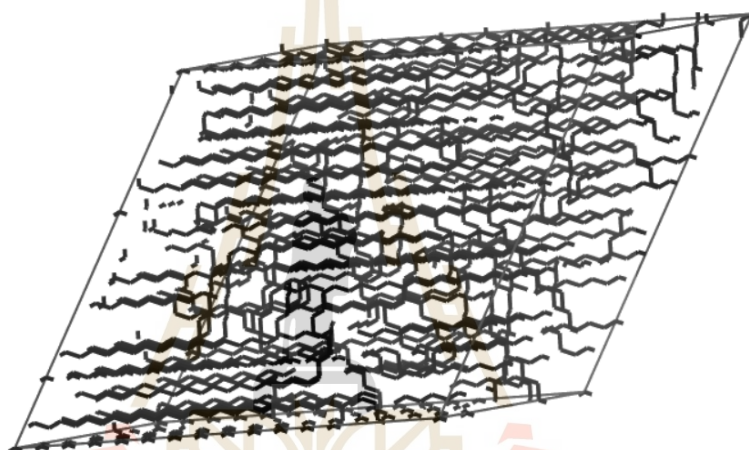
Figure 4.3.2 (a) The OACFs of the chain end-to-end vectors (b) the MSDs of the chain center of mass and (c) the MSDs of individual CG beads of PE-like models with different intermolecular interactions at 298 K (continued).

Figure 4.3.3 presents the final structures at 298 K after 100 million MCS trajectories. Denser structures are seen for chains with more attractive interactions while the less-dense structures are observed for chains with stronger repulsion. When the intermolecular interaction becomes more attractive, chains can be located closer to each other so that the “local packing” with nearby CG beads up to the 8th shell in the 2nd lattice becomes denser with the magnitudes of the pair correlation functions (PCF) ordered as $E205 > E185 > E165 > E145 > E125$ (see Figure 4.3.9). In addition, the averaged values of *trans* fractions and the relative amplitude of chain ordering become lower in cases of too repulsive or too attractive interaction. The fraction of *trans* conformation and the magnitude of chain order parameters are $E145 > E165 > E185 > E205 > E125$ (Figure 4.3.4) and $E165 > E185 > E145 > E205 > E125$ (Figure 4.3.5), respectively. Thus, polymers still have some *gauche* conformation with a lower degree of chain ordering, especially for the most repulsive ($\epsilon/k = 125$ K) and the most attractive ($\epsilon/k = 205$ K) interactions.

(a) $E = 125$



(b) $E = 145$



(c) $E = 165$

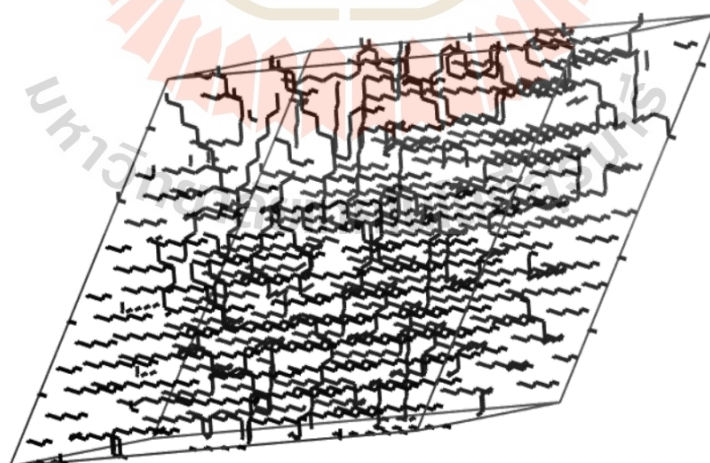


Figure 4.3.3 The final structures after 100 million MCS trajectories at 298 K of PE-like models with different intermolecular interactions (a) E125, (b) E 145 (c) E165 (d) E185 and (d) E205 systems.

(d) $E = 185$



(e) $E = 205$

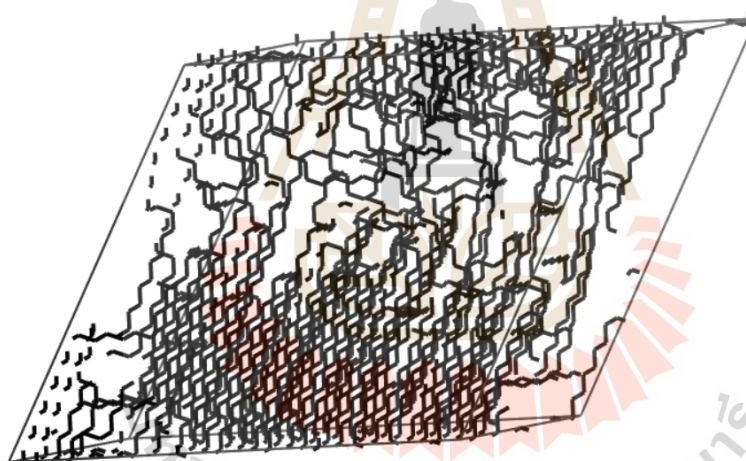


Figure 4.3.3 The final structures after 100 million MCS trajectories at 298 K of PE-like models with different intermolecular interactions (a) E125, (b) E 145 (c) E165 (d) E185 and (d) E205 systems (continued).

4.3.2 Conformation

Figure 4.3.4 presents the *trans* fraction of polymer chains at different temperatures upon cooling from the melts. The smallest magnitudes of the *trans* fractions are seen at 473 K and become higher at lower temperatures. At 298 K (during

50-100 million MCS), the averaged values of the *trans* fractions, are 0.762 ± 0.057 , 0.810 ± 0.059 , 0.829 ± 0.071 , 0.825 ± 0.086 , and 0.814 ± 0.081 for chains in E125, E145, E165, E185, and E205 systems, respectively.

Generally, the amplitudes of *trans* fraction tend to be larger for chains with more repulsive interaction except in the E125 system (the most repulsive chains) which exhibits the smallest amount of *trans* fraction than other cases. This is probably because polymers can have more space to interchange the conformation between *trans* and *gauche* states. For chains with more attractive interaction than normal PE, polymer chains in the E205 system can adopt a lower fraction of *trans* conformation. As polymers adopt a larger amount of *gauche* state in the melts (473 K), it should be more difficult for chains with stronger attractive interaction to convert their conformation to the *trans* state at 298 K. Thus, chains with too repulsive and too attractive intermolecular interactions could adopt a lower amount of *trans* conformation at 298 K upon cooling from the melts.

In addition, the magnitude of the *trans* fraction can be increased significantly during 20-30 million MCS (350 K) for chains with different intermolecular interactions in the order of $E185 > E205 > E165 > E145 \geq E125$. These results show that the normal PE chains have the fastest growth to adopt the *trans* conformation at 350 K followed by chains with slightly more attractive (E205) and slightly more repulsive (E165) intermolecular interaction. Note that even though the normal PE exhibits the fastest growth at 350 K, the final magnitude of the *trans* fraction is not the largest, but it is still smaller than that of the E165 system. Note that there is still a slight increase of the *trans* fraction. Longer simulation at 298 K up to 200 million MCS was also done but the overall results are not significantly different for comparing all systems. Thus, all results reported in this work are based on this 100 million MCS trajectory to focus on the initial stage of structural formation at this temperature.

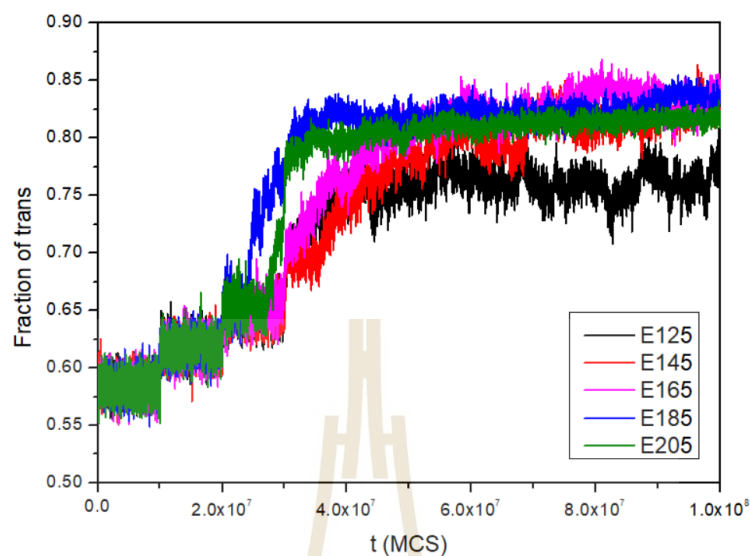


Figure 4.3.4 The fraction of trans conformation of PE-like models with different intermolecular interactions.

4.3.3 Chain dimension

The mean square radius of gyrations, $\langle R_g^2 \rangle$, is used to represent the chain dimension as presented in Figure 4.3.5. At 400 K and 473 K, the magnitudes of $\langle R_g^2 \rangle$ are relatively fluctuated around the constant values and become larger for more repulsive chains. Then, $\langle R_g^2 \rangle$ is increased during 20 - 40 million MCS (at 350 K) in most systems, especially for more attractive chains in E205 with the fastest growth comparable to the normal PE chains. At 298 K, the molecular dimension, averaged during 50-100 MCS, for all the chains can be ordered as $E145 \geq E165 > E185 \geq E125 > E205$ with the averaged magnitude and the standard deviation of 125.93 ± 7.22 , 136.66 ± 8.01 , 133.40 ± 7.19 , 126.18 ± 3.45 and 122.94 ± 2.66 respectively. Except for the E125 systems (the most repulsive chains), the more repulsive chains generally tend to have larger chain dimensions and larger fluctuations. This is because the CG beads tend to stay away from others and polymer chains are more expanded and have more frequent conformational changes. As expected, the more attractive chains (E205 system) have the smallest magnitude of chain dimension and standard deviation as polymers become more compact and get denser structures. Chains with too repulsive

and attractive interactions exhibit smaller chain dimensions because polymers can adopt a larger amount of *gauche* conformation as described in the previous section. Thus, only polymers with the appropriate intermolecular interaction parameters (close to normal PE) can exhibit the largest chain dimension upon stepwise cooling from the molten state.

4.3.4 Chain orientation

To monitor the signal of crystal formation, the overall orientation order parameter of polymer chains, S_G , can be calculated according to In this calculation, polymer coils are viewed as the ellipsoid shape with three molecular axes ($L_3 < L_2 < L_1$) obtained from the diagonalization of the radius gyration tensor. The longest (L_1) axis was chosen to determine for chain orientation. Here, the angle (θ) is formed between two L_1 axes from different chains so that the random and parallel orientation can be represented by $S_G = 0$ and 1, respectively.

$$S_G = \frac{1}{2}[3\langle \cos^2 \theta \rangle - 1] \quad (4.3.1)$$

In this calculation, polymer coils are viewed as the ellipsoid shape with three molecular axes ($L_3 < L_2 < L_1$) obtained from the diagonalization of the radius gyration tensor. The longest (L_1) axis was chosen to determine for chain orientation. Here, the angle (θ) is formed between two L_1 axes from different chains so that the random and parallel orientation can be represented by $S_G = 0$ and 1, respectively.

As seen in Figure 4.3.6, S_G for all systems is about zero (random orientation) during the first 20 million MCS (473 and 400 K). Then, S_G for normal PE and slightly more attractive chains (E185 and E205) start to increase during 20-30 million MCS (350K) while chains with more repulsive interaction still assume random orientation but their S_G starts to increase at 298 K. The MCS for chains starting to have more ordered orientation can be arranged as E185 > E205 > E165 = E125 > E145. These results imply that only chains with the appropriated intermolecular interaction close to normal PE can exhibit a faster growth of chain orientation. Slightly attractive chains can draw nearby molecules to induce the ordered orientation even at 350 K. At 298 K, the

magnitudes of S_G averaged during 50-100 million MCS are E125 (0.346 ± 0.093), E145 (0.677 ± 0.104), E165 (0.778 ± 0.061), E185 (0.767 ± 0.042), E205 (0.553 ± 0.024).

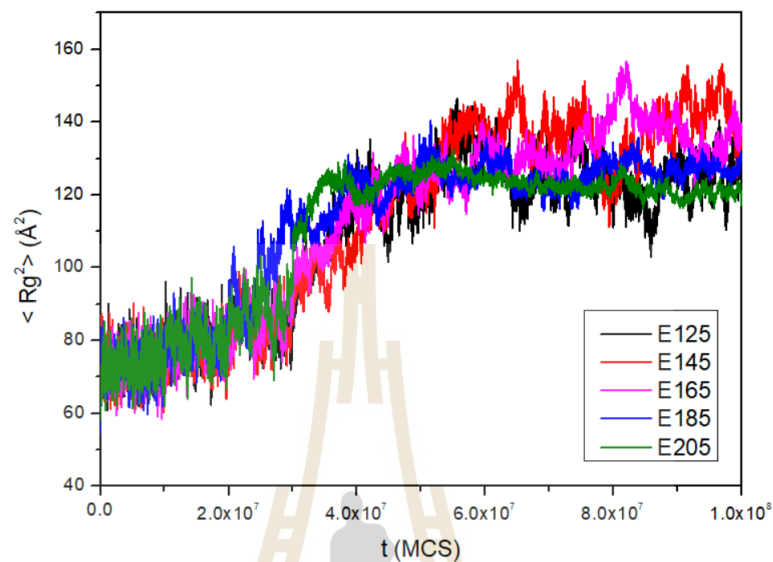


Figure 4.3.5 The mean square radius of gyration of PE-like models with different intermolecular interactions.

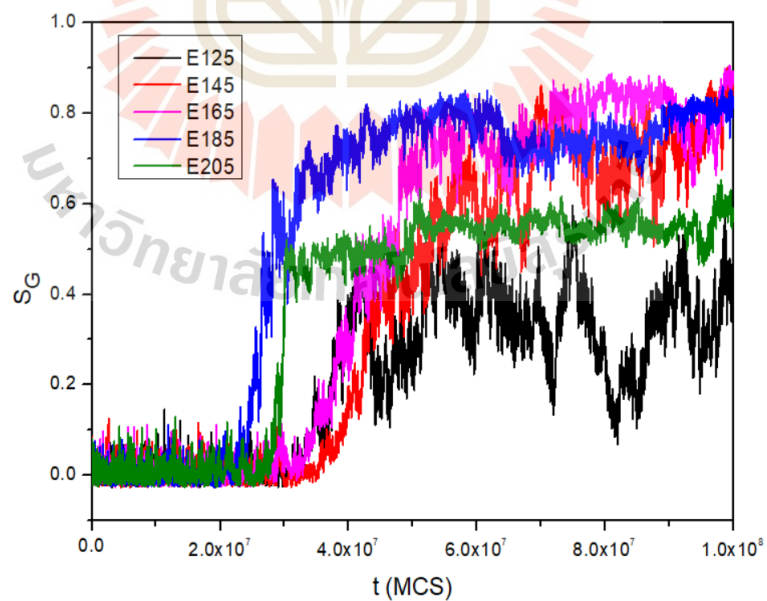


Figure 4.3.6 The global order parameter for PE-like models with different intermolecular interactions.

Upon crystallization, PE chains should gain a larger fraction of *trans* state and have a higher degree of intramolecular bond correlation. The first-order intramolecular bond order parameter, $M_1(j)$ can be calculated to evaluate the bond correlation in the same molecule according to

$$M_1(j) = \langle m_i \cdot m_{i+j} \rangle = \langle \cos \theta_{i,i+j} \rangle \quad (4.3.2)$$

Here, $\theta_{i,i+j}$ is the angle between $(i+j)$ th and (i) th bonds within the same chain. The characteristics of $M_1(j)$ for intramolecular bonds in the ordered structures formed at 298 K are presented in Figure 4.3.7. Generally, the magnitudes of $M_1(j)$ should be smaller as a function of the bond index (j) as polymers adopt a larger amount of the *gauche* state at the further bonds apart. For all systems, $M_1(j)$ reaches 0.0 (disordered) around the 10th bond. For comparison, $M_1(j)$ for chains in E205 dropped to 0.0 at the fastest growth followed by E185 and E125, respectively. Thus, chains with slightly more attractive interaction can have a more disordered intramolecular bond correlation for $j \leq 10$ even though chains with more repulsive interaction in E125 have a larger fraction of *gauche* conformation (see Figure 4.3.4). For bond index $j > 10$, the magnitudes of $M_1(j)$ can be less than 0.0 and can be generally proportional to the strength of intermolecular interaction in the ordered as E205 < E125 < E145 < E165 < E185. Note that the data for E205 has the lowest amplitude at the j index around 10 but then exhibits the upturn to have the largest value at $j \geq 16$ with $M_1(j)$ close to zero. These results suggest that intramolecular bonds in E205 exhibit the most disordered orientation due to the attractive interaction between chains.

For chains with more repulsive intermolecular interaction, $M_1(j)$ exhibits monotonically decayed profiles with the magnitude for bond $j > 10$ closer to 0.0 for more repulsive chains. These findings suggest that the anisotropy of intramolecular bond correlation should be related to the intermolecular interaction between chains and the intramolecular bond orientation becomes more disordered for more repulsive chains at $j > 10$ bonds. Thus, for chains with too repulsive or attractive interaction, the bonds within the same chains tend to exhibit more disordered orientation in their crystal structures formed under stepwise cooling from the molten state. For chains

with too repulsive interaction, bonds in the same chains can adopt a larger amount of gauche conformation resulting in a lower degree of intramolecular bond correlation. For chains with too attractive interaction, the gauche conformation that occurred in the melt state can not be effectively converted to the trans state. Thus, there is still some amount of gauche conformation which also results in a lower degree of intramolecular bond correlation. The more repulsive chains, the more disordered the orientation for bonds within the same chains.

Next, the intermolecular bond orientation order (S_L) is calculated to determine the bond orientation between different molecules according to

$$S_L(n) = \frac{1}{2} [3 \langle \cos^2 \psi(n) \rangle - 1] \quad (4.3.3)$$

where $\psi(n)$ is the angle between two bonds at the reference position and the n th shell in the $2nd$ lattice.

Figure 4.3.8 presents the intermolecular bond orientation order for each system at 298 K. Generally, the magnitudes of S_L are near 0.0 in the first shell (bonds tend to be random orientation) due to the most repulsive non-bonded interaction so that the bond can be oriented in any direction. Then bonds show the largest degree of anisotropic arrangement in the second shell (equivalent to the distance at 0.5 nm). For bonds in the further shells, the magnitudes of S_L are monotonically lower implying that intermolecular bond orientation tends to be a more random arrangement at the longer separated distance. The relative magnitudes of S_L in each system can be ordered as: E165 < E185 << E205 < E145 << E125. A large magnitude of S_L (higher degree of intermolecular bond correlation) can be observed for the E185 and E165 systems. Thus, bonds in normal PE and the chains with slightly more repulsive interaction exhibit the highest correlation due to the most ordered structures formed upon stepwise cooling from the melts. Note that for chains with more attractive interaction (E205), intermolecular bond orientation can have a higher correlation than those bonds in more repulsive chains (E205 < E145 << E125). Thus, chains with excessive attractive or repulsive interaction should induce the intermolecular bonds to become more random orientation.

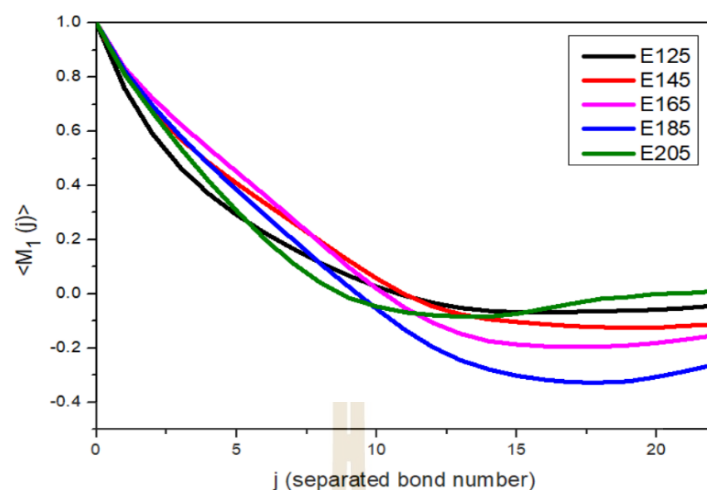


Figure 4.3.7 The intramolecular bond orientation correlation functions for PE-like models with different intermolecular interactions.

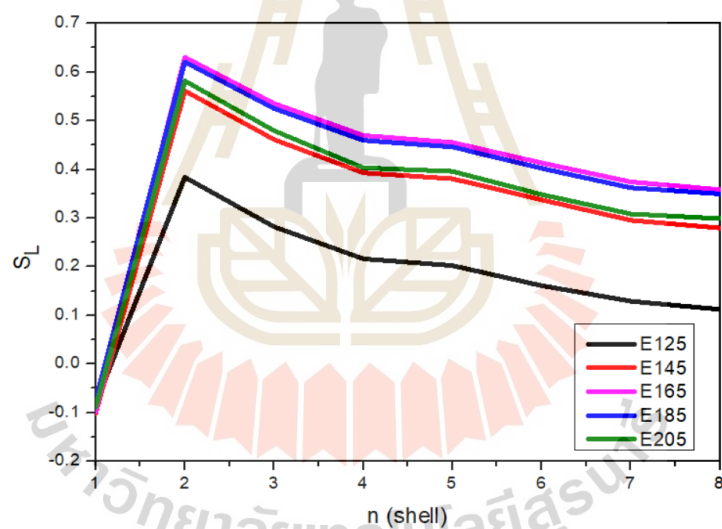


Figure 4.3.8 The correlation function of intermolecular bond orientation for PE-like models with different intermolecular interactions.

4.3.5 Structural packing

Structural packing was evaluated in terms of the intermolecular pair correlation function (PCF) calculated from the probability of having two CG beads at different shells on the 2nd lattice according to

$$g_{AA}(i) = \frac{\langle n_{AA}(i) \rangle}{(10i^2 + 2)V_A} \quad (4.3.4)$$

where, $n_{AA}(i)$ is the number of CG beads at the i th shell from the reference bead; V_A is the volume fraction of CG beads in 2nd lattice ($V_A = 0.225$). $10i^2 + 2$ is the coordination number of the i^{th} shell. Figure 4.3.9 depicts the PCFs for *PE-like* chains with different intermolecular interactions at 298 K. The PCFs exhibit the maxima in the third shell due to the most attractive interaction of the discretized LJ energies on the 2nd lattice. The magnitudes of PCFs tend to be smaller for further shells and have almost the same values after the 7th shell. The magnitudes of PCFs can be generally compared as: E205 > E185 > E165 > E154 > E125. These data suggest that CG beads can stay closer to each other as a function of the intermolecular interaction parameters. For more attractive interaction, the chain packing becomes denser. The trend seen in the PCFs is different from the behavior of the order parameter (S_G) and the amount of *trans* conformation as the PCFs are evaluated at the scale of CG beads. For example, chain properties (order parameter and *trans* fraction) in the more attractive (E205) system can be lower even though the magnitudes of PCFs are higher.

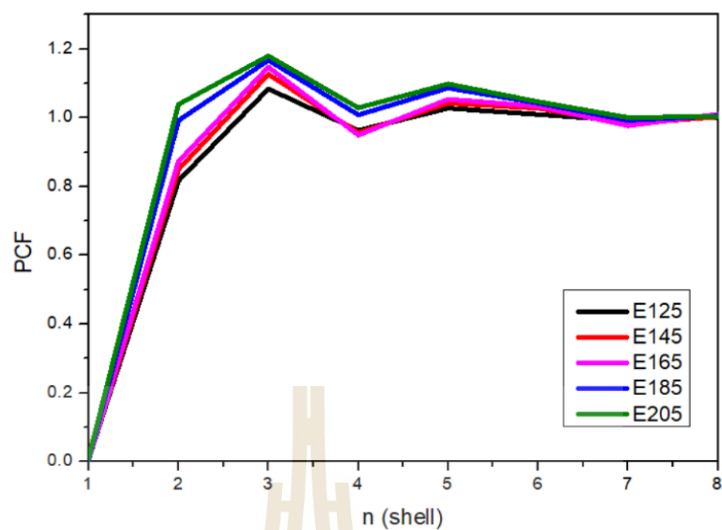
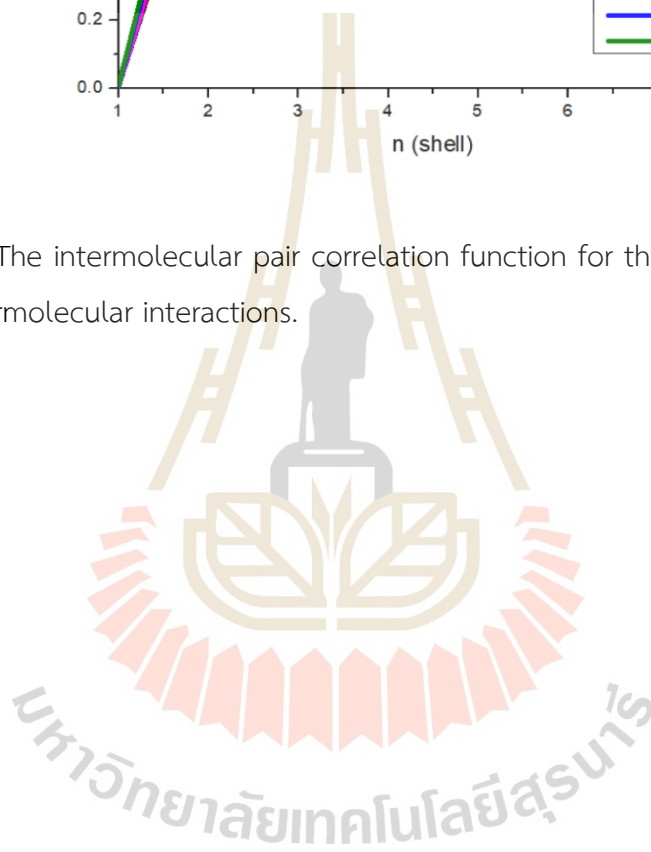


Figure 4.3.9 The intermolecular pair correlation function for the *PE-like* models with different intermolecular interactions.



4.4 Molecular dynamics (MD) simulation of detailed structures and ion transportation of polymerized ionic liquid/ionic liquid blends

This section will mainly focus on both molecular dynamics simulations and experimental studies of polymerized ionic liquids (Pbvim-TFSI) and polymerized ionic liquids-ionic liquids blends (PbvimTFSI-BmimTFSI). Characterizing transport properties of such blends and thereby address the manner by which conductivity can be tuned by the addition of pure ILs to polyILs.

4.4.1 Validated method for equilibration: PolyIL-IL Blends at 600K.

4.4.1.1 Indicating a sufficient structural equilibration for the simulated systems

Equilibration of the polymer systems such as IL, PolyIL and PolyIL-IL blends can be determined by evaluating the potential energy and density. As depicted in Figure 4.4.1 and Figure 4.4.2, after initial setup or after change of parameters, system is out of equilibrium. And its properties will not be stationary, so we are interested in equilibrium, must wait for a number of time steps to reach equilibrium before measuring observables. In most cases, there are two types of checks that the system enters equilibrium as follows: density and radius of gyration is molecular size values. And the reason for not using potential energy determines to enter equilibrium because sometimes the energy is stationary but has not yet reached equilibrium. So that the system reaches its equilibrium, show that no drift in density and the radius of gyration (R_g) of polymer chains were observed. So, the structures in IL, PolyIL and PolyIL-IL blends in Figure 4.4.3 are reached equilibrium.

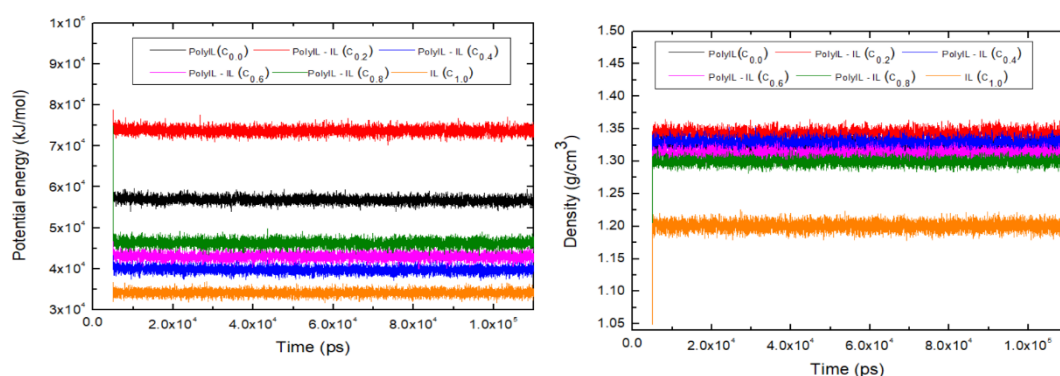


Figure 4.4.1 Time evolution of potential energy (left) and density (right).

4.4.1.2 Radius of gyration (R_g): Molecular size

Results for chain dimension are presented in Table 3.2 and Figure 4.4.2 The R_g and R_{ee} for chains in the PolyIL-IL blend systems decreased slightly from the pure PolyIL. But the value of R_g and R_{ee} for blend systems are a significant decrease. For previous experiment from Matsumoto et al. (Matsumoto, 2019), they studied about the rheological properties of PIL in IL solutions are strongly influenced by the electrostatic screening between IL and PIL chains. These their results indicate that polymerized ionic liquid chains shrink as the ionic liquid concentration increases at lower concentrations due to the charge screening effect by the same mechanism as that for ordinary polyelectrolytes in salt solutions but start to expand at higher ionic liquid concentrations due to the charge underscreening effect. In our study, chains in the PolyIL-IL blends and in the pure PolyIL gave similar R_g and R_{ee} values (see Table 3.2 : Chapter III), and the behavior mentioned above possibly also occurred in our simulated systems.

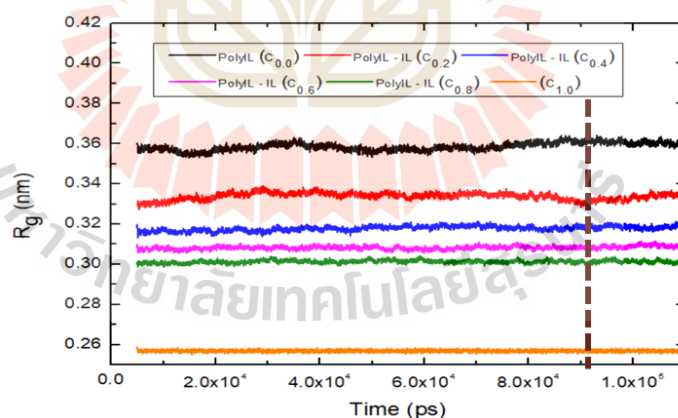


Figure 4.4.2 Time evolution of the radius of gyration (R_g) for IL, PolyIL and PolyIL-IL blends from the 110 ns equilibration runs. The dashed lines indicate the equilibration time of the R_g .

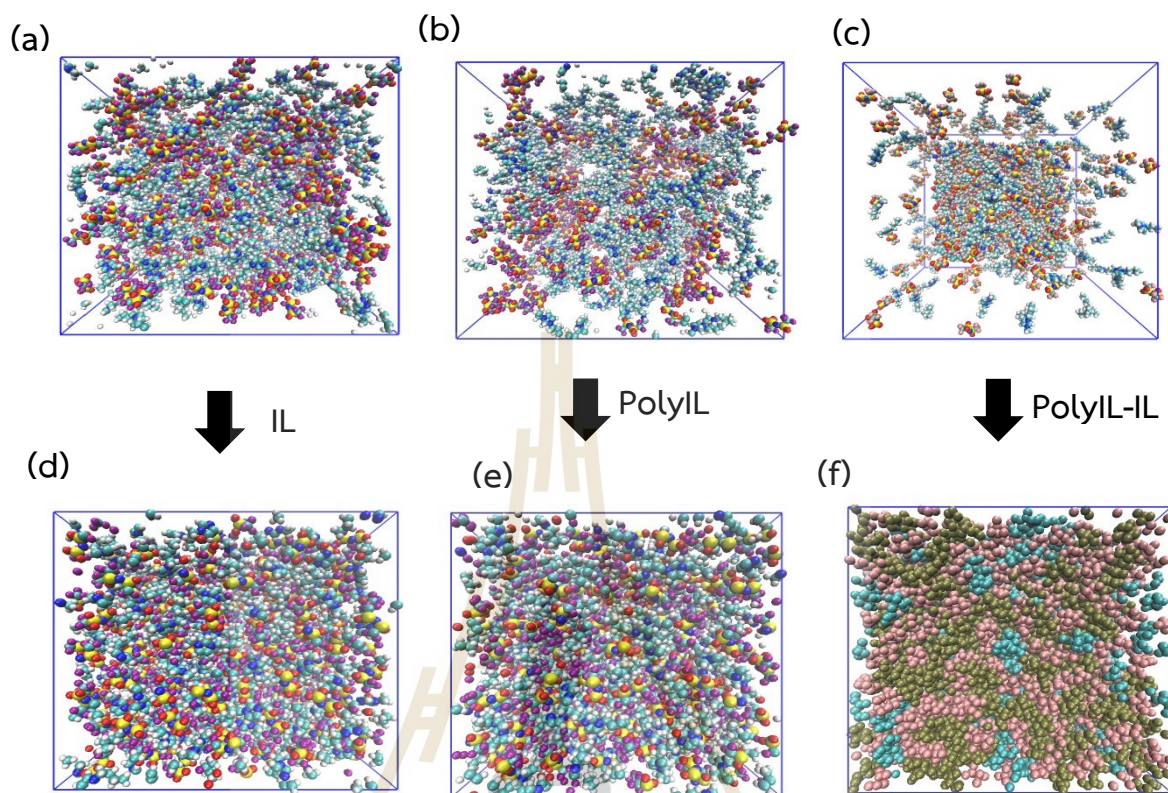


Figure 4.4.3 The initial [non-equilibrium] : (a), (b) and (c) and final structures [equilibrium] : (d), (e) and (f) at 600 K.

4.4.2 Polymer dynamics: PolyIL-IL Blends

4.4.2.1 The mean squared displacement (MSD) and Diffusion coefficient (D)

The dynamics of polymer chains were studied both in terms of translational and orientational mobility. For the definition of MSD at the time of reaching equilibrium at infinity because if the system moves in a straight line, the system enters a diffusive regime, meaning it moves in a straight line with no change in slope. Therefore, if the running time increases but the system's trajectory remains constant, we conclude that time is used in simulation is infinite time of system to reach equilibrium. For the definition of time-dependent diffusion coefficient (D), derived from the mean squared displacement (MSD) using the Einstein relation. Form the results of MSD from figure 4.4.4: (a), (b) and (c), indicated that the translational motion of systems, BMIM⁺ and

TFSI⁻ ions increases monotonically with increasing IL concentrations. And Bmim⁺ has the fastest motion in reaching equilibrium. In addition for figure 4.4.4(d), polycation motions and diffusivities are not easy to obtain for longer polymer chains, we neglect the diffusive calculation of polycations (Zhang, 2020). For the results of diffusion coefficients in Figure 4.4.5(a), (b) and (c), showed that increasing of temperature and concentration of ionic liquids (ILs) effect to improve for diffusion coefficient of all species in PolyIL-IL blends. For figure 4.4.5(d), from the example of diffusion at a temperature of 300 K, it is found that when in the PolyIL system, TFSI⁻ anions move the fastest. But when ionic liquids are added, the results show that they will be found that cations move the fastest in the blend system but both of Bmim⁺ and TFSI⁻ gave similar of diffusion coefficient. Therefore, it can be concluded that the diffusion coefficients increase after adding IL into the PolyIL system and increases temperature.

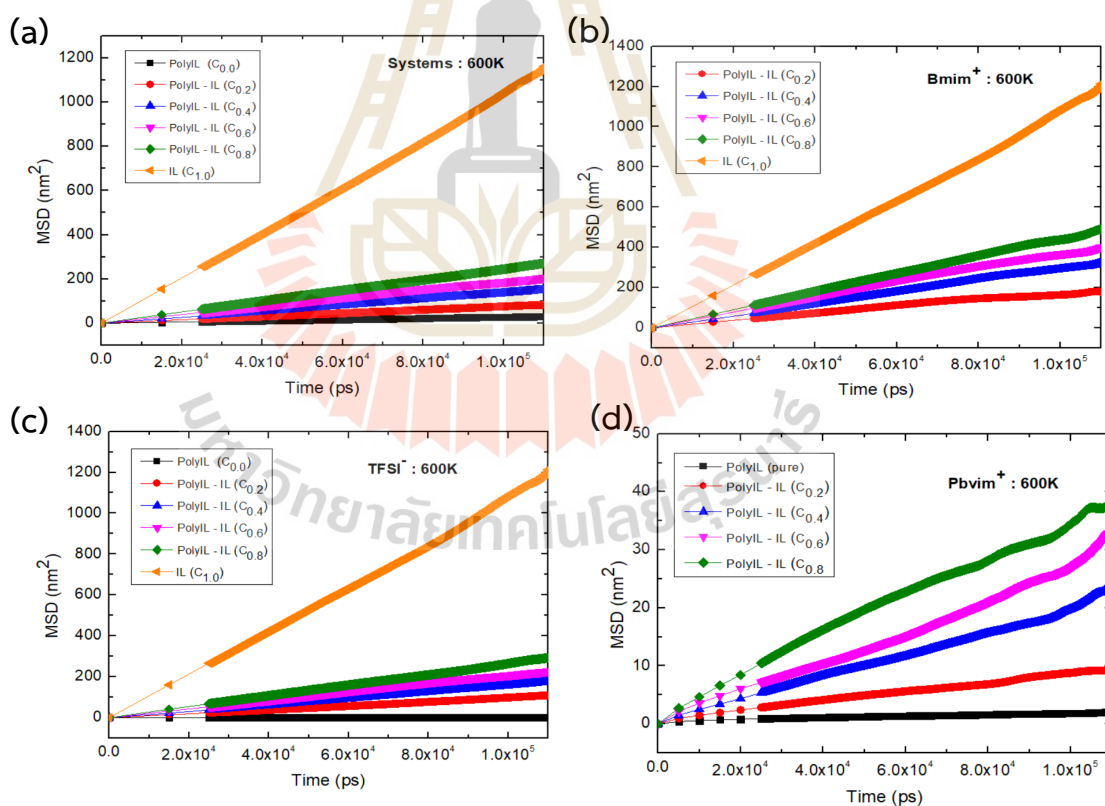


Figure 4.4.4 The mean-square displacement for the center of mass of (a) PolyIL-IL blends, (b) Bmim⁺ cation, (c) TFSI⁻ anion and (d) Pbvim⁺ (polycation).

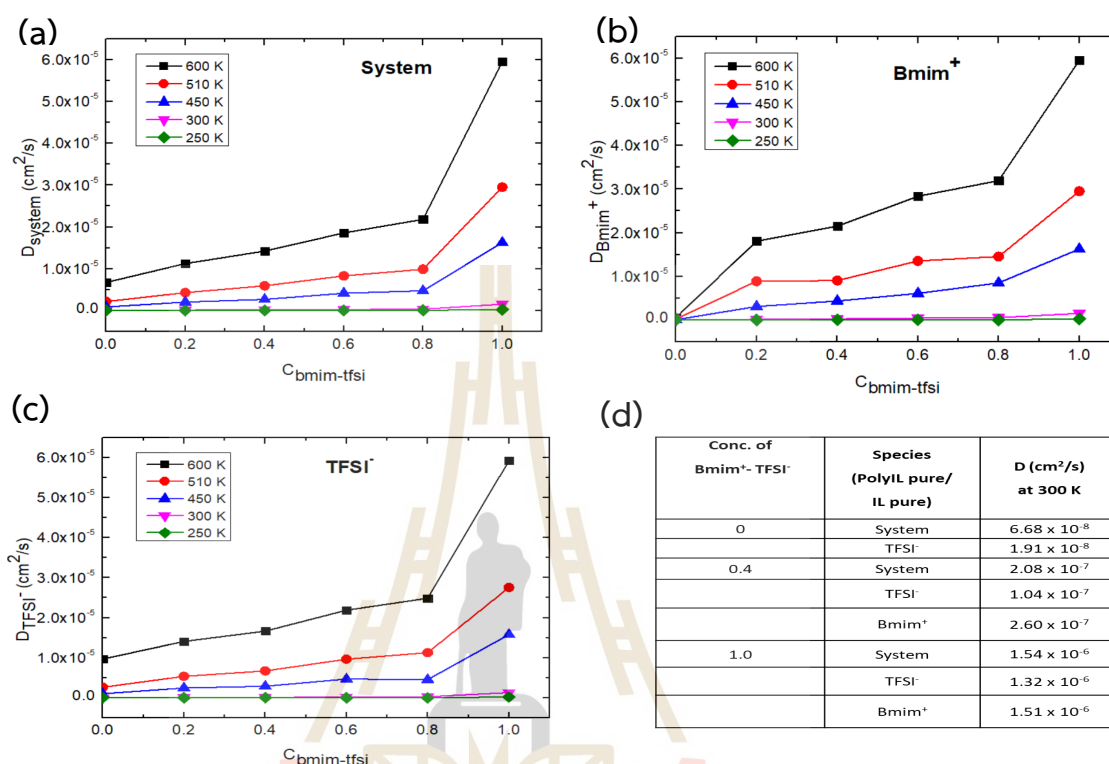


Figure 4.4.5 The Diffusion coefficient of (a) PolyIL-IL blends, (b) Bmim⁺ cation, (c) TFSI⁻ anion and (d) Comparisons between PolyIL, PolyIL-IL blends and IL, respectively.

4.4.2.2 Ion Diffusivities for PolyIL-IL Blends

From the results displayed in Figure 4.4.6(a) and 4.4.6(b), we monitor that at all the temperatures examined the diffusion coefficients of both Bmim⁺ and TFSI⁻ ions increase monotonically with expanding IL concentrations. Each effect verifies the assumption underlying our research and illustrates that blending polyILs with pure ILs can actually result in an improvement in the ion mobilities relative for ILs. Interestingly, we also note that the enlarge of diffusivities upon addition of pure ILs to polyILs is less than for TFSI⁻ compared to those seen for Bmim⁺ ions. Such trends can be understood at a qualitative level by considering that with expanding fraction of ILs, there is a consisting escalate in the number of cations, accrue mobile BMIM⁺ cations. The coordination of TFSI⁻ ions to such counterions is expected to lead to a significant

fasting of the dynamics of anions. And In Figure 4.4.6(c) and 4.4.6(d), we display the above diffusivity results in the plane of T/T_g (T_g corresponding to the glass transition at the considered loading of IL). The TFSI^- ion mobilities are seen to display a “decoupling” in this representation.

Explicitly, we observe that the mobilities of polyIL-IL at IL concentrations: 0.2-0.6 and pure ILs are higher (at a specified T/T_g) than the polyIL-IL of IL concentrations: 0.8 at low temperatures because there is a large competition between Bmim^+ cations and TFSI^- anions. This can be seen from the Transference Numbers for PolyIL-IL Blends data (Figure 4.4.19 at PolyIL-IL $C_{0.8}$). Both cations and anions have higher transfer values. Therefore, the mobilities of the blend system at 0.8 of IL concentrations is the slowest mobility at low temperature (specified T/T_g) and are sensitive to the loading at high temperatures. The overhead results demonstrate that once the coordination of polycations is soaked, the anions diffuse independently without being affected by the polymer chains and exhibit a decoupling phenomenon. A surprising investigation is that very similar decoupling properties also manifest in the cation diffusivities.

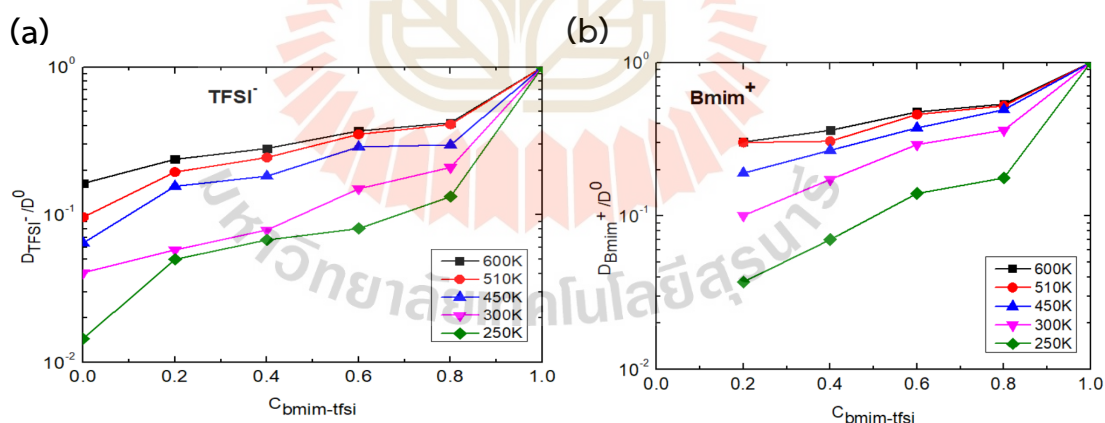


Figure 4.6 The Diffusion coefficient of (a) TFSI^- , (b) Bmim^+ ions in polyIL-IL blends as a function of IL concentrations at different temperatures. In the figure, D_0 is the respective value obtained for pure ILs. (c) TFSI^- and (d) Bmim^+ ions in polyIL-IL blends as a function of T/T_g at different IL concentrations.

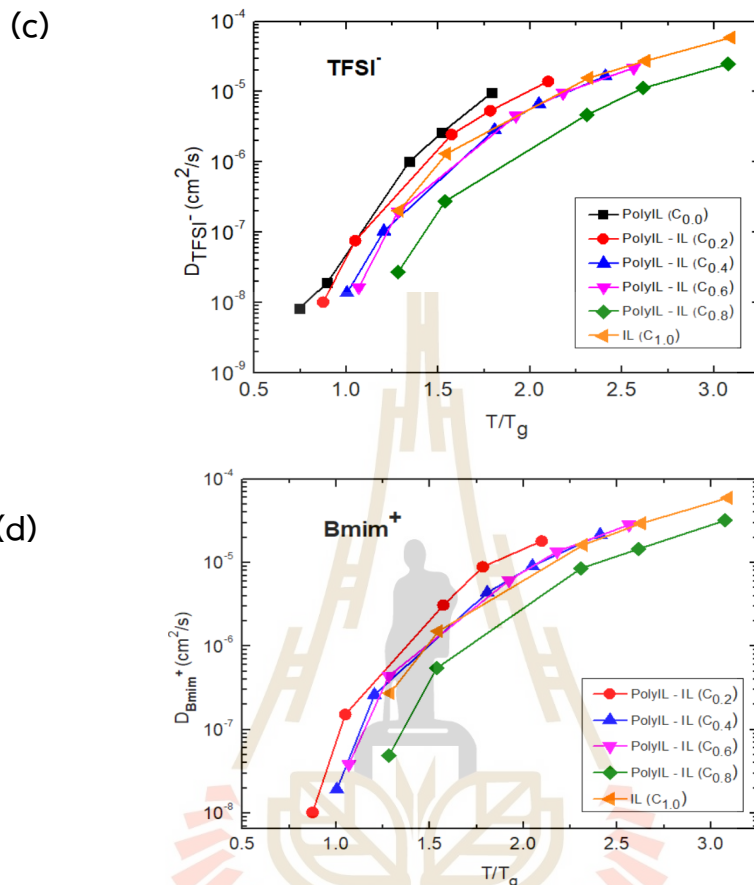


Figure 4.6 The Diffusion coefficient of (a) TFSI⁻, (b) Bmim⁺ ions in polyIL-IL blends as a function of IL concentrations at different temperatures. In the figure, D_0 is the respective value obtained for pure ILs. (c) TFSI⁻ and (d) Bmim⁺ ions in polyIL-IL blends as a function of T/T_g at different IL concentrations (continued).

4.4.2.3 The orientational autocorrelation functions (ACF) and KWW relaxation times for PolyIL-IL Blends at 600 K

From ACF data as depicted in Figure 4.4.7(a), we observe that the autocorrelation functions of the polymer chains in the blends systems decayed more quickly than that of the pure polyIL system. And then (Figure 4.4.7(b)), we calculated the timescale of backbone auto-correlation function of relaxation times of polymer chains by fitting the Kohlrausch Williams-Watts (KWW) stretched-exponential function (τ_{KWW}) of the polymer as a measure of the polymer segmental dynamics. τ_{KWW}

decreases monotonically with increase in IL concentrations, indicating that the addition of ILs (Bmim-TFSI) indeed facilitates faster segmental dynamics of the polymer chains.

The above results indicate that inspection by advising that the addition of ILs reduce the extent of coordination between the anions (TFSI⁻) and the polycations (Pbvim⁺) while expanding the coordination of the anions with the cations (Bmim⁺). And the relaxation times of polymer chains is consistent with Matsumoto et al. 's research (Matsumoto, 2019). Specifically, they identified three regions, but from MD simulation results are consistent with second region that at an intermediate of c_s (concentration of the ionic liquid Bmim-TFSI), η_{sp} and λ decreased with increasing c_s . These results indicate that polymerized ionic liquid chains shrink as the ionic liquid concentration increases at lower concentrations due to the charge screening effect by the same mechanism as that for ordinary polyelectrolytes in salt solutions. And the phenomena refer to over probably also happened in our simulation models.

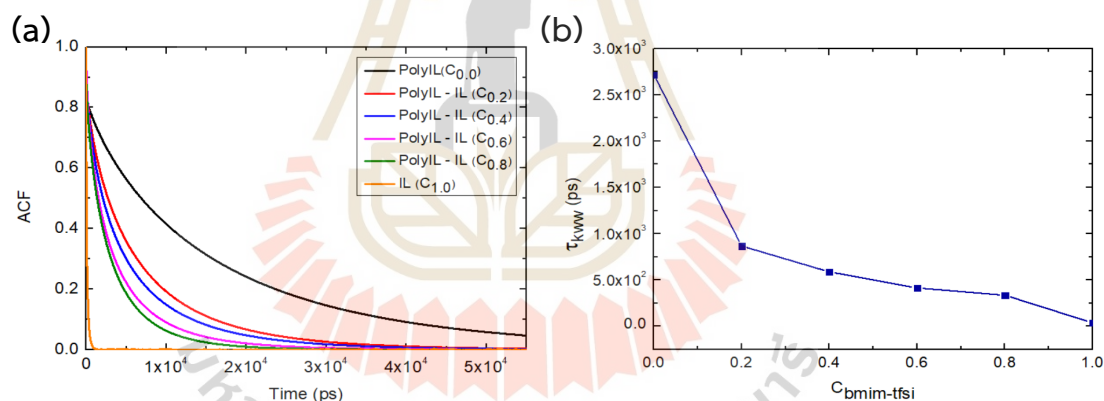


Figure 4.4.7 (a) The Orientational autocorrelation functions and (b) KWW fitting of PolyIL-IL blends in various IL concentrations. Corresponding KWW relaxation times (τ_{KWW}) for each system.

4.4.2.4 Short time dynamics

For Figure 4.4.8, we observe that for as expected, the largest movement is seen for Bmim⁺ while TFSI⁻ and the Pbvim⁺ exhibit a much smaller magnitude of displacement. These results are indicated that Pbvim⁺, Bmim⁺ and TFSI⁻. All three species had improved displacement with the addition of ionic liquids due to when the system are no ionic concentrations, it will be found that the polymer moves very

slowly. This causes the polymer to aggregate together rather than diffusion of their motion. If the ionic concentrations are gradually increased, this will result of each system in the polymer having a better distribution of movement.

And Figure 4.4.9 and Table 4.4.1. For quantitative, the absolute displacement indicate that rigidity of the coordinating structures can be ordered as: $\text{Pbvim}^+ < \text{TFSI}^- < \text{Bmim}^+$. This all data of the absolute displacement for PolyIL-IL Blends at 600 K suggest that TFSI^- interact strongly with the Pbvim^+ and move cooperatively on a relatively smaller scale while Bmim^+ have much larger amplitudes of the displacement. And the fluctuation indicating that Bmim^+ are quite weaker interact with TFSI^- and other species. Therefore, this information will confirm the information mentioned above that indicating that the addition of ILs (Bmim-TFSI) indeed accommodates faster segmental dynamics of the polymer chains.

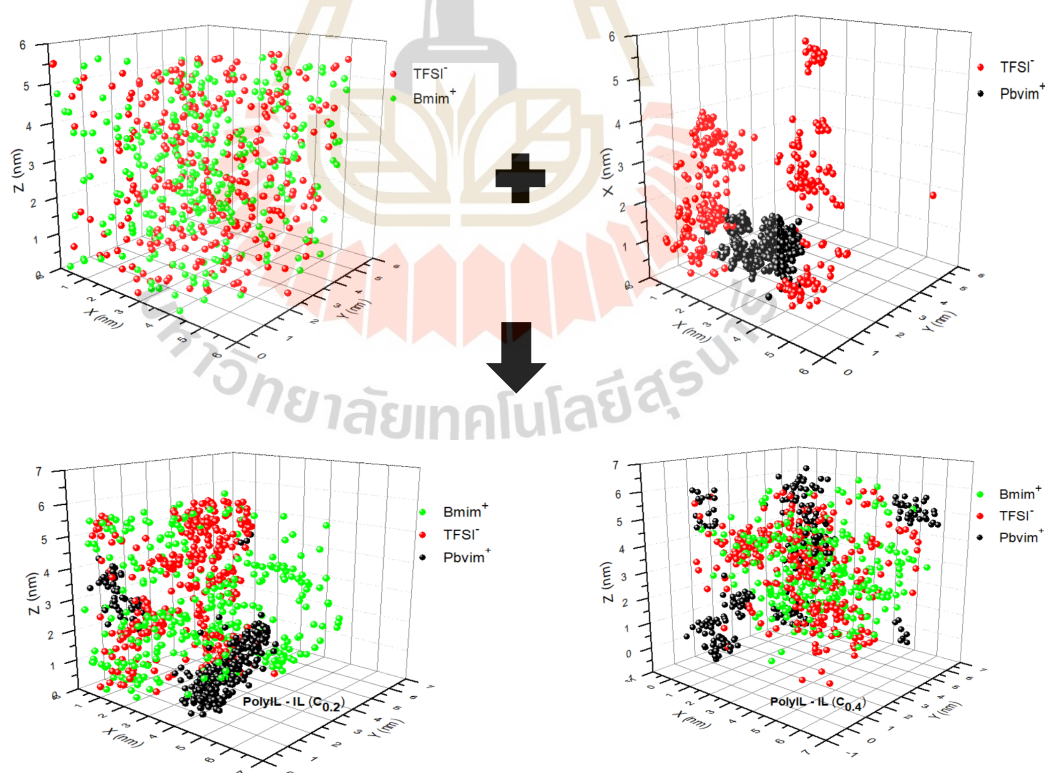


Figure 4.4.8 The Trajectories of Bmim^+ , TFSI^- and Pbvim^+ recorded every 500 ps.

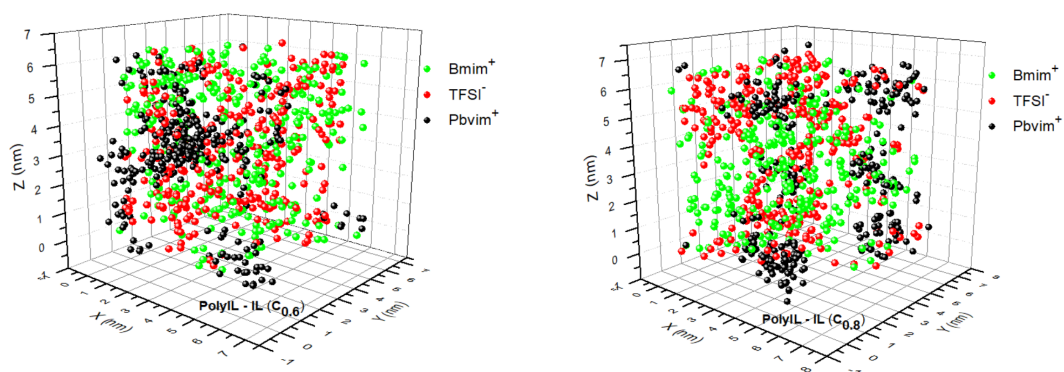


Figure 4.4.8 The Trajectories of Bmim^+ , TFSI^- and Pbvim^+ recorded every 500 ps (continued).

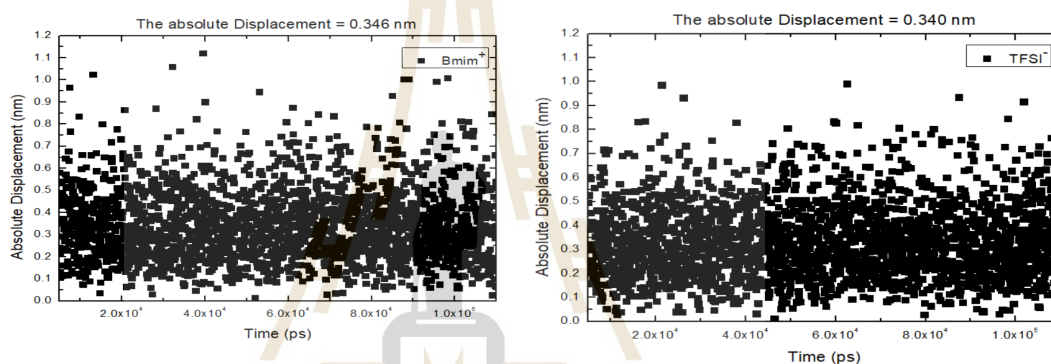


Figure 4.4.9 The absolute displacement of ILs system (a) Bmim^+ and (b) TFSI^- every 500 ps interval.

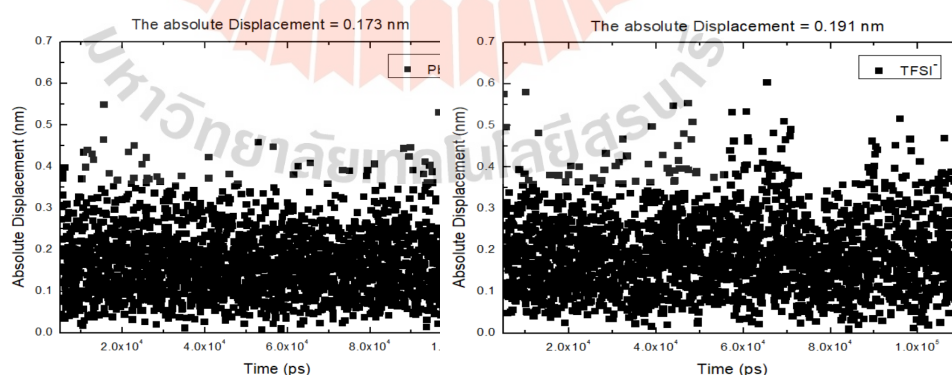


Figure 4.4.10 The absolute displacement of PolyILs system (a) Pbvim^+ and (b) TFSI^- every 500 ps interval.

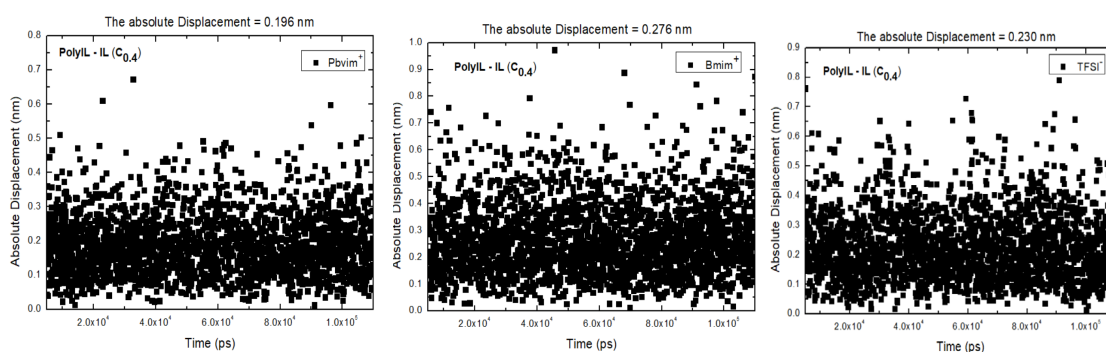


Figure 4.4.11 The absolute displacement of PolyIL-IL system (a) Pbvim⁺ and (b) Bmim⁺ and (c) TFSI⁻ every 500 ps interval; Give an example (at ILs conc = 0.4) of a blend systems from all systems.

Table 4.4.1 The absolute displacement (in 500 ps increments) of ILs, PolyILs and PolyIL-IL blends.

Conc for IL	Species	The absolute displacement (nm)	Conc for IL	Species	The absolute displacement (nm)
IL pure	Bmim ⁺	0.346	0.6	Pbvim ⁺	0.205
	TFSI ⁻	0.340		TFSI ⁻	0.234
0	Pbvim ⁺	0.173		Bmim ⁺	0.286
	TFSI ⁻	0.191	0.8	Pbvim ⁺	0.210
	Bmim ⁺	—		TFSI ⁻	0.246
0.2	Pbvim ⁺	0.185		Bmim ⁺	0.296
	TFSI ⁻	0.216	1.0	Pbvim ⁺	0.217
	Bmim ⁺	0.259		TFSI ⁻	0.270
0.4	Pbvim ⁺	0.196		Bmim ⁺	0.305
	TFSI ⁻	0.230			
	Bmim ⁺	0.276			

4.4.3 Radial Distribution Functions (RDF) and Coordination numbers (CN)

For RDFs, the illustrative atoms chosen for anion, cation, and polycation were identical to those adopted for the analysis of the mean squared displacement (MSD) and Diffusion coefficient (D). Further, the cutoffs for evaluating the anion-cation/polycation coordination were determined by the position r where $g(r) = 1.0$ after the first peak (Zhang, 2020). From the results in Figure 4.4.12(a), we see that the value of peak for the association of Pbvim⁺ - TFSI⁻ is higher than that of Bmim⁺ - TFSI⁻, indicating a stronger binding of TFSI⁻ with the Pbvim⁺ monomers attached to the

polyIL chains at the same temperature, indicating that IL concentrations are dominated. With results confirming this behavior by the absolute displacement in Figure 4.4.9, 4.4.10 and 4.4.11. For Figure 4.4.12(b), at the same temperature, it is found that the CN of ILs increases and decreases in the polyILs systems with increasing ILs concentration.

In summary for RDFs and CNs can be found that at the same temperature, It will indicate that for polymers and anions, the interaction becomes more gradually stronger as the ionic concentrations increases because the ILs will help the anions move along the polymer faster. And from the behavior mentioned above, the binding of IL will gradually decrease because the cations will interact with the anions to help the anions move faster.

After that, we were studying RDF at different temperatures. For Figure 4.4.13(a), 4.4.13(b) and 4.4.13(c), this indicates that there is no difference in both polymer and ionic properties. Therefore, we can be concluded that the ILs concentration is more prominent than the effect of temperature.

For Figure 4.4.14(a), we observe that CNs data indicate a decrease in the Pbvim^+ system enclosing TFSI^- because TFSI^- are switched to bind with Bmim^+ . From Figure 4.4.14(b), it will be found that when the temperature is increased, the value of CN changes very little. We can be concluded that the IL concentrations is more prominent than the effect of temperature.

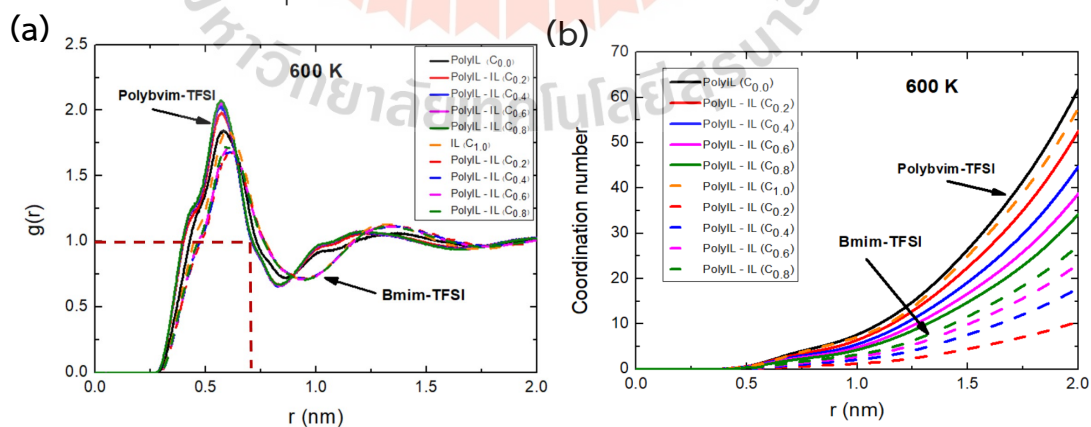


Figure 4.4.12 Radial distribution function between (a) the centers of mass for Pbvim^+ , TFSI^- and Bmim^+ and (b) Coordination numbers (CN) at 600 K.

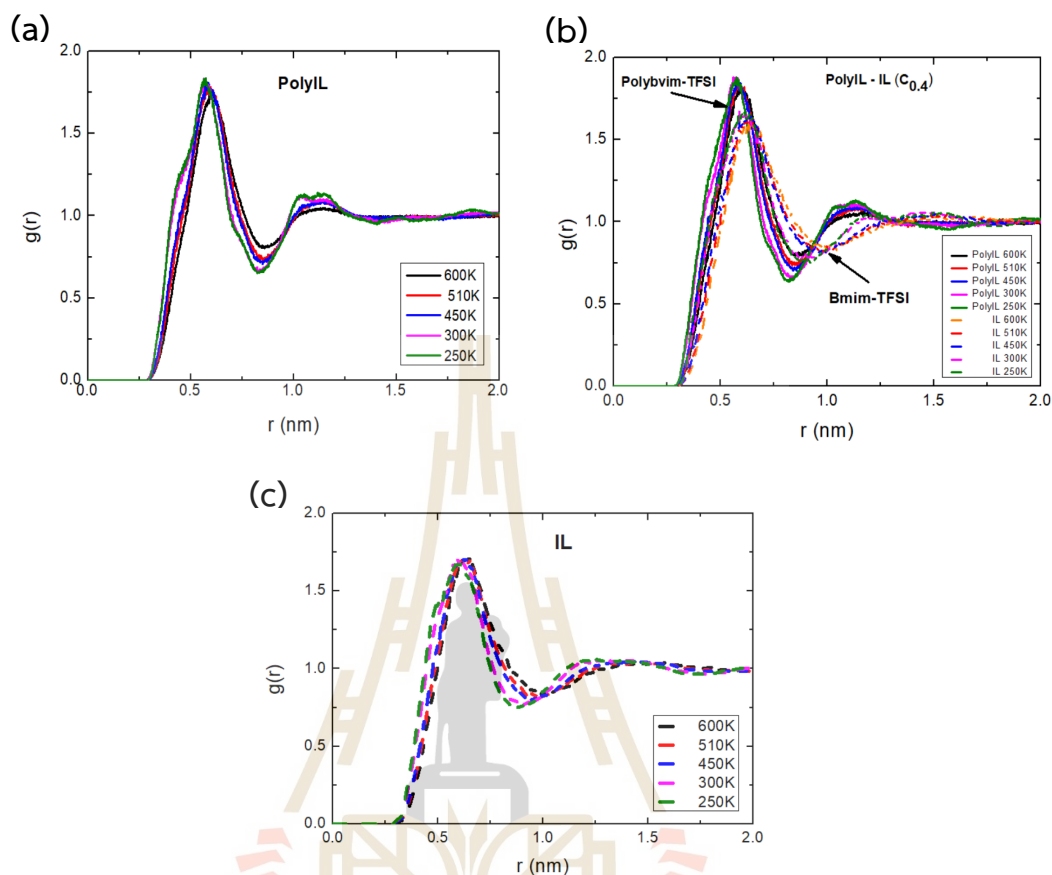


Figure 4.4.13 Radial distribution function between (a) the centers of mass for PolyILs, (b) PolyIL-IL blends and (c) ILs at different temperatures.

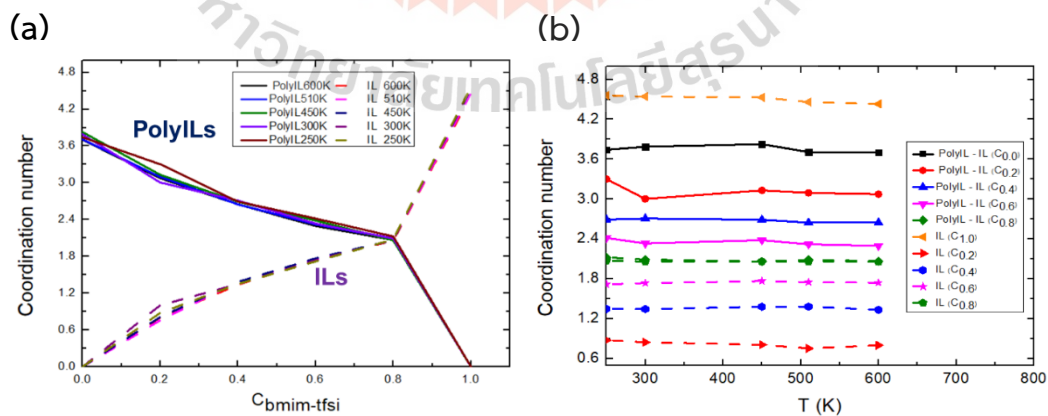


Figure 4.4.14 Coordination numbers (CN), (a) for PolyILs, ILs at different IL concentrations and (b) for PolyILs, ILs at different temperatures.

4.4.4 Ion Transport Mechanisms

4.4.4.1 Anion Association Statistics

To understand the influence of IL concentrations (Bmim-TFSI) on the TFSI⁻ coordination characteristics, we calculated the probability, P_n , that a given TFSI⁻ is associated with n cations/polycations and the probability P_N that an anion is associated with N number of chains at different loadings of the ILs electrolyte at 600 K. Form Santosh et al (Mogurampelly, 2018). In the absence of polymer chains (i.e., pure ILs), the anions are expected to be in only one of two states: (a) stay free from any kind of association; (b) associate with non-polymerized cations. Whence, for pure ILs, P_N and P_n are expected to be zero for $N, n > 0$.

It is observed from Figure 4.4.15(a), that $P(n)$ exhibits a maximum at $n = 4$ in the absence of pure ILs. However, as the IL concentrations increases, the location of the peak is seen to gradually shift to $n = 3$, while the association with four cations constitutes the second major coordination group. For blend systems display peaks of $P(n)$ at $n = 3$ and $n = 2$, suggesting that such anions swap out either one or two cations and engage with non-polymerized cations as a third and/or fourth partner for their coordination. Moreover, when increasing IL concentrations show that the number of free ions IL concentrations larger than low IL concentrations.

Next, we turn to the influence of IL concentrations on the coordination of anion with distinct polymer chains in Figure 4.4.15(b), we quantify such features through the consideration of the probability P_N that an anion is coordinated with N distinct polymer chains. This data show that peak of P_N at $N = 2$ is observed in the absence of IL concentrations. Further, with an increase in IL concentrations, the peak is seen to transition from $N = 2$ to $N = 1$. PolyIL-IL blends are seen to preferentially associate with a single polymer chain. Together, the results of the coordination statistics presented in Figure 4.15 and Figure 4.4.16 suggest that the co-coordinated anions dissociate from the second polymer chain and instead preferentially engage in coordination with the cations of a single polymer chain.

In summary for anion association statistics. From the both graphs of Figure 4.4.15 indicate that, when increasing the concentration of ionic liquids, P_N and P_n are

seen to peak at $N = 2$ and $n = 4$, indicative of the anion association with four monomers of two different polymer chains in pure polyIL electrolyte. And P_N and P_n exhibit a maximum for $N = 1$ and $n = 3$ or 2 , suggesting that a given anion prefers to be associated with three polymerized cations of the single polymer chain in PolyIL-IL Blends. The decreasing of number of cations and polymer chains associated with anion because there is a switching of the coordinated interaction of anions between the polymer chains and cations.

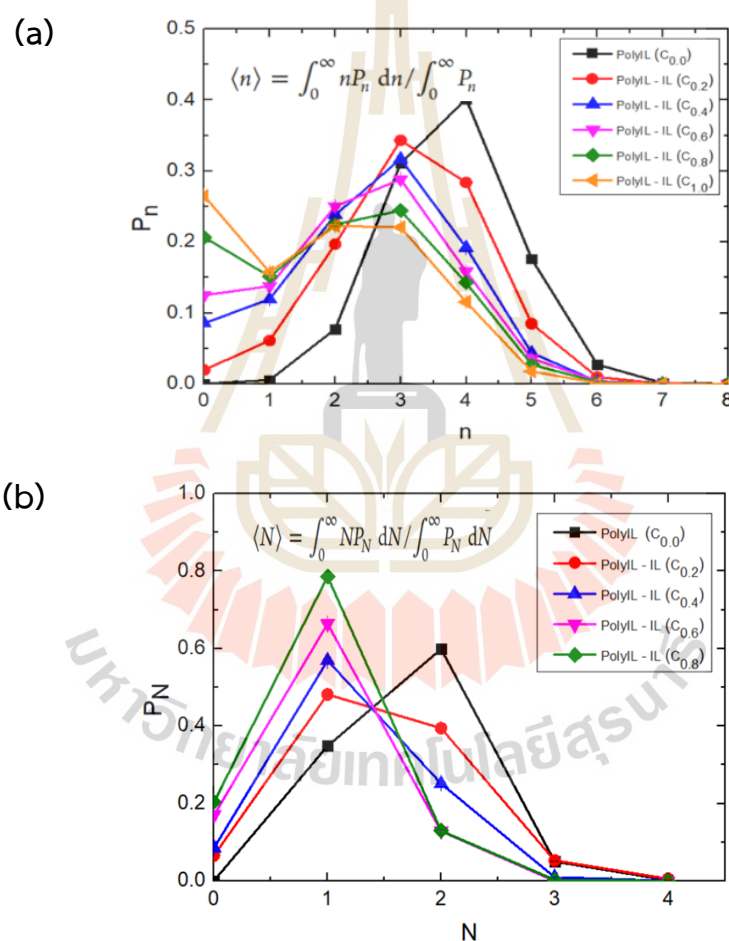


Figure 4.4.15 Probability that a given TFSI⁻ is associated with (a) n cations and (b) N polymer chains. The error bars are smaller than the size of the symbol where invisible.

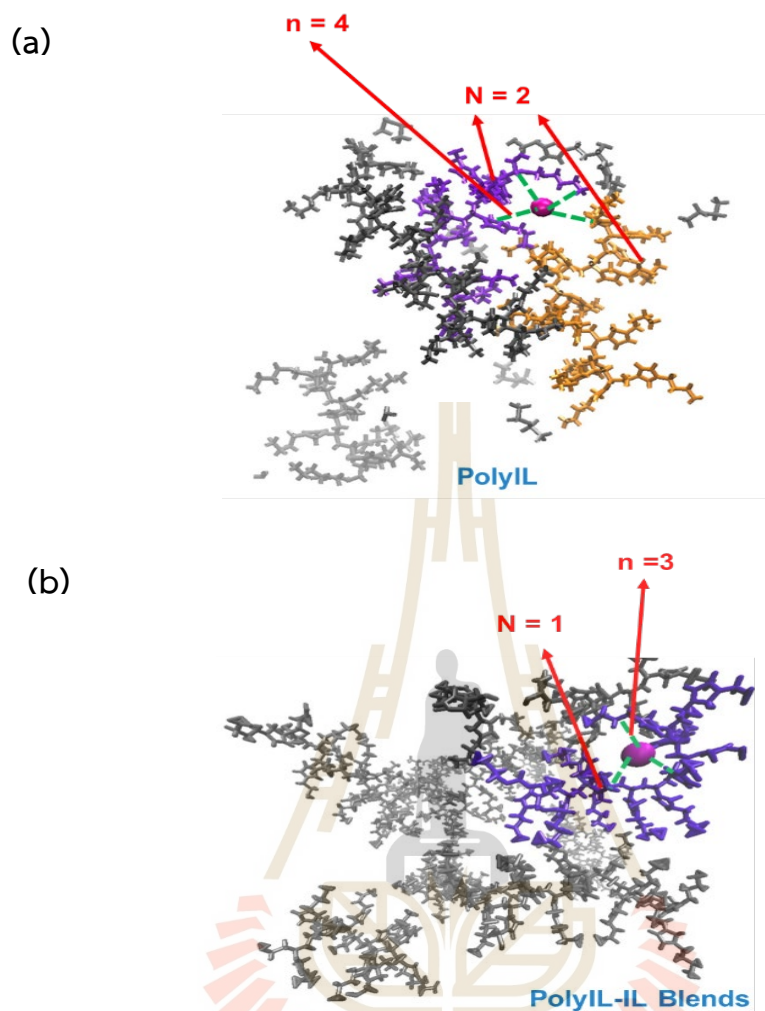


Figure 4.4.16 A snapshot of anion (magenta) association to polymerized cations and polymer chains in (a) PolyIL and (b) PolyIL-IL blends. The represent an ion-association determined from a distance cutoff of 6.5 Å. Only the polymer chains within 20 Å spherical radius from the centered anion are shown without any other ions for clarity.

4.4.5 Glass Transition Temperatures (T_g) for PolyIL-IL Blends:

The blend systems were then cooled from 600 K stepwise to 160 K by decrements of 10 K. Using cooling rate = 1×10^{10} K/s and the system density was calculated from the last 1ns from 2ns of NPT simulation (Mogurampelly, 2017). The increase of V_{specific} with increasing temperature was less pronounced below T_g yielding a kink separating rubbery and the glassy states (Khongvit, 2020).

T_g values for all simulated systems are presented in Figure 4.4.17. The T_g for all blend systems were lower than for the pure polyILs. For all the V_{specific} curves have only one transition between the high- and low-temperature regimes. One transition is usually interpreted as evidence of miscibility, while two transitions imply immiscibility of polymers (Kikkawa, 2009; Thomas, 2014; Saha, 2016). The fact that only one kink is observed in the V_{specific} curves argues for miscibility of PolyILs, ILs and PolyIL-IL blend systems. In Figure 4.4.18(a), T_g from experiment show that the all blend systems have two glass transition temperature (T_g) follows as $T_{g, \text{low}}$ and $T_{g, \text{high}}$. Because T_g from blend systems have broad range, when increasing temperature make them transform glassy state to the liquid state indicated that enriched local concentration of polyIL are dominantly, so this effect is called $T_{g, \text{high}}$ and when decreasing temperature make them behavior like float state indicated that enriched local concentration of ILs are dominantly, so this effect is called $T_{g, \text{low}}$.

And what's interesting is that when calculating the T_g value for pure ILs and pure polyILs in Figure 4.4.17, it was found that both linear lines are very good. But when observing the blend systems, we were finding that both lines of high and low temperature deviate from the linear lines. We hypothesize this phenomenon that the simulated results may behave like the experimental results, so the broad range is the cause of the two lines leading to T_g line of both temperatures deviating from the linear line.

The generally, polymer blends can be divided into three categories: miscible, semimiscible (or partially miscible), and immiscible blends (Thomas, 2014). A blend of miscible polymers exhibits a single T_g as well as a single homogeneous phase. Two distinct T_g values arising from two phase-segregated components are often interpreted as an indicator of immiscibility (Kikkawa, 2009; Thomas, 2014). An alternative view has been proposed by Lodge and McLeish (Lodge, 2000). According to their self-concentration model, chain connectivity of polymers leads to an increased local concentration of monomers in blends compared to an average bulk concentration. For this reason, one should normally expect two glass transitions in any single-phase

polymer blend. Thus, it was suggested that the presence of two distinct T_g values cannot be used as a reliable criterion of immiscibility and semimiscibility (Lodge, 2006).

Together, the results discussed above indicate that we cannot say all blend systems have separated because in simulation results show that all snapshots were created using VMD open-source software, the polyIL-IL blend systems are homogeneous. But in the experimental results of T_g , the high T_g and the low T_g blend components exhibit, respectively, stronger and weaker variations with the blend composition. As already mentioned, we believe that the estimates of $\{T_g\}$ obtained from relaxation time and specific heat measurements may be different. Jacek et al, their theory predicts that spontaneous concentration fluctuations may lead to the appearance of two mesoscopic regions of enriched local concentration in macroscopically homogeneous, but locally inhomogeneous, one-phase binary polymer blends. These mesoscopic concentration fluctuations, a universal property of blends of semiflexible polymers not shared by mixtures of non-associating small molecule liquids. Moreover, the relatively large concentration fluctuations naturally explain the existence of two relaxation time and two T_g in miscible blends with sufficient dynamical asymmetry between the blend components (Jacek Dudowicz, 2014).

In Figure 4.4.18(b). When the experimental results are compared with the simulation results. It was found that the simulation results for T_g in good agreement with experimental values.

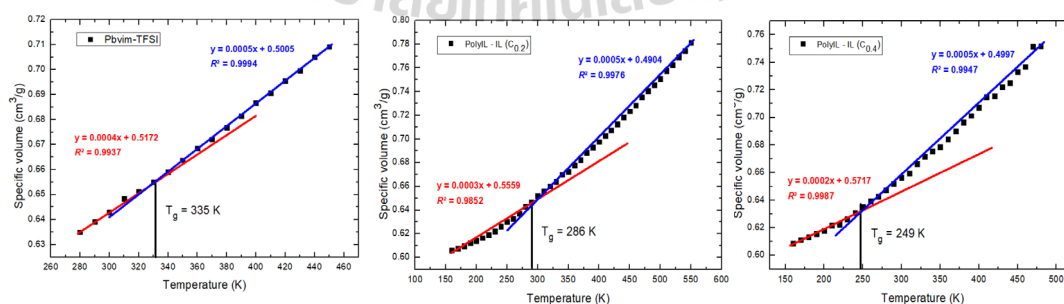


Figure 4.4.17 Plots of specific volume versus temperature to determine T_g values for various IL concentrations of blend systems.

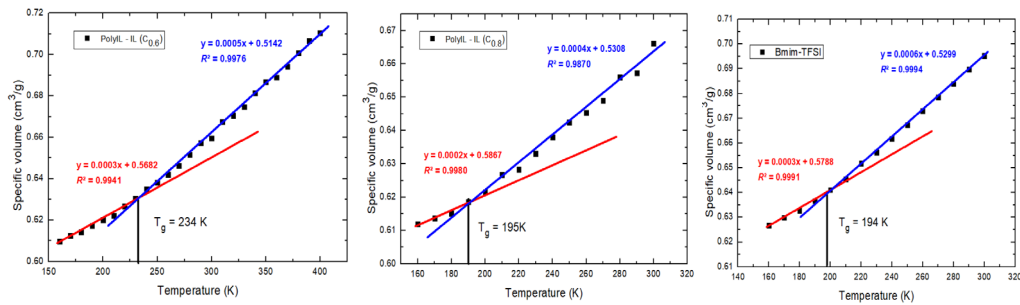


Figure 4.4.17 Plots of specific volume versus temperature to determine T_g values for various IL concentrations of blend systems (continued).

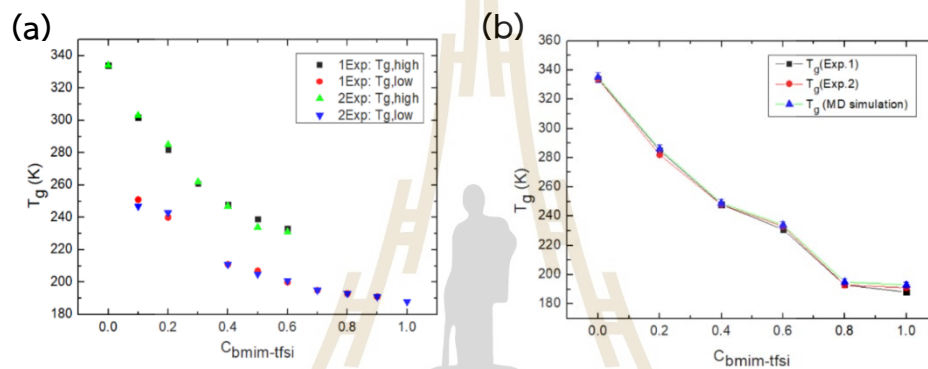


Figure 4.18 (a) T_g from experiment and (b) Comparison (Exp.& Sim.) of Glass Transition Temperatures (T_g).

4.4.6 Transference Numbers for PolyIL-IL Blends

Amount of relevancy in defining the accomplishment of polymer electrolytes is the transference number. The transference number amounts the current transported by the identity of attention (in our case, the anion) relative to the overall current. Each a number is of regard as its relevancy in quantifying the predisposition for concentration polarization features resulting from the evacuation and hoarding of the contrast charged ions at the electrodes (Mogurampelly, 2018). While several definitions of transference number exist (Balsara, 2015), in the present context, we use the definition that only relies on ion mobilities and the number of mobile species.

From Figure 4.4.19(a) and 4.4.19(b), we can observe that the transfer numbers of TFSI⁻ anion have irregular fluctuation as the temperature increases. Addition of mobile ions, such as in our case through the cations of pure IL, is prospective to increase the conductivity but concurrently lower the transference numbers of TFSI⁻ anion. Each

datum is surprising, as one would have prospective that the transference numbers would display a monotonic inflate with ILs adding to the value of unity for pure ILs. Again, our results illustrate a recantation arising from effect with enlarged ILs loading and temperature, viz., the increasing of the anion mobilities relative to the cations.

For polyIL, we will be found that polycations move very slowly. Therefore, anions are highly transferable. Therefore, it is to move like a free ion in the simulation. Then when they come to a blends system is to add ILs. Therefore, a competition occurred between polycations or cations with anions. And then there is a change in the coordination numbers of anions, which is to switch between polycations and anion or cation and anion. For pure IL, there will be a very poor amount of anion transfer because anions interact with cations because they have the same number of both. So, we can be concluded that transference numbers of anions have the addition of pure ILs to pure polyILs as the dominant than influence the temperature.

From Figure 4.4.20, all graphs regarding the transfer number of anions. It will be higher than cations because anions are more numbers than cations at PolyIL-ILs (0.0-0.8). And there will be a gradual decrease in transfers until the number of cation and anion ions is equal at PolyIL-ILs (1.0). It is found that cations have a higher transfer amount than anions because cations have more diffusion. And there will be equal transfer at a temperature of 600 K. In their recent study (Zhang, 2020), their found that, even with relatively long-time simulation times extending 400 ns, polycation diffusivities are not easy to obtain for longer polymer chains (Zhang, 2020). Therefore, we find that the simulation time 110 ns run of our simulation systems is sufficient to reach equilibrium with other ion species. Because even if it takes more time to run longer than 110 ns, it will hardly affect the diffusion of the long polymer chain.

For transference Numbers for PolyIL-IL Blends data, it was found that when increasing the ionic concentration, there will be a gradual decrease in the transfer of anions. This is the result of binding with cations to help move them along long polymer chains. Therefore, all information will indicate in evaluating the efficiency of this system that only ion transfer cannot be used in studies alone. The information in Sections 4.4.1-4.4.5 and 4.4.7, as well as simulation trajectory, must be used to more accurately confirm the behavior of the mixed system.

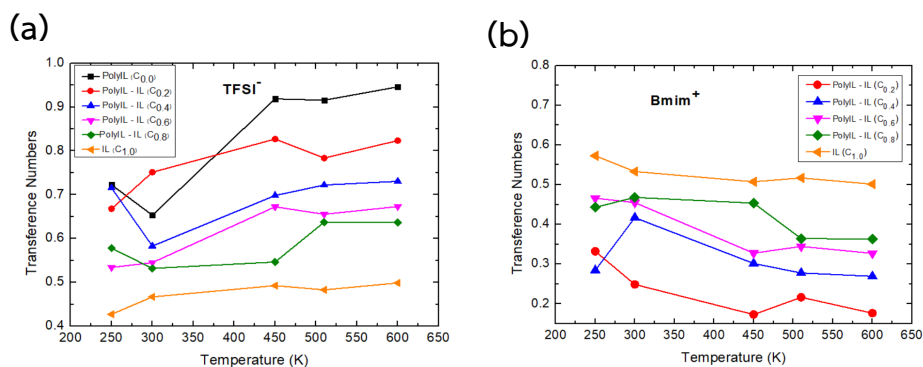


Figure 4.4.19 (a) the anions and (b) cations transference number as a function of the ILs loading at different temperatures.

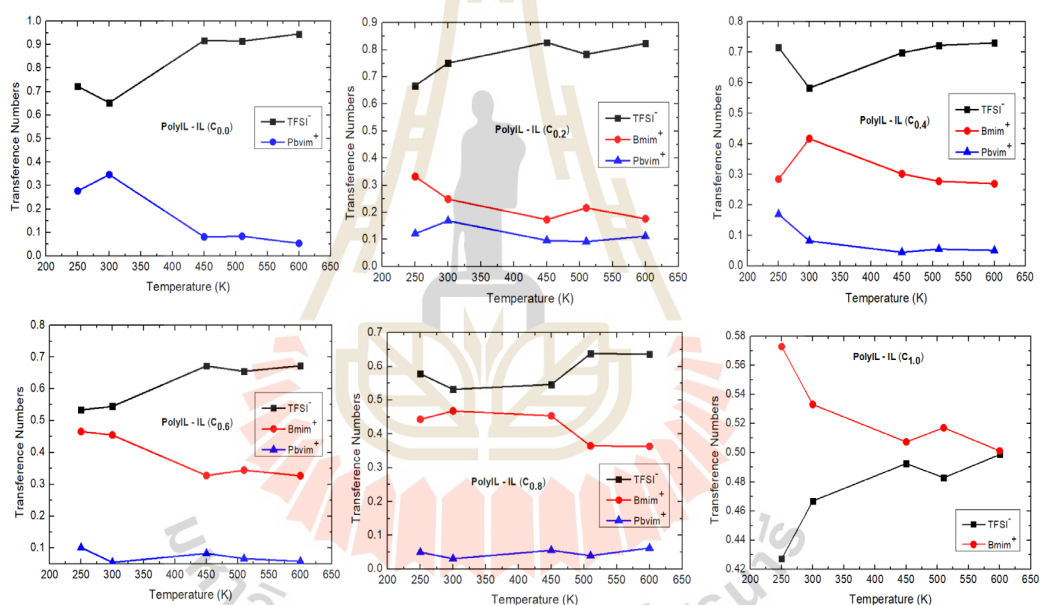


Figure 4.4.20 The comparison of the anions and cations transference number as a function of the ILs loading at different temperatures.

4.4.7 The ideal ionic conductivity in PolyIL-IL Blends

In Figure 4.4.21(a)–(d) and Table 4.4.2, we display the experiment and simulation results for the total ionic conductivity and the NE values as a function of the IL concentrations, respectively.

For Figure 4.4.21(a) and 4.4.21(b), when the experimental results are compared with the simulation results. Although the large numerical errors would make the values of conductivities unreliable, we found that this trend was observed [66]. It was found that the simulation results for the ideal ionic conductivity in good agreement with experimental values in qualitative.

In all results from Figure 4.4.21(a)–(d) and Table 4.4.2, we can confirm that the hypothesis underlying our work and demonstrates that blending pure ILs with polyILs can indeed lead to an enhancement in the conductivity relative to ILs. Therefore, it can be concluded that the ionic conductivity increases after adding IL into the PolyIL system and increases temperature.

Interestingly, in Figure 4.4.22(a)–(c), we show that the NE conductivities exhibit a “decoupling” from T/T_g , the degree of such effects becomes significantly reduced when compared to the ion mobilities (Figure 4.4.6(c)–(d)). Indeed, the conductivity of polyIL-IL blends and pure ILs are still seen to be greater than that of the pure polyILs. And the NE values display a nonmonotonic behavior as a function of pure ILs loading (exhibiting a maximum around 100% ($C_{\text{bmim-TFSI}} = 1.0$) loading of pure ILs). Such trends can be understood to arise as a consequence of the competing effects of the increased number of mobile ions resulting from the addition of pure ILs (to polyILs) and the greater mobilities (at a specified T/T_g) of the systems containing a greater fraction of pure ILs.

At this time, there is no clear reason why the simulated conductivity values are too high from the experimental values. Many assumptions have been made in various studies regarding conductivity in simulations such as Neglecting ionic correlations between free ions, intrinsic into the Nernst-Einstein equation, seemingly overestimates the ionic conductivity and on the other hand, ignoring the contribution from bound ions would underestimate the conductivity. But no clear conclusion. Even if the cross-

correlation term is taken into account or the simulation run time is longer, there are still large errors.

Thus, the simulations may be missing some key dynamical aspect. Additional studies using more advanced techniques and force fields may help discover the source of the differences. Nevertheless, the simulation will focus on describing qualitative data for ionic conductivity and Nernst–Einstein conductivities and offer insight at the molecular level.

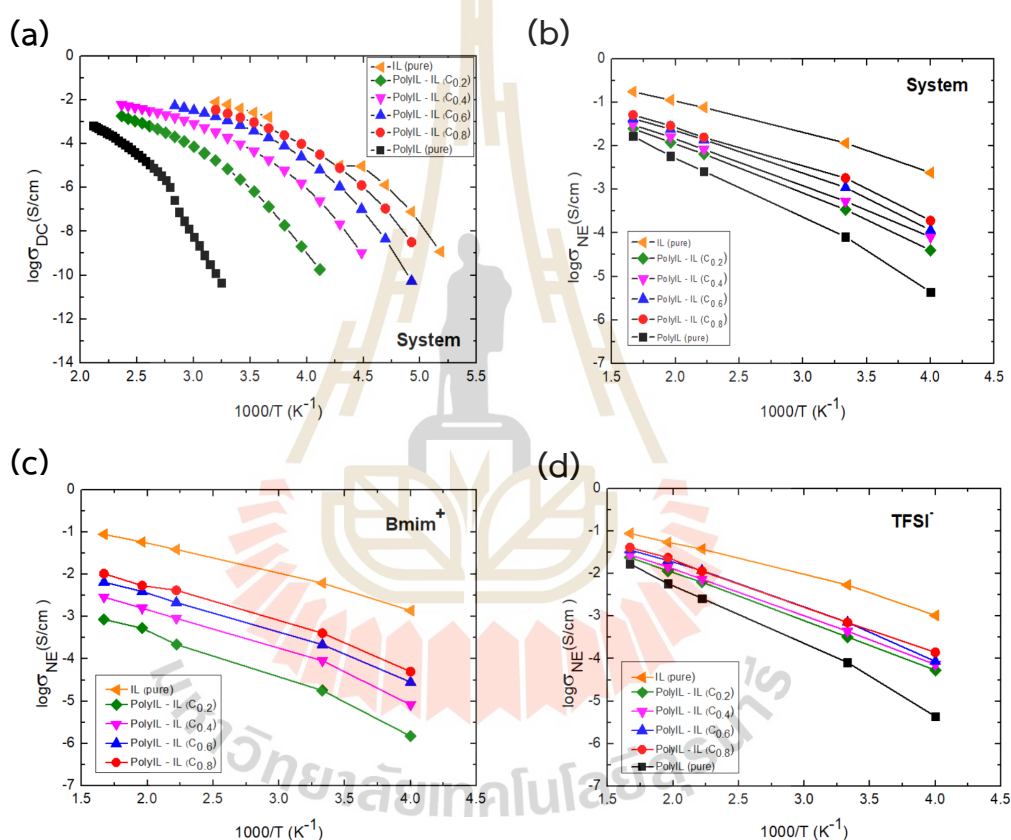
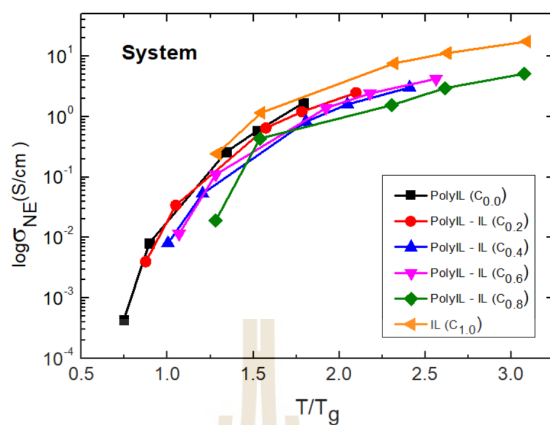


Figure 4.21 The ideal ionic conductivity of PolyIL-ILs blend systems obtained as plotted versus $1000/T$ (a) Total ionic conductivity from experiment, (b) Total of systems, (c) $Bmim^+$ and (d) $TFSI^-$ for ideal ionic conductivity from MD simulation.

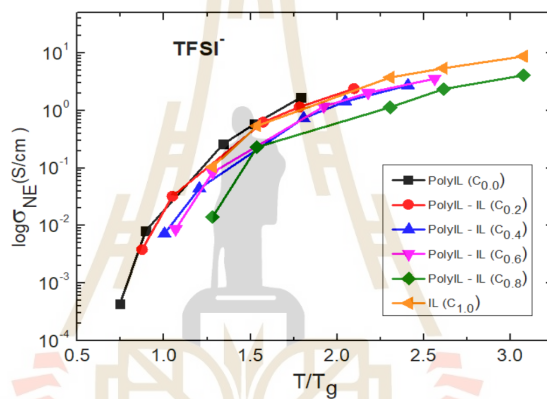
Table 4.4.2 Comparison between the total ionic conductivity from the experiment and the ideal ionic conductivity from MD simulation of PolyIL-ILs blend systems at different temperatures.

Conductivity		MD Simulations (S/m)					Experiments (S/m)
Pbvim-TFSI (pure)	Species	600K	510K	450K	300K	250K	453K
	system	1.685	0.579	0.261	0.00813	0.000437	0.037
	TFSI ⁻	1.685	0.579	0.261	0.00813	0.000437	
Mix0.2 Concentration of Bmim-TFSI	Species	600K	510K	450K	300K	250K	303K
	system	2.487	1.205	0.649	0.0341	0.00398	0.000698
	TFSI ⁻	2.401	1.152	0.627	0.0323	0.00383	
	Bmim ⁺	0.0858	0.053	0.0219	0.00178	0.000149	
Mix0.4 Concentration of Bmim-TFSI	Species	600K	510K	450K	300K	250K	303K
	system	3.028	1.593	0.826	0.0531	0.00806	0.0187
	TFSI ⁻	2.739	1.435	0.735	0.0441	0.00724	
	Bmim ⁺	0.289	0.158	0.0909	0.00902	0.000824	
Mix0.6 Concentration of Bmim-TFSI	Species	600K	510K	450K	300K	250K	303K
	system	4.231	2.424	1.389	0.110	0.0115	0.116
	TFSI ⁻	3.579	2.025	1.175	0.0836	0.00863	
	Bmim	0.652	0.393	0.215	0.0262	0.00282	
Mix0.8 Concentration of Bmim-TFSI	Species	600K	510K	450K	300K	250K	303K
	system	5.12	2.956	1.555	0.434	0.0191	0.237
	TFSI ⁻	4.085	2.357	1.136	0.231	0.0141	
	Bmim ⁺	1.035	0.539	0.419	0.203	0.00499	
Bmim-TFSI (pure)	Species	600K	510K	450K	300K	250K	303K
	system	17.542	11.271	7.616	1.158	0.243	0.4878
	TFSI ⁻	8.749	5.442	3.751	0.541	0.104	
	Bmim ⁺	8.793	5.829	3.865	0.618	0.139	

(a)



(b)



(c)

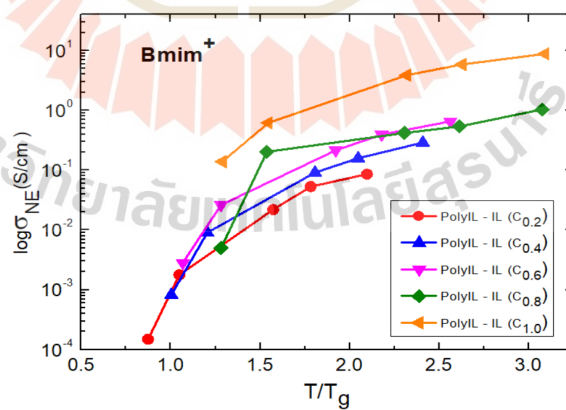


Figure 4.4.22 The Nernst-Einstein predictions a function of the loading of ILs for (a) system, (b) $TFSI^-$ and (c) $Bmim^+$ as a function of T/T_g .

4.4.8 Ion Transport Events in PolyIL-IL Blends at 600 K

To realize the mechanisms underlying ion movement in the polyIL electrolytes, we also examined different hopping cases, revealed by the anions which are especially correlated with polymerized cations (Mogurampelly, 2018). To this aim, we degraded the transport cases into three principal categorizations as schematically displayed in Figure 4.4.23: (a) type 1: anion hopping events along polymer backbone by means of the formation and breaking of ion pairs with polymerized cations; (b) type 2: ion hopping events between different polymer chains; and (c) type 3: the to and from transition events occurring between the polymer chains and the rest of the medium; i.e., if an anion is coordinated to polymer chain(s) at time t and uncoordinated to any polymer chain at a different time t' , then it is a type 3 event and in the absence of polymer chains (i.e., pure ILs), the anions are expected to be in only one of two states: (i) stay free from any kind of association; (ii) associate with non-polymerized cations.

From Figure 4.4.24, we observe that intrachain interaction gradually decreased but it is still a dominant mechanism because discussion in Section 4.4.2 in the subtopic is short time dynamics and Section 4.4.3, the interactions between anions and polycations are seen to be stronger than those between anion and non-polymerized cations. After that, competition between polycations and cations arose that compete to form bonds with anions where the main movement is anions interact to polymer chains so it will be the behavior of prominent intrachain hopping.

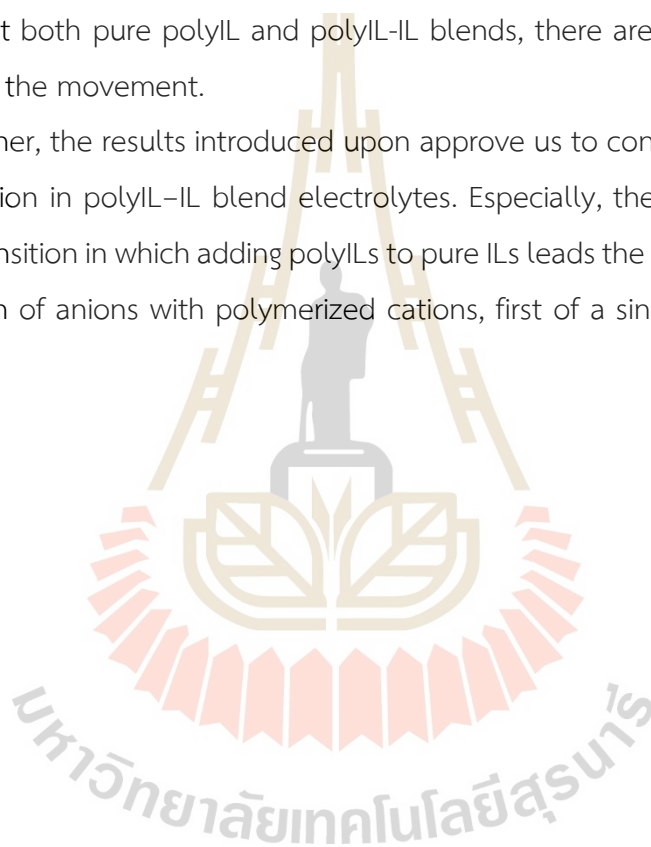
Later, ionic concentrations were added, this causes the cation to escape from the anion in the free state. The cations then compete for bonding with the polymer chains, this effect causes anions to escape from the polymer chains. And then binds with cations at a certain time. Therefore, this type 3 of behavior is second only to intrachain hopping. And another possible movement behavior is type 2 is the formation of bonds between anions and different polymer chains. From the MD simulation results, it was found that this was the least likely to happen due to the larger number of available non-polymerized cations.

From Inoue et al. (Inoue, 2013), they explained about sub-Rouse mode and proposed that the observation of these local motions is caused by the plasticizing

effect by dissociated large counter-anions. They showed that sub-Rouse mode is often observed for solutions where intrachain interaction is dominant for local motions. Appearance of the sub-Rouse mode for PC₄VITFSI was attributed to the decreasing of interchain interaction due to ionized large counterions which behaves like a solvent.

From the experimental research referenced above. It was found that the movement of PC₄-TFSI, this indicates that there is intrachain interaction that is more prominent than interchain interaction. This is consistent with MD simulation results, indicating that both pure polyIL and polyIL-IL blends, there are prominent intrachain interaction in the movement.

Altogether, the results introduced upon approve us to conclude the mechanism of anion motion in polyIL-IL blend electrolytes. Especially, the all effects indicate a moderate transition in which adding polyILs to pure ILs leads the way a raised tendency of connection of anions with polymerized cations, first of a single chain and then of two chains.



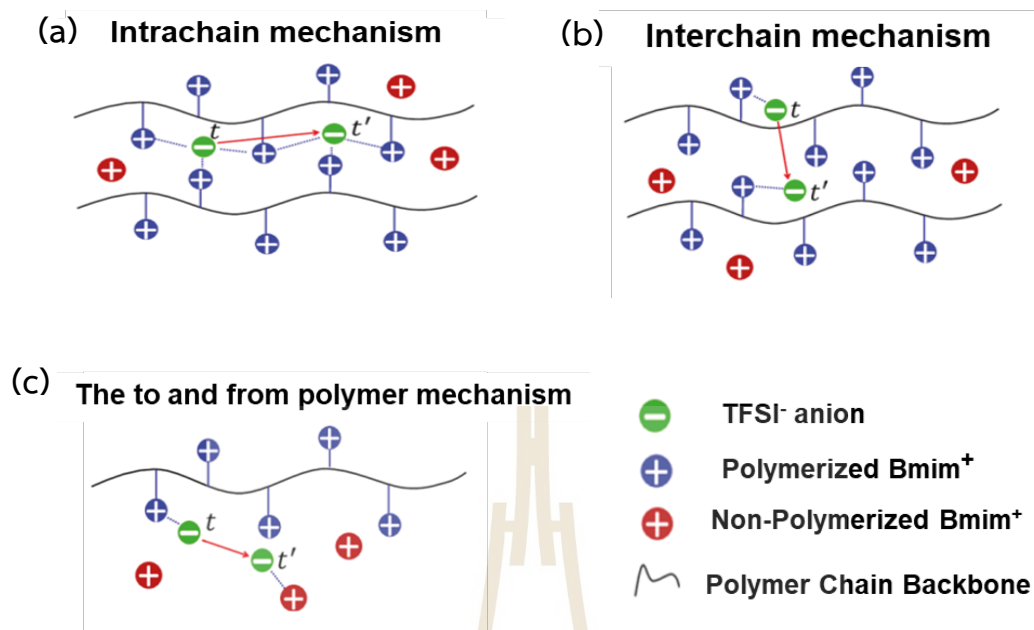


Figure 4.4.23 Definition of ion hopping mechanisms adopted in this work to distinguish different types of ion hopping events in poly(IL)-IL blend electrolytes from Mogurampelly et al. (Mogurampelly, 2018). The transition events are categorized into three types to represent (a) intrachain, (b) interchain, and (c) the to and from polymer chain hopping events.

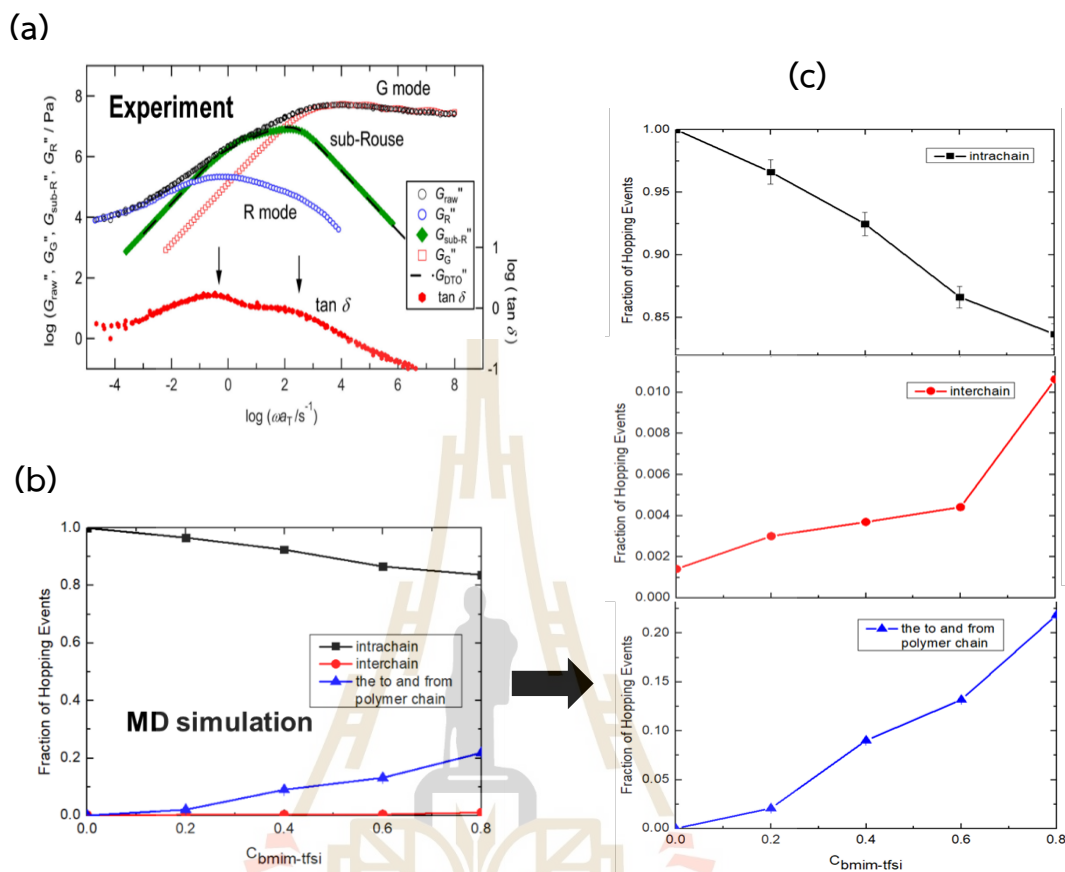


Figure 4.4.24 Fraction of transition rate of different hopping types as a function of pure ILs loading at 600K (a) Experimental result from (Inoue, 2013) (b) Result from MD simulation and (c) Individual result from MD simulation.

CHAPTER V

CONCLUSION

This thesis investigates multiscale computer simulations were applied to examine molecular determinants that can control structural properties of the host polymers in electrolyte application. To improve the ionic conductivity of polymer electrolytes, some possible paths are proposed to modify the repeating units to adjust the intrachain stiffness and intermolecular interaction that can affect conformational characteristics, molecular dimension, chain perturbation near the surface, crystallization, upon cooling from the melts, atomistic amorphous structures and the degree of ionic dissociation in polymerized ionic liquids.

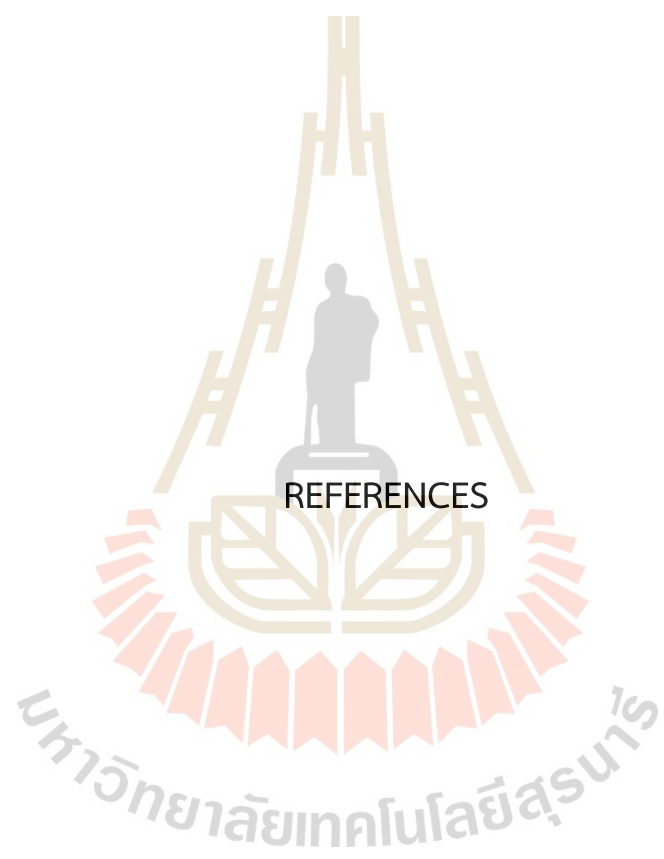
The First part is multiscale molecular simulations of two polymer hosts for gel electrolytes: PVC and PVF. This part illustrates a multiscale molecular modeling method to generate and equilibrate PVC and PVF models at their amorphous state. The method starts from quantum chemistry calculation to derive the statistical weights of the rotational isomeric state (RIS) model. PVC and PVF chains were then mapped to the coarse-grained (CG) model using the modified RIS model onto the 2nd lattice. The mapping of PVC and PVF chain can be done by grouping each monomer to one CG bead. The average non-bonded interactions were estimated using the discretized Lennard-Jones (LJ) potential. Coarse-grained PVC and PVF at the bulk density were then generated and readily equilibrated by lattice Monte Carlo simulation. The on-lattice properties were determined including chain conformational statistics and molecular mobility (rotational and translational modes). Dynamics of PVF is faster than PVC about one order of magnitude. The equilibrated PVC and PVF structures from the 2nd lattice were then reverse-mapped to fully atomistic models. Chain dimension, conformational statistics, structural and thermodynamic properties were determined for both neat PVC and PVF structures. All these results are comparable well with experiment data.

The second part is film stiffness, The effect of chain stiffness on structural and molecular properties of the free surfaces of polymer melts was studied by MC simulation of CG polyethylene-like models. The effect of chain stiffness on structural and molecular properties of the free surfaces of polymer melts was studied by MC simulation of CG polyethylene-like models. For polymer surfaces with more flexible chains, higher bulk densities with sharper surface profiles are obtained. Near the surface, end-bead monomers are more segregated for more flexible chains while middle-bead monomers are more depleted. As a function of chain stiffness, bulk densities become higher and accompanied by sharper surfaces. In general, both bonds and chains adopt random orientation in the structures but tend to have anisotropic orientation near the surface, especially more pronounced for stiffer chains. The molecular dimension has a more compact shape for more flexible chains because of a larger fraction of gauche conformation. Near the surface, chains are more flattened for stiffer chains, especially in the perpendicular direction to the surface. In the bulk region, more flexible chains adopt a larger amount of gauche conformation and have denser structures as evidenced by higher/lower intramolecular/intermolecular energies. In the surface region, however, chains tend to gain more trans conformation and the structures become less dense as indicated by lower/higher intramolecular/intermolecular energies.

The third part is the role of the intermolecular interaction related to the chain packing in the condensed phase, which can be intimately associated with polymer crystallization. Lattice Monte Carlo simulation has been developed to determine the effect of intermolecular interaction of CG PE-like chains on the structural formation during an initial stage under stepwise cooling from the molten state. The conformational characteristics, the bond and molecular orientation, structural packing, intra- and intermolecular bond order parameters were evaluated. The growth of structure formation is generally faster, and the chains can have better-ordered orientation for chains with intermolecular interaction parameters close to the normal PE. The PE-like chains with too attractive or too repulsive intermolecular interaction exhibit poorer crystallization characteristics as chains can adopt a lower amount of trans conformation and have more difficulty in forming the ordered structures. For PE-

like polymers with too repulsive interaction, larger fluctuations of the magnitudes of the conformational state and the order parameter are evidenced. For PE-like polymers with too attractive interaction, chains still adopt some amount of gauche conformation at lower temperatures with less degree of chain ordering. Thus, only PE-like chains with intermolecular interaction parameters close to the normal PE can exhibit the ordered structures with a large degree of trans conformation and chain orientation in the ordered structure formation under stepwise cooling from the molten state.

The final part is MD simulation of detailed structures and ion transportation of polymerized ionic liquid/ionic liquid blends. To summarize for the overall results from above, we reported molecular dynamics simulations of the structure, dynamical and ion transport properties of imidazolium-based polymerized ILs blended with IL electrolytes by GROMACS 2020.1 package. Our study is interested in the hypothesis that the addition of ionic liquids to polyILs can improve or accelerate the polymer/ion dynamics and simultaneously encourage mobile ions to the overall conductivity. To illustrate polymerized cations at the classical level within the framework of the OPLS-AA force field model, we tackled force field evolution by circumventing intramolecular interactions with the help of quantum mechanical calculations. Afterwards, atomistic molecular dynamics simulations at different IL concentrations were conducted to examine the mechanisms underlying ion transport in polyIL-IL blends. We illustrated results for the structural peculiarities, polymer dynamics, ion transport mechanisms, glass transition temperature (T_g), transference numbers, the ideal ionic conductivities and compared the behavior of polyIL-IL blends at different IL concentrations by MD simulation and experiment (T_g and conductivity). All properties above, indicating that are agreed between simulations and experiment results.



REFERENCES

REFERENCES

- Abe, A., Jernigan, R. L. and Flory, P. J. (1965). Conformational energies of n-alkanes and the random configuration of higher homologs including polymethylene. *Journal of the American Chemical Society*, 88, 631-639.
- Abraham, M., Hess, B., van der Spoel, D. and Lindahl, E. (2020). GROMACS Documentation Release 2020.1. *Royal Institute of Technology and Uppsala University: Sweden*. <https://doi.org/10.5281/zenodo.3685920>.
- Abraham, K. M., Jiang, Z. and Carroll, B. (1997). Highly conductive PEO like polymer electrolytes. *Chemistry of Materials Journal*. 9, 1978–19.
- Acevedo, O. (2018). Ionic liquid force field parameters (OPLS-2009IL and OPLS-VSIL). (accessed Dec 24, 2019). <https://github.com/orlandoacevedo/IL>.
- Akten E. D. and Mattice W. L. (2001). Monte Carlo simulation of head-to-head, tail-to-tail polypropylene and its mixing with polyethylene in the melt. *Macromolecules*. 34, 3389–3395.
- Allen, M. P. and Tildesley, D. J. (1987). *Computer simulation of liquids*, Oxford: Clarendon Press.
- Anogiannakis, S. D., Tzoumanekas, C. and Theodorou, D. N. (2012). Microscopic description of entanglements in polyethylene networks and melts: strong, weak, pairwise, and collective attributes. *Macromolecules*. 45(23), 9475–9492.
- Anwar, M. and Schilling, T. (2015). Crystallization of polyethylene: A molecular dynamics simulation study of the nucleation and growth mechanisms. *Polymer*. 76, 307–312.
- Balsara, N. P. and Newman, J. (2015). Relationship between steady-state current in symmetric cells and transference number of electrolytes comprising univalent and multivalent ions. *Journal of The Electrochemical Society*. 162, A2720–A2722.

- Baschnagel, J., Binder, K., Doruker P., Gusev, A., Hahn, O., Kremer, K., Mattice, W. L., Muller-Plathe, F., Murat, M., Paul, W., Santos, S., Suter, U. W. and Tries, V. (2000). Bridging the gap between atomistic and coarse-grained models of polymers: status and perspectives. *Advances in Polymer Science*. 152, 41–156.
- Bocharova, V. and Sokolov, A. P. (2020). Perspectives for Polymer Electrolytes: A View from Fundamentals of Ionic Conductivity. *Macromolecules*. 53, 4141-4157.
- Bovey, F. A., Hood, F. P., Anderson, E. W. and Kornegay, R. L. (1967). Polymer nuclear magnetic resonance spectroscopy. XII. The stereoregularity of poly(vinyl chloride) and its dependence on polymerization temperature. *The Journal of Physical Chemistry*. 71, 312.
- Boyd, R. H. and KESNER, L. (1981). Conformational properties of polar polymers. I. poly(vinyl chloride). *Journal of Polymer Science*. 19, 375-391.
- Brandrup, J. and Immergut, E. H. (2004). Polymer Handbook. John Wiley and Sons, New York.
- Cadogan, D. F. and Howick, C. J. (2000). Plasticizers. *Kirk-Othmer Encyclopedia of Chemical Technology*.
- Capiglia, C., Mustarelli, P., Quartarone, E., Tomasi, C. and Magistris, A. (1999). Effects of nanoscale SiO₂ on the thermal and transport properties of solvent-free, poly(ethylene oxide) (PEO)-based polymer electrolytes. *Solid State Ion*. 118, 73–79.
- Carballeira, L., Pereiras, A. J. and Rios, M. A. (1989). Conformational properties of poly(vinyl bromide) and poly(vinyl fluoride). *Macromolecules*. 22(6), 2668–2673.
- Chen, C. M. and Higgs, P. G. (1998). Monte-carlo simulations of polymer crystallization in dilute solution. *The Journal of Chemical Physics*. 108, 4305–4314.
- Choi, P. and Mattice, W. L. (2004). Molecular origin of demixing, prior to crystallization, of atactic polypropylene/isotactic polypropylene blends upon cooling from the melt. *The Journal of Chemical Physics*. 121(17), 8647-8651.
- Choi, U. H., Ye, Y., Salas de la Cruz, D., Liu, W., Winey, K. I., Elabd, Y. A., Runt, J. and Colby, R. H. (2014). Dielectric and viscoelastic responses of imidazolium-

- based ionomers with different counterions and side chain lengths. *Macromolecules*. 47, 777– 790.
- Cho, J. and Mattice, W. L. (1997). Estimation of long-Range interaction in coarse-grained rotational isomeric state polyethylene chains on a high coordination lattice. *Macromolecules*. 30(3), 637-644.
- Clancy, T. C. and Mattice, W. L. (2000). Rotational isomeric state chains on a high coordination lattice: Dynamic Monte Carlo algorithm details. *The Journal of Chemical Physics*. 112(22), 10049–10055.
- Correia, D. M., Sabater i Serra, R., Gómez Tejedor, J. A., de Zea Bermudez, V., Andrio Balado, A., Meseguer-Dueñas, J. M. and Costa, C. M. (2018). Ionic and conformational mobility in poly(vinylidene fluoride)/ionic liquid blends: Dielectric and electrical conductivity behavior. *Polymer*. 143, 164–172.
- Daniel, T., Hallinan, Jr. and Nitash P. B. (2013). Polymer electrolytes. *Annual Review of Materials Research*. 43, 503-525.
- De la Rosa, A., Heux, L., Cavaille J. Y. and Mazeau, K. (2002). Molecular modeling of the mobility of poly(allyl alcohol), PAA, and poly(vinyl alcohol), PVA. *Polymer*. 43, 5665–5677.
- Demir, B., Chan, K. Y., Searles, J. and Searles, D. J. (2020). Structural electrolytes based on epoxy resins and ionic liquids: A molecular-level investigation. *Macromolecules*. 53, 7635– 7649.
- Dionne P. J., Ozisik, R. and Picu C. R. (2005). Structure and dynamics of polyethylene nanocomposites. *Macromolecules*. 38, 9351–9358.
- Dionne, P. J., Picu, C. R. and Ozisik, R. (2006). Adsorption and desorption dynamics of linear polymer chains to spherical nanoparticles: a monte carlo investigation. *Macromolecules*. 39(8), 3089–3092.
- Dobrynin, A. V., Colby, R. H. and Rubinstein, M. (1995). Scaling theory of polyelectrolyte solutions. *Macromolecules*. 28, 1859–187.
- Doherty, B., Zhong, X., Gathiaka, S., Li, B. and Acevedo, O. (2017). Revisiting OPLS force field parameters for ionic liquid simulations. *Journal of Chemical Theory and Computation*. 13, 6131–6145.

- Doruker, P. and Mattice, W. L. (1997). Reverse mapping of coarse-grained polyethylene chains from the second nearest neighbor diamond lattice to an atomistic model in continuous space. *Macromolecules*. 30(18), 5520-5526.
- Doruker, P. and Mattice, W. L. (1998). Dynamics of Bulk Polyethylene on a High Coordination Lattice. *Macromolecular Symposia*. 133, 47-70.
- Doruker, P. and Mattice, W. L. (1998). Simulation of polyethylene thin films on a high coordination lattice, *Macromolecules*. 31, 1418-1426.
- Doruker, P. and Mattice, W. L. (1999). Mobility of the surface and interior of thin films composed of amorphous polyethylene. *Macromolecules*. 32, 194-198.
- Ergoz, E., Fatou, J. G. and Mandelkern, L. (1972). Molecular weight dependence of the crystallization kinetics of linear polyethylene. I. experimental results. *Macromolecules*. 5, 147-157.
- Esselink, K., Hilbers, P. A. J. and Van Beest, B. W. H. (1994). Molecular dynamics study of nucleation and melting of n-alkanes. *The Journal of Chemical Physics*. 101, 9033-9041.
- Feast, W. J. and Munro, H. S. (Eds). (1987). Polymer surfaces and surfaces. *John Wiley and Sons, New York*. 33(12), 2092.
- Feng, G., Chen, M., Bi, S., Goodwin, Z. A. H., Postnikov, E. B., Brilliantov, N., Urbakh, M. and Kornyshev, A. A. (2019). Free and bound states of ions in ionic liquids, conductivity, and underscreening paradox. *Physical Review X*. 9, 021024.
- Fenton, D. E., Parker, J. M. and Wright, P. V. (1973). Complexes of alkali metal ions with poly(ethylene oxide). *Polymer*. 14, 589.
- Flory, P. J. (1969). Statistical Mechanics of Chain Molecules. *Wile, New York*.
- Flory, P. J., Sundararajan, P. R. and DeBolt, L. C. (1974). Configurational statistics of vinyl polymer chains. *Journal of the American Chemical Society*. 96, 5015-5024.
- Forrest, J. A., Dalnoki-Veress, K., Stevens, J. R. and Dutcher, J. R. (1992). Effect of free surfaces on the glass transition temperature of thin polymer films. *Physical Review Letters*. 77(10), 2002-2005.
- Forsyth, M., Porcarelli, L., Wang, X., Goujon, N. and Mecerreyes, D. (2019). Innovative electrolytes based on ionic liquids and polymers for next-generation solid-state batteries. *Accounts of Chemical Research*. 52, 686-694.

- Foteinopoulou, K., Karayiannis, N. C., Laso, M. and Kröger, M. (2009). Structure, dimensions, and entanglement statistics of long linear polyethylene chains. *The Journal of Physical Chemistry B*. 113, 442-455.
- Fujiwara, S. and Sato, T. (1997). Molecular dynamics simulations of structural formation of a single polymer chain: Bond-orientational order and conformational defects. *The Journal of Chemical Physics*. 107, 613-622.
- Fujiwara, S. and Sato, T. (1998). Molecular dynamics simulation of structural formation of short polymer chains. *Physical Review Letters*. 80, 991-994.
- Fujiwara, S. and Sato, T. (1999). Molecular dynamics simulation of structure formation of short chain molecules. *The Journal of Chemical Physics*. 110, 9757-9764.
- Fujiwara, S. and Sato, T. (2001). Structure formation of a single polymer chain. I. Growth of trans domains. *The Journal of Chemical Physics*. 114, 6455-6463.
- Garbassi, F., Morra, M. and Occhiello, E. (1994). Polymer surfaces — from physics to technology. *John Wiley & Sons. Chichester*.
- Gee, R. H., Lacevic, N. and Fried, L. E. (2006). Atomistic simulations of spinodal phase separation preceding polymer crystallization. *Nature Materials*. 5, 39-43.
- Graham, W. and Watts, D. C. (1970). Non-symmetrical dielectric relaxation behaviour arising from a simple empirical decay function. *Transactions of the Faraday Society*. 66, 80-85.
- Haliloglu, T. and Mattice, W. L. (1998). Mapping of rotational isomeric state chains with asymmetric torsional potential energy functions on a high coordination lattice: Application to polypropylene. *The Journal of Chemical Physics*. 108(16), 6989-6995.
- Hallinan, D. T., and Balsara, N. P. (2013). Polymer electrolytes. *Annual Review of Materials Research*. 43, 503.
- Harmandaris, V. A., Mavrantzas, V. G. and Theodorou, D. N. (1998). Atomistic molecular dynamics simulation of polydisperse linear polyethylene melts. *Macromolecules*. 31, 7934-7943.
- Helfand, E. and Tagami, Y. (1972). Theory of surface between immiscible polymers. *The Journal of Chemical Physics*. 56, 3592-3601.

- Holbrey, J. and Seddon, K. (1999). Ionic liquids. *Clean Products and Processes*. 1, 223–236.
- Humphrey, W., Dalke, A. and Schulten, K. (1996). VMD: Visual molecular dynamics. 14(1), 33–38.
- Hu, W. and Frenkel, D. (2005). Polymer crystallization driven by anisotropic interactions. In: allegro, G. (eds) interphases and mesophases in polymer crystallization III. *Advances in Polymer Science*. 191, 1–35.
- Inoue, T., Matsumoto, A. and Nakamura, K. (2013). Dynamic viscoelasticity and birefringence of poly (ionic liquids) in the vicinity of glass transition zone. *Macromolecules*. 46(15), 6104–6109.
- Itoh, T., Fujita, K., Uno, T. and Kubo, M. (2017). Polymer electrolytes based on vinyl ethers with various EO chain length and their polymer electrolytes cross-linked by electron beam irradiation. *Ionics*. 23, 257–264.
- Jabbari-Farouji, S., Rottler, J., Lame, O., Makke, A., Perez, M. and Barrat, J. L. (2015). Correlation of structure and mechanical response in solid-like polymers. *Journal of Physics: Condensed Matter*. 27(19), 194131.
- Jacek Dudowicz, J., Douglas, J. F. and Freed, K. F. (2014). Two glass transitions in miscible polymer blends?. *The Journal of Chemical Physics*. 140(24), 244905.
- Jamornsuriya, S. and Vao-soongnern, V. (2022). Molecular simulation of an initial stage of the ordered-structure formation of linear and ring polymers upon cooling from the melts. *Journal of Molecular Liquids*. 363, 119833.
- Jang, J. H. and Mattice, W. L. (2000). A monte carlo simulation for the effect of compression on an amorphous polyethylene melt in very thin confined geometry. *Macromolecules*. 33(4), 1467–1472.
- Jorgensen, W. L., Maxwell, D. S. and Tirado-Rives, J. (1996). Development and testing of the OPLS All-Atom force field on conformational energetics and properties of organic liquids. *Journal of the American Chemical Society*. 118, 11225-11236.
- Karayiannis, N. C., Giannousaki, A. E., Mavrantzas, V. G. and Theodorou, D. N. (2002). Atomistic monte carlo simulation of strictly monodisperse long polyethylene

- melts through a generalized chain bridging algorithm. *The Journal of Chemical Physics*. 117, 5465–5479.
- Karayiannis, N. C., Mavrantzas, V. G. and Theodorou, D. N. (2002). A novel monte carlo scheme for the rapid equilibration of atomistic model polymer systems of precisely defined molecular architecture. *Physical Review Letters*. 88, 105503.
- Kavassalis, T. A. and Sundararajan, P. R. (1993). A molecular-dynamics study of polyethylene crystallization. *Macromolecules*. 26, 4144–4150.
- Keith, J. R., Mogurampelly, S., Aldukhi, F., Wheatle, B. K. and Ganesan, V. Influence of molecular weight on ion-transport properties of polymeric ionic liquids. *Physical Chemistry Chemical Physics*. 19, 29134–29145.
- Khongvit, P. and Orrasa, N. N. (2020). Functionalized graphenes as nanofillers for polylactide: Molecular dynamics simulation study. *Polymer Composites*. 41, 294-305.
- Khongvit, P. (2016). A coarse-grained model for polylactide: glass transition temperature and conformational properties. *Journal of Polymer Research*. 23, 139.
- Kikkawa, Y., Suzuki, T., Kaneshato, M., Doi, Y. and Abe, H. (2009). Effect of phase structure on enzymatic degradation in poly(L-lactide)/Atactic Poly(3-hydroxybutyrate) blends with different miscibility. *Biomacromolecules*. 10(4), 1013–1018.
- Kisliuk, A., Bocharova, V., Popov, I., Gainaru, C. and Sokolov, A. P. (2019). Fundamental parameters governing ion conductivity in polymer electrolytes. *Electrochimica Acta*. 299, 191–196.
- Kivelson, D., Jr, E. B. W. and Jr, D. R. L. (1960). Microwave spectrum, structure, dipole moment, and nuclear quadrupole effects in vinyl chloride. *The Journal of Chemical Physics*. 32, 205–209.
- Ko, M. J., Waheed, M. J., Lavine, M. S. and Rutledge, G. C. (2004). Characterization of polyethylene crystallization from an oriented melt by molecular dynamics simulation. *The Journal of Chemical Physics*. 121, 2823–2832.
- Kotelyanskii, M. and Theodorou, D. N. (2004). Simulation methods for polymers. *Marcel Dekker. New York*.

- Koyama, A., Yamamoto, T., Fukao, K. and Miyamoto, Y. (2002). Molecular dynamics simulation of polymer crystallization from an oriented amorphous state. *Physical Review E*. 65, 050801.
- Koyama, A., Yamamoto, T., Fukao, K. and Miyamoto, Y. (2003). Molecular dynamics studies on polymer crystallization from a stretched amorphous state. *Journal of Macromolecular Science Part B-Physics*. 42, 821–831.
- Koyama, A., Yamamoto, T., Fukao, K. and Miyamoto, Y. (2008). Molecular dynamics studies on spatial scale of low energy excitation in a simple polymer system. *Physical Review*. E. 4-7.
- Kremer, F. and Schönhals, A. (2003). Broadband Dielectric Spectroscopy. *Springer-Verlag: Berlin*.
- Kumar, S. K., Russell, T. P. and Hariharan, A. (1994). Monte carlo simulations of the free surface of polymer melts. *Chemical Engineering Science*. 49, 2899–2906.
- Kusinram, C. and Vao-soongnern, V. (2022). A multiscale simulation of amorphous poly(vinyl alcohol). *Materials Today Communications*. 30, 103029.
- Lavine, M. S., Waheed, N. and Rutledge, G. C. (2003). Molecular dynamics simulation of orientation and crystallization of polyethylene during uniaxial extension. *Polymer*. 44, 1771-1779.
- Lee, K. J. and Mattice, W. L. (1992). Modeling of glassy poly (vinyl chloride) starting from a random model. *Computational and Theoretical Polymer Science*. 2, 55-63.
- Lei, Z., Chen, B., Koo, Y.-M. and MacFarlane, D. R. (2017). Introduction: ionic liquids. *Chemical Reviews*. 117(10), 6633–6635.
- Li, C., Choi, P. and Sundararajan, P. R. (2010). Simulation of chain folding in polyethylene: A comparison of united atom and explicit hydrogen atom models. *Polymer*. 51, 2803–2808.
- Lodge, T. P. and McLeish, T. C. B. (2000). Self-concentrations and effective glass transition temperatures in polymer blends. *Macromolecules*. 33(14), 5278–5284.

- Lodge, T. P., Wood, E. R. and Haley, J. C. (2006). Two calorimetric glass transitions do not necessarily indicate immiscibility: The case of PEO/PMMA. *Journal of Polymer Science Part B: Polymer Physics*. 44(4), 756– 763.
- Ludovice, P. J. and Suter, U. W. (1992). In computational modeling of polymers. *Bicerano, J., Ed. Marcel Dekker, New York*. 401.
- Luo, C. and Sommer, J. U. (2009). Coding coarse grained polymer model for LAMMPS and its application to polymer crystallization. *Computer Physics Communications*. 180, 1382-1391.
- Luo, C. and Sommer, J. U. (2011). Growth pathway and precursor states in single lamellar crystallization: MD simulations. *Macromolecules*. 44, 1523-1529.
- Luo, C. and Sommer, J. U. (2013). Disentanglement of linear polymer chains toward unentangled crystals. *ACS Macro Letters*. 2, 31-34.
- Luo, C. and Sommer, J. U. (2016). Role of thermal history and entanglement related thickness selection in polymer crystallization. *ACS Macro Letters*. 5(1), 30-34.
- Luo, C., Kroger, M. and Sommer, J.-U. (2017). Molecular dynamics simulations of polymer crystallization under confinement: "Entanglement effect. *Polymer*. 109, 71–84.
- Luo, X. B., Liu, H. J. and Paddison, S. J. (2021). Molecular dynamics simulations of polymerized ionic liquids: mechanism of ion transport with different anions. *ACS Applied Polymer Materials Journal*. 3, 141– 152.
- Mansfield, K. F. and Theodorou, D. N. (1990). Atomistic simulation of a glassy polymer surface. *Macromolecules*. 23, 4430–4445.
- Manthiram, A., Yu, X. and Wang, S. (2017). Lithium battery chemistries enabled by solid-state electrolytes. *Nature Reviews Materials*. 2, 16103.
- Mark, J. E. (1972). Random-coil dimensions and dipole moments of vinyl chloride chains. *The Journal of Chemical Physics*. 56, 451-458.
- Matsumoto, A., Del Giudice, F., Rotrattanadumrong, F. and Shen, A. Q. (2019). Rheological scaling of ionic-liquid-based polyelectrolytes in ionic liquid solutions. *Macromolecules*. 52, 2759– 2771.

- Mattice, W. L. and Suter, U. W. (1994). Conformational Theory of Large Molecules. The Rotational Isomeric State Model in Macromolecular Systems. *Wiley, New York*.
- Mavrantza, I. E., Prentzas, D., Mavrantzas, V. G. and Galiotis, C. (2001). Detailed atomistic molecular-dynamics simulation of the orthorhombic phase of crystalline polyethylene and alkane crystals. *The Journal of Chemical Physics*. 115, 3937-3950.
- Mavrantzas, V. G. and Theodorou, D. N. (1998). Atomistic simulation of polymer melt elasticity: Calculation of the free energy of an oriented polymer melt. *Macromolecules* 31, 6310–6332.
- Mayo, S. L., Olafson, B. D. and Goddard W. A. (1990). III, DREIDING: A generic force field for molecular simulations. *The Journal of Chemical Physics*. 94, 8897–8909.
- McDaniel, J. G. and Son, C. Y. (2018). Ion correlation and collective dynamics in BMIM/BF₄-based organic electrolytes: From dilute solutions to the ionic liquid limit. *The Journal of Physical Chemistry B*. 122, 7154–7169.
- Meyer, H. and Muller-Plathe, F. (2001). Formation of chain-folded structures in supercooled polymer melts. *The Journal of Chemical Physics*. 115, 7807-7810.
- Meyer, H. and Muller-Plathe, F. (2002). Formation of chain-folded structures in supercooled polymer melts examined by MD simulations. *Macromolecules*. 35, 1241-1252.
- Mecerreyes, D. (2011). Polymeric ionic liquids: Broadening the properties and applications of polyelectrolytes. *Progress in Polymer Science*. 36, 1629–1648.
- Misra, S., Fleming, P. D. and Mattice, W. L. (1995). Structure and energy of thin films of poly-(1,4-cis-butadiene): a new atomistic approach. *Journal of Computer-Aided Materials Design*. 2, 101–112.
- Mittal, K. L. (Ed). (1983). Physicochemical aspects of polymer surfaces. *Plenum Press, New York*. 1.
- Mittal, K. L. (Ed). (1983). Physicochemical aspects of polymer surfaces, *Plenum Press, New York*. 2.

- Mogurampelly, S. and Ganesan, V. (2018). Ion transport in polymerized ionic liquid–ionic liquid blends. *Macromolecules*. 51, 9471– 9483.
- Mogurampelly, S., Keith, J. R. and Ganesan, V. (2017). Mechanisms underlying ion transport in polymerized ionic liquids. *Journal of the American Chemical Society*. 139, 9511– 9514.
- Muthukumar, M. (2005). Modeling polymer crystallization. *Advances in Polymer Science*. 191, 241.
- Nakajima, A. and Kato, K. (1966). Unperturbed chain dimension of poly(vinyl chloride) polymerized at different temperatures. *Die Makromolekulare Chemie*. 95, 52-63.
- Nguyen, H. T., Smith, T. B., Hoy, R. S. and Karayiannis, N. C. (2015). Effect of chain stiffness on the competition between crystallization and glass-formation in model unentangled polymers. *The Journal of Chemical Physics*. 143, 144901.
- Nicholson, D. A. and Rutledge, G. C. (2016). Molecular simulation of flow-enhanced nucleation in n-eicosane melts under steady shear and uniaxial extension. *The Journal of Chemical Physics*. 145, 244903.
- Ohno, H. (2001). Molten salt type polymer electrolytes. *Electrochimica Acta*. 46(10-11), 1407–1411.
- Olivier-Bourbigou, H., Magna, L. and Morvan, D. (2010). Ionic liquids and catalysis: recent progress from knowledge to applications. *Applied Catalysis A: General*. 373, 1–56.
- Paul, W., Yoon, D. Y. and Smith, G. D. (1995). An optimized united atom model for simulations of polymethylene melts. *The Journal of Chemical Physics*. 103, 1702–1709.
- Piorkowska, E. and Rutledge, G. C. (2013). Handbook of Polymer Crystallization. *John Wiley & Sons, New Jersey*.
- Poling, B. E., Prausnitz, J. M. and O’Connell, J. P. (2000). Properties of Gases and Liquids 5th Ed. *McGraw-Hill, New York*.
- Poling, B. E., Prausnitz, J. M. and O’Connell, J. P. (2002). Properties of Gases and Liquids 5th Ed. *McGraw-Hill, New York*.

- Qian, W. J., Texter, J. and Yan, F. (2017). Frontiers in poly (ionic liquid)s: Syntheses and applications. *Chemical Society Reviews*. 46, 1124–1159.
- Quartarone, E. and Mustarelli, P. (2011). Electrolytes for solid-state lithium rechargeable batteries: recent advances and perspectives. *Chemical Society Reviews*. 40, 2525-2540.
- Ramos, J., Vega, J. F. and Martinez-Salazar, J. (2015). Molecular dynamics simulations for the description of experimental molecular conformation, melt dynamics, and phase transitions in polyethylene. *Macromolecules*. 48, 5016-5027.
- Rane, S. S. and Mattice, W. L. (2004). Relative magnitudes of the short-term motions of the cyclic and linear components of a homopolyrotaxane in θ media. *Macromolecules*. 37(18), 7056–7060.
- Rane, S. S. and Mattice, W. L. (2005). Structure and internal dynamics of poly(ethylene oxide) catenanes in the melt. *Macromolecules*. 38, 3708–3712.
- Ratner, M. A. and Shriver, D. F. (1988). Ion transport in solvent-free polymers. *Chemical Reviews*. 88, 109–124.
- Rehahn, M., Mattice, W. L. and Suter, U. W. (1997). Rotational isomeric state models in macromolecular systems. *Advances in Polymer Science*. 131/132.
- Reith, D., Meyer, H. and Mu, F. (2001). Mapping atomistic to coarse-grained polymer models using automatic simplex optimization to fit structural properties. *Macromolecules*. 35(7), 2335-2345.
- Rigby, D. and Roe, R. J. (1987). Molecular dynamics simulation of polymer liquid and glass. I. Glass transition. *The Journal of Chemical Physics*. 87, 7285–7292.
- Rochow, E. T., Coeler, M., Pospiech, D., Kobsch, O., Mechtaeva, E., Vogel, R., Voit, B., Nikolowski, K. and Wolter, M. (2020). In situ preparation of crosslinked polymer electrolytes for lithium ion batteries: a comparison of monomer systems. *Polymers*. 12, 1707.
- Saha, S. and Bhowmick, A. K. (2016). Computer simulation of thermo-plastic elastomers from rubber-plastic blends and comparison with experiments. *Polymer*. 103, 233–242.
- Sangoro, J. R., Iacob, C., Agapov, A. L., Wang, Y., Berdzinski, S., Rexhausen, H., Strehmel, V., Friedrich, C., Sokolov, A. P. and Kremer, F. (2014). Decoupling of ionic

- conductivity from structural dynamics in polymerized ionic liquids. *Soft Matter*. 10, 3536–3540.
- Sangoro, J. R., Jacob, C., Naumov, S., Valiullin, R., Rexhausen, H., Hunger, J., Buchner, R., Strehmel, V., Karger, J. and Kremer, F. (2011). Diffusion in ionic liquids: the interplay between molecular structure and dynamics. *Soft Matter*. 7, 1678–1681.
- Scott, M. P., Brazel, C. S., Benton, M. G., Mays, J. W., Holbrey, J. D. and Rogers, R. D. (2002). Application of ionic liquids as plasticizers for poly(methyl methacrylate). *Chemical Communications*. 1370–1371.
- Shaplov, A. S., Ponkratov, D. O. and Vygodskii, Y. S. (2018). Poly(ionic liquid)s: synthesis, properties, and application. *Polymer Science, Series B*. 58, 73–142.
- Sirirak, K. and Vao-soongnern, V. (2023). Molecular simulation for the effect of chain stiffness on polymer crystallization from the melts. *Journal of Molecular Liquids*. 387, 122650.
- Sirirak, K. and Vao-soongnern, V. (2023). Molecular simulation of structural properties of polymer blend nanofilms. *Journal of Polymer Research*. 30(1), 46.
- Smith, G. D., Jaffe, R. L. and Yoon, D. Y. (1994). Conformational characteristics of poly(tetrafluoroethylene) chains based upon ab Initio electronic structure calculations on model molecules. *Macromolecules*. 27, 3166–3173.
- Smith, G. D., Ludovice, P. J., Jaffe, R. L. and Yoon, D. Y. (1995). Conformations of 2,4-dichloropentane and 2,4,6-trichloroheptane and a force field for poly (vinyl chloride) based upon ab Initio electronic structure calculations. *The Journal of Physical Chemistry*. 99, 164–172.
- Solc, K. and Stockmayer, W. H. (1971). Shape of random-flight chains. *The Journal of Chemical Physics*. 54, 2756–2757.
- Song, J. Y., Wang, Y. Y. and Wan, C. C. (1999). Review of gel-type polymer electrolytes for lithium-ion batteries. *Journal of Power Sources*. 77, 183–197.
- Stamm, M. (1992). Polymer surfaces on a molecular scale: comparison of techniques and some examples. *Advances in Polymer Science*. 100, 357.
- Sundararajan, P. R. and Kavassalis, T. A. (1995). Molecular dynamics study of polyethylene chain folding: The effects of chain length and the torsional

- barrier. *Journal of the Chemical Society, Faraday Transactions.* 91, 2541–2549.
- Takeuchi, H. (1998). Structure formation during the crystallization induction period of a short chain-molecule system: A molecular dynamics study. *The Journal of Chemical Physics.* 1095, 614–5621.
- Tarascon, J. M. and Armand, M. (2001). Issues and challenges facing rechargeable lithium batteries. *Nature.* 414, 359-367.
- Theodorou, D. H. and Suter, U. W. (1985). Detailed molecular structure of a vinyl polymer glass. *Macromolecules.* 18, 1467–1478.
- Thomas, S., Grohens, Y. and Jyotishkumar, P. (2014). Characterization of polymer blends: miscibility, morphology and interfaces. Eds. *Wiley-VCH Verlag: Weinheim, Germany.*
- Vao-soongnern, V. and Jamornsuriya, S. (2021). Molecular simulation of structural and surface properties of poly(ethylene-ran-propylene) thin films. *Journal of Polymer Research.* 28, 340.
- Vao-soongnern, V. and Mattice, W. L. (2000). Topological effects on static and dynamic properties in an amorphous nanofiber composed of cyclic polymers. *Macromolecular Theory and Simulations.* 9, 570–577.
- Vao-soongnern, V., Doruker, P. and Mattice, W. L. (2000). Simulation of an amorphous polyethylene nanofiber on a high coordination lattice. *Macromolecular Theory and Simulations.* 9, 1-13.
- Vao-soongnern, V., Ozisik, R. and Mattice W. L. (2001). Monte carlo simulation of the structures and dynamics of amorphous polyethylene nanoparticles. *Macromolecular Theory and Simulations.* 10, 553-563.
- Vao-soongnern, V., Sukhonthamethirat, N., Rueangsri, K., Sirirak, K. and Matsuba, G. (2023). Molecular simulation of the structural formation of mono- and bidisperse polyethylene upon cooling from the melts. *Journal of Molecular Liquids.* 376, 121434.
- Vao-soongnern, V., Xu, G. and Mattice, W. L. (2004). Structure formation in the crystallization and annealing of tetracontane nanoparticles. *Macromolecular Theory and Simulations.* 13(6), 539-549.

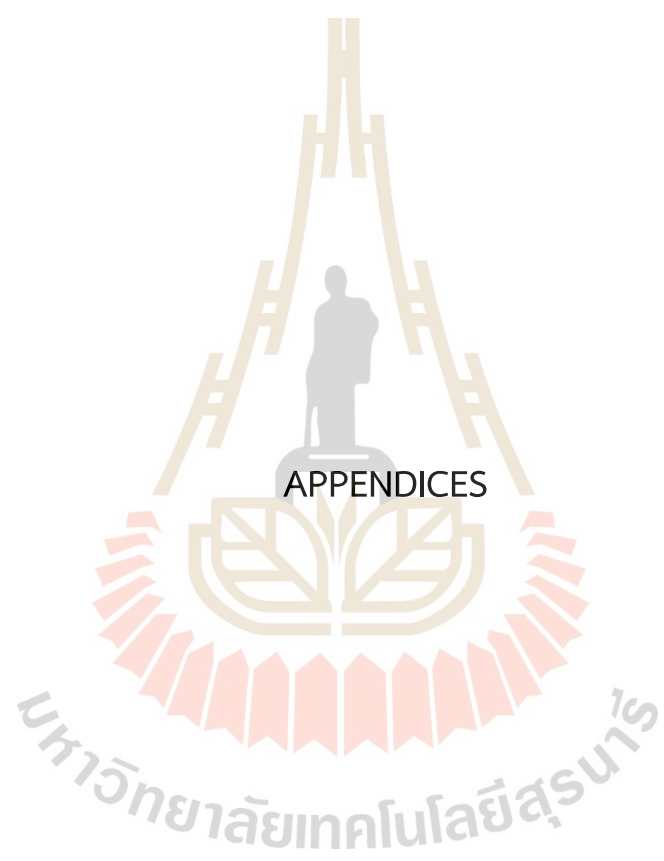
- Vao-soongnern, V. (2006). Nanostructure of the interface modified by grafted polymers: a monte carlo simulation. *Journal of Nanoscience and Nanotechnology*. 6, 3977-3980.
- Vao-soongnern, V. (2010). Monte carlo simulations of structures and dynamics of cyclic and linear poly(ethylene oxide) melts. *Computational Materials Science*. 49(4), S369–S371.
- Vao-soongnern, V. (2014). A multiscale simulation model for poly (ethylene oxide). *Polymer Science Series*. 56, 928–935.
- Verho, T., Paajanen, A., Vaari, V. and Laukkanen, A. (2018). Crystal growth in polyethylene by molecular dynamics: The crystal edge and lamellar thickness. *Macromolecules*. 51, 4865–4873.
- Waheed, N., Ko, M. J. and Rutledge, G. C. (2005). Molecular simulation of crystal growth in long alkanes. *Polymer*. 46, 8689–8702.
- Waheed, N., Lavine, M. S. and Rutledge, G. C. (2002). Molecular simulation of crystal growth in n-eicosane. *The Journal of Chemical Physics*. 116, 2301–2309.
- Watanabe, M. and Mizumura, T. (1996). Conductivity study on ionic liquid/polymer complexes. *Solid State Ionics*. 86–88, 353-356.
- Welch, P. M. (2017). Examining the role of fluctuations in the early stages of homogenous polymer crystallization with simulation and statistical learning. *The Journal of Chemical Physics*. 146, 044901.
- Wichai, S. and Vao-soongnern, V. (2021). A multiscale simulation of amorphous polystyrene. *Journal of Polymer Research*. 28, 109.
- Wichai, K. and Vao-soongnern, V. (2021). Monte carlo simulation of molecular and structural properties of random copolymer thin films. *Journal of Molecular Modeling*. 27(10), 301.
- Wright, P. V. (1975). Electrical conductivity in ionic complexes of poly(ethylene oxide). *British Polymer Journal*. 7, 319-327.
- Xiao, H., Luo, C., Yan, D. and Sommer, J.-U. (2017). Molecular dynamics simulation of crystallization cyclic polymer melts as compared to their linear counterparts. *Macromolecules*. 50, 9796–9806.

- Xu, G. and Mattice, W. L. (2001). Study on structure formation of short polyethylene chains via dynamic Monte Carlo simulation. *Computational and Theoretical Polymer Science*. 11(6), 405–413.
- Xu, G. and Mattice, W. L. (2002). Monte carlo simulation of the crystallization and annealing of a freestanding thin film of n-tetracontane. *The Journal of Chemical Physics*. 116(5), 2277–2283.
- Xu, G., Lin, H. and Mattice, W. L. (2003). Configuration selection in the simulations of the crystallization of short polyethylene chains in a free-standing thin film. *The Journal of Chemical Physics*. 119(13), 6736–6743.
- Xu, G., Vao-soongnern, V. and Mattice, W. L. (2002). Similarities and differences in the rapid crystallization induced in n-tetracontane by an instantaneous deep quench of the free-standing nanofiber and free-standing thin film. *Macromolecular Theory and Simulations*. 11(5), 494-500.
- Yabe, M., Mori, K., Ueda, K. and Takeda, M. (2019). Development of PolyPreGen software to facilitate the determination of molecular dynamics simulation parameters for polymers. *Journal of Computer Chemistry, Japan International Edition*. 5, 2018-0034.
- Yamamoto, T. (2005). Molecular dynamics modeling of the crystal-melt interfaces and the growth of chain folded lamellae. *Advances in Polymer Science*. 191, 37-85.
- Yamamoto, T. (2009). Computer modeling of polymer crystallization - Toward computer-assisted materials' design. *Polymer*. 50(9), 1975-1985.
- Yamamoto, T. (2013). Molecular dynamics of polymer crystallization revisited: Crystallization from the melt and glass in longer polyethylene. *The Journal of Chemical Physics*. 139, 054903.
- Yamamoto, T. (2014). Molecular dynamics in fiber formation of polyethylene and large deformation of the fiber. *Polymer*. 54, 3086-3097.
- Yamamoto, T. (2014). Molecular dynamics of crystallization in a helical polymer isotactic polypropylene from the oriented amorphous state. *Macromolecules*. 47, 3192-3202.

- Yao, P., Yu, H., Ding, Z., Liu, Y., Lu, J., Lavorgna, M., Wu, J. and Liu, X. (2019). Review on polymer-based composite electrolytes for lithium batteries. *Frontiers in Chemistry*. 7, 522.
- Yi, P. and Rutledge, G. C. (2009). Molecular simulation of crystal nucleation in n-octane melts. *The Journal of Chemical Physics*. 131, 134902.
- Yi, P. and Rutledge, G. C. (2011). Molecular simulation of bundle-like crystal nucleation from n-eicosane melts. *The Journal of Chemical Physics*. 135, 24903.
- Yi, P., Locker, C. R. and Rutledge, G. C. (2013). Molecular dynamics simulation of homogeneous crystal nucleation in polyethylene. *Macromolecules*. 46, 4723-4733.
- Yoshizawa-Fujita, M., Ishii, J., Takeoka, Y. and Rikukawa, M. (2021). Oligoether/Zwitterion diblock copolymers: synthesis and application as cathode-coating material for Li batteries. *Polymers*. 13, 800.
- Zhang, H., Liu, C., Zheng, L., Xu, F., Feng, W., Li, H., Huang, X., Armand, M., Nie, J. and Zhou, Z. (2014). Lithium bis(fluorosulfonyl)imide/poly(ethylene oxide) polymer electrolyte. *Electrochimica Acta*. 133, 529–538.
- Zhang, J., Liang, Y., Yan, J. and Lou, J. (2007). Study of the molecular weight dependence of glass transition temperature for amorphous poly(L-lactide) by molecular dynamics simulation. *Polymer*. 48, 4900-4905.
- Zhang, Q., Liu, K., Ding, F. and Liu, X. (2017). Recent advances in solid polymer electrolytes for lithium batteries. *Nano Research*. 10, 4139–4174.
- Zhang, S.Y., Zhuang, Q., Zhang, M., Wang, H., Gao, Z.M., Sun, J. K. and Yuan, J. Y. (2020). Poly(ionic liquid) composites. *Chemical Society Reviews*. 49, 1726–1755.
- Zhang, Z. J., Lu, Z. Y., Li, Z. S. and Sun, C. C. (2005). Conformational properties of poly(vinyl Fluoride) based upon ab initio electronic structure calculations. *Chemical Physics Letters*. 406(4-6), 504–508.
- Zhang, Z., Nasrabadi, A. T., Aryal, D. and Ganesan, V. (2020). Mechanisms of ion transport in lithium salt-doped polymeric ionic liquid electrolytes. *Macromolecules*. 53, 6995– 7008.

Zhang, Z., Wheatle, B. K., Krajniak, J., Keith, J. R. and Ganesan, V. (2020). Ion mobilities, Transference Numbers, and Inverse Haven Ratios of Polymeric Ionic Liquids. *ACS Macro Letters Journal*. 9, 84–89.

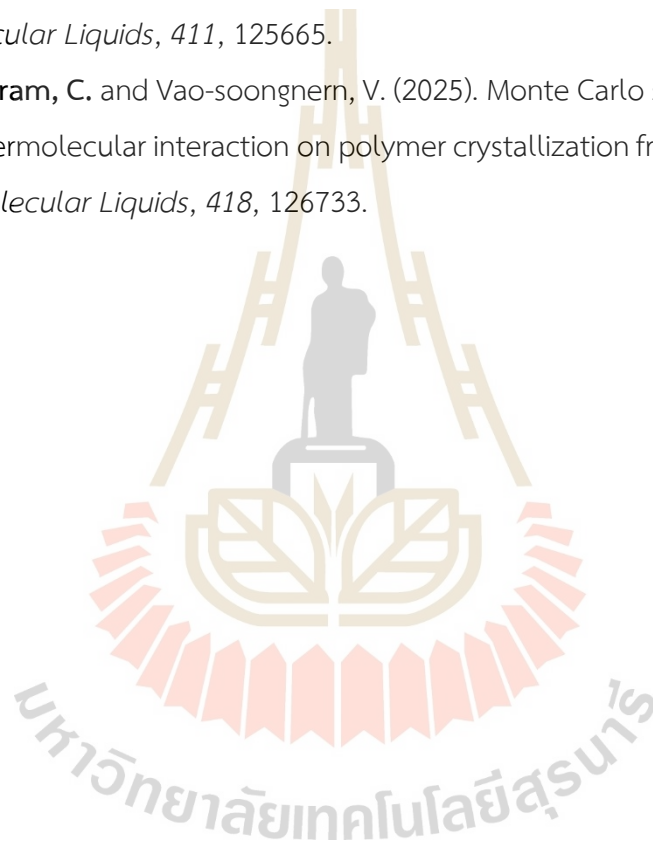




APPENDIX A

THESIS OUTPUT (PUBLICATIONS)

1. **Kusinram, C.** and Vao-soongnern, V. (2024). Monte Carlo simulation for the effect of chain stiffness on the free surface of polymer melts. *Journal of Molecular Liquids*, 411, 125665.
2. **Kusinram, C.** and Vao-soongnern, V. (2025). Monte Carlo simulation for the role of intermolecular interaction on polymer crystallization from the melts. *Journal of Molecular Liquids*, 418, 126733.



APPENDIX B

INTERNATIONAL CONFERENCE I

The 17th International Workshop for East Asian Young Rheologists (IWEAYR-17), Busan, Korea.

The 16th International Workshop for East Asian Young Rheologists Conference
IWEAYR-16, Udon Thani, Thailand, Feb 18-21, 2023

P39

Multiscale Molecular Simulation of Structures and Dynamics Poly(vinyl chloride) Blends with Different Stereochemical Sequences

Chidapha Kusinram, Visit Vao-soongnern*

School of Chemistry, Suranaree University of Technology, Nakhon Ratchasima, 30000, THAILAND

*Email: visit@sut.ac.th

Abstract

A multiscale simulation of amorphous polymeric materials has been developed for vinyl polymer with polar atoms *i.e.* polyvinylchloride, (PVC), $-\text{[CH}_2\text{-CH(Cl)]}_n$ melts and binary blends with different chain tacticity (iPVC, sPVC and aPVC) at the bulk density. The model starts from an *ab initio* quantum chemistry to get the statistical weights of the rotational isomeric state (RIS) model to describe the conformational characteristics of polymer molecule. PVCs chains were coarse-grained by grouping one monomer in one bead and then mapped onto the second nearest neighbor diamond (2nd) lattice. The average non-bonded interactions were treated by the discretized Lennard-Jones (LJ) potential. The on-lattice properties can be determined including chain dimension, intermolecular packing, conformational statistics and molecular mobility (rotational and translational modes). Dynamics of PVC chains with different stereochemistry were generally in the order as: iPVC > aPVC >> sPVC. For binary mixtures composed of chains with different stereochemical sequences, sPVC melt has a tendency for the formation of “local structure” than other types. The binary mixtures containing sPVC experience demixing during the simulations. Fully atomistic amorphous PVC models can be obtained by the reverse-mapping procedure to restore the missing atoms. After energy minimization, material properties including torsional angle distribution, solubility parameter, radial distribution function and static neutron scattering structure factor were calculated for neat structures and blends with different tacticity.

Keywords: Poly(vinyl chloride), Tacticity, Multiscale molecular simulation

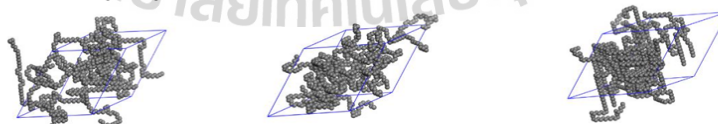


Fig. 1 Specific snapshots of (a) isotactic (b) atactic and (c) syndiotactic PVC models



Fig. 2 (a) The pair correlation function (chain packing) of *i*PVC chains in pure melt and blend mixtures. (b) the mean-square displacement of the center-of-mass (MSD) of *i*PVC chains in pure melts and *i*PVC/*s*PVC, *i*PVC/*a*PVC blends.

References

1. V. A Multiscale Simulation Model for Poly(ethylene oxide), Polym., Sci. A, 2014, 56(6), 928.

APPENDIX C

INTERNATIONAL CONFERENCE I

International Discussion Meeting on Polymer Crystallization (IDMPC 2024), Yonezawa, Yamagata, Japan.

P1-30

Molecular simulation for the effect of interchain interaction on polymer crystallization upon step-wise cooling from the melts

Chidapha Kusinram¹ and Visit Vao-soongnern¹

¹School of Chemistry, Institute of Science, Suranaree University of Technology,
Nakhon Ratchasima 30000, Thailand.

Monte Carlo (MC) simulation of coarse-grained models on the high coordination lattice was employed to investigate the effect of interchain interaction on the structural formation of “polyethylene-like” model upon stepwise cooling from the melt states. Polymer chains were represented by the Rotational Isomeric State model for intrachain energetics of polyethylene (PE) whereas the Lennard-Jones potential function for the interchain interactions ($\sigma = 0.44$ nm, $\epsilon/k = 185$ K) for PE; ($\sigma > 0.44$ nm, $\epsilon/k < 185$) or ($\sigma < 0.44$ nm, $\epsilon/k > 185$) for polymer chains more repulsion or more attraction than that of normal PE, respectively). The evolution of the ordered structure was analyzed regarding the fraction of *trans* state, the length of *trans* sequence, the orientational order parameter at bond and molecular scale, the intermolecular pair correlation function, and the anisotropic change of chain dimension. Simulation results indicate that the rate of structural formation is faster and the degree of crystallinity is higher for normal PE chains. Chains with too strong attractive or too repulsive interaction adopt less amount of *trans* conformation and are harder to form the ordered structure upon cooling from the melts. Our study implies that only polymers with the appropriate range of interchain interaction can exhibit clear evidence for crystallization. [1-4].

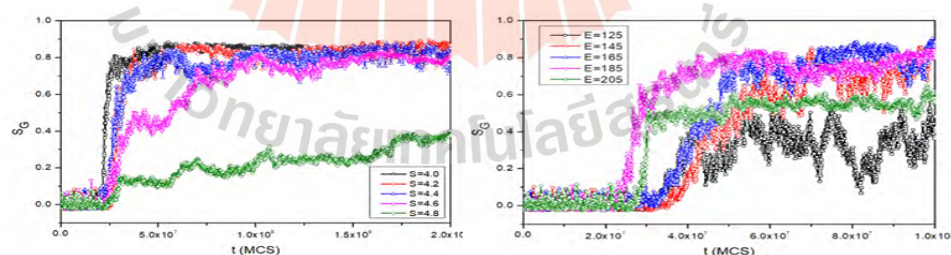


Figure 1 The evolution of the overall orientation correlation function for *polyethylene-like* models with different interchain interaction [left: varied σ and right: varied ϵ/k].

References

- [1] S. Jamornsuriya and V. Vao-soongnern, J. Mol. Liq. **363**, 119833 (2023).
- [2] V. Vao-soongnern, N. Sukhonthamethira, K. Rueansri, K. Sirirak, G. Matsuba, J. Mol. Liq. **376**, 121434 (2023)
- [3] K. Rueansri and V. Vao-soongnern, J. Mol. Liq. **390**, 123134 (2023).
- [4] K. Rueansri and V. Vao-soongnern, Macromol. Symp. **409**, 2200146 (2023).

CURRICULUM VITAE

Name: Chidapha Kusinram

Date of Birth: 17th March 2000 at Buriram Thailand

Education:

2022- 2025	M.Sc. Chemistry International Program, Suranaree University of Technology, DPST scholarship.
2018 - 2022	B.Sc. Chemistry (First class honors :Gold Medal), Suranaree University of Technology, DPST scholarship, the scholarship in the category of talent in science and technology from SUT and NRCT Research Assistantship.
2015 – 2018	Suranaree Witthaya School, Science-Mathematics program.

Publications:

1. **Kusinram, C.** and Vao-soongnern, V. (2025). Monte Carlo simulation for the role of intermolecular interaction on polymer crystallization from the melts. *Journal of Molecular Liquids*, 418, 126733.
2. **Kusinram, C.** and Vao-soongnern, V. (2024). Monte Carlo simulation for the effect of chain stiffness on the free surface of polymer melts. *Journal of Molecular Liquids*, 411, 125665.
3. Wichai K., Sukhonthamethirat N., **Kusinram C.** and Vao-soongnern V. (2023). An efficient method to generate dense amorphous structures for molecular simulation of vinyl polymers. *Macromolecular Symposia*, 408, 2100443.
4. **Kusinram C.** and Vao-soongnern V. (2022). A multiscale simulation of amorphous poly(vinyl alcohol). *Materials Today Communications*, 30, 103029.

Government scholarship:

The Development and Promotion of Science and Technology Talented (DPST) scholarship (fully supported).